Preparation and characterization of carbon micro/nano hybrids and their functional composites

Hang Zhao

université PARIS-SACLAY

CentraleSupélec

NNT : 2015SACLC020

THESE DE DOCTORAT
DE
L'UNIVERSITE PARIS-SACLAY
PREPAREE A
"CENTRALESUPELEC"

ECOLE DOCTORALE N° 579
Intitulé complet de l'école doctorale

Spécialité de doctorat Génie Mécanique

Par

M. Hang ZHAO

COMPORTEMENT MULTIFONCTIONNEL DES COMPOSITES COMPORTANT DES NANO/MICRO RENFORTS

Thèse présentée et soutenue à «CentraleSupélec», le «2015-11-16»:

Composition du Jury :

M. RANGANATHAN, Narayanaswami	Professeur des Universités, LMR, Ecole Polytechnique de l'Université de Tours	Président
M. SYLVESTRE, Alain	Professeur des Universités, G2Elab, University Joseph Fourier - Grenoble 1	Rapporteur
M. LUBINEAU, Gilles	Professeur des Universités, OHMAS Laboratory, King Abdullah University of Science and Technology (KAUST)	Rapporteur
Mme, DIANI, Julie	Directrice de Recherche CNRS, PIMM- ENSAM	Examinatrice
M. TAINE, Emmanuel	Ingénieur de recherche, SBM Offshore	Examinateur
Mme, JEAN-MISTRAL, Claire	Maître de Conférences, LaMCos, Université de Lyon -INSA Lyon	Examinatrice
M. BAI, Jinbo	Directeur de Recherche CNRS, MSSMat, CentraleSupélec	Directeur de thèse

Université Paris-Saclay
Espace Technologique / Immeuble Discovery
Route de l'Orme aux Merisiers RD 128 / 91190 Saint-Aubin, France

université PARIS-SACLAY
ÉCOLE DOCTORALE
Sciences mécaniques et énergétiques, matériaux et géosciences (SMEMAG)

Titre: Comportement multifonctionnel des composites comportant des nano/micro renforts

Mots clés: Composites Polymère ; Nano/Micro Renforcement ; Propriétés Mécaniques ; Propriétés Electriques ; Piézorésistivité

Résumé: En raison de leurs propriétés mécaniques, électriques et thermiques exceptionnelles, les nanotubes de carbone (NTC) ont reçu une importante attention mondiale. Les NTC ont un grand potentiel dans différents domaines d'applications tels que le stockage d'énergie et la microélectronique. Grâce à leur structure unidimensionnelle, leur important facteur d'aspect et leur faible densité, les NTC servent comme charges dans les composites. Par contre, en raison des fortes interactions entre eux, il est difficile de les disperser et de les aligner dans une matrice de polymère.

Il est connu qu'une bonne conception d'hybrides, constitués de NTC verticalement lignés sur des substrats, améliore de manière significative la dispersion de ces derniers dans la matrice. Ces hybrides sont préparés par le procédé de dépôt chimique en phase vapeur (CVD). Une fois, ces hybrides sont dispersés dans la matrice du composite cela conduit à une nette amélioration des propriétés multifonctionnelles de ce composite. Les substrats utilisés dans cette thèse sont les nanoplaquettes de graphite (NPG) pour donner des hybrides NPG-NTC que nous appellerons par la suite GCHs. Les GCHs ont l'avantage d'avoir une faible densité et une structure totalement conductrice qui améliore les propriétés diélectriques et électriques des composites.

Dans l'état de l'art, les relations entre l'organisation des GCHs et les conditions de synthèse par CVD et entre l'ajout des GCHs dans les composites et les réseaux conducteur interne dans les composites n'ont jamais été étudiées. Pour cela, dans cette thèse, nous allons soigneusement étudier et discuter ces problèmes mentionnés.

Nous présentons tout d'abord la synthèse des NTC sur les NPG par CVD. Ensuite, l'influence des paramètres de la CVD, la température, la composition du gaz et le temps de la réaction, ont été étudié. Les résultats qualitatifs et quantitatifs obtenus d'après les caractérisations des ces hybrides peuvent servir comme base de données pour l'intégration et l'influence des ces hybrides dans les composites. Les composites binaires polyvinylidene fluoride/GCHs et leurs propriétés diélectriques qui sont nettement améliorées par rapport aux composites ternaires composés de polyvinylidene fluoride/NPG/NTC. Les composites obtenus par dispersion des GCHs dans la matrice à l'aide du procédé d'extrusion-injection, présentent un seuil de percolation fortement réduit et une stabilité thermique relativement élevée. Leurs propriétés diélectriques améliorées peuvent être attribuées à des réseaux sous forme de micro-condensateurs et le changement de la cristallinité de la matrice peut être attribué à la bonne conception des hybrides. Le composite GCHs/polydiméthylsiloxane (PDMS) présente un seuil de percolation ultra-bas et une grande sensibilité piézo-résistive. En particulier, les autres améliorations des propriétés électriques obtenues dans les composites GCHs/PDMS par rapport à celles des composites à base de NTC/PDMS, de NPG/PDMS ou encore de NTC-NPG/PDMS. Les légers mouvements des doigts peuvent être détectés grâce à l'usage de ces films composites en tant que capteurs de mouvement.

Université Paris-Saclay
Espace Technologique / Immeuble Discovery
Route de l'Orme aux Merisiers RD 128 / 91190 Saint-Aubin, France

Université Paris-Saclay
Espace Technologique / Immeuble Discovery
Route de l'Orme aux Merisiers RD 128 / 91190 Saint-Aubin, France

Title: Preparation and characterization of micro/nano hybrids and their functional composites

Keywords: Polymer Composites; Nano/Micro Hybrids; Mechanical Properties; Electrical Properties; Piezo-Resistivity

Abstract : Due to the outstanding mechanical, electrical and thermal properties, carbon nanotubes (CNTs) received worldwide attentions and intensive investigations in last decades. CNTs are greatly potential in applications such as energy storage and microelectronics. The one-dimensional structure, high aspect ratio and low density, promote CNTs serving as the excellent fillers in composites field. However, due to the strong interactions, CNTs are usually difficult to be dispersed and aligned in a polymer matrix.

Designing the CNTs construction reasonably is an effective way to ameliorate the dispersion states of CNTs in matrix. These specific hybrid constructions allowed CNTs arrays synthesized vertically onto the substrates through catalyst chemical vapor deposition method. These CNT arrays effectively overcome the problem of CNTs aggregation and promote the interconnection among CNTs. The considerable improvement of multi-functional properties of composites can be also achieved. Graphite nanoplatelets (GNPs) served as substrate make their synthesizing products-GNP-CNTs hybrids (GCHs) possess distinctive merits of all-carbon composition, totally-conductive coupling structure and the low intrinsic density. These GCHs constructions provide a particular improvement in the dielectric and electrical properties of composites. However, the relationship between GCHs organization and synthesizing conditions during CVD process and the influence of the addition of GCHs to internal conductive networks have not been reported in detail.

The first chapter makes a general review of structures, properties, applications and synthesis of CNTs and GNP substrates, and the main procedures of fabricating composites and surface functionalization of CNTs. Moreover, a short introduction of the development of micro-nano hybrids applied to the functional composites is made. Most importantly, the developing electrical states and (di) electrical characteristics of composites with ever-increasing conducting filler loading are reviewed in detail at the last part.

The second chapter discusses firstly the synthesis process through the CCVD approach and the relationship between CVD parameters and the corresponding construction of GCHs, where the temperature, gas composition and reaction time were controlled. The constructions CNT arrays are dependent on the synthesis conditions. Furthermore, the results obtained from analysis can provide a structural foundation for the huge application potential of GCHs constructions.

The third chapter introduces the poly(vinylidene fluoride)-based nanocomposites containing GCH particles, the dielectric properties of which are improved more greatly than the ternary composites loading equivalent mixture of GNPs and CNTs. The composites achieved by dispersing GCH particles into matrix using the mechanical melt-mixing process, showing a strongly reduced percolation threshold (5.53 vol.%) and the relatively high thermal stability. Their improved dielectric properties can be attributed to the formed microcapacitor networks and the change of crystalline formation of matrix, caused by well-designed CNT arrays constructions.

The fourth chapter investigates the advanced GCHs/ polydimethylsilicone (PDMS) composites with high piezo-resistive performance at wide temperature range. The synthesized GCHs can be well dispersed in the matrix through the mechanical blending process. The flexible composite shows an ultra-low percolation threshold (0.64 vol.%) and high piezo-resistive sensitivity. Particularly, the much improvements of electrical properties achieved in GCHs/PDMS composites compared with composites filled with equivalent CNT, GNP or mixture of CNTs/GNPs. Slight motions of finger can be detected and distinguished accurately using the composites film as typical wearable sensor.

Université Paris-Saclay
Espace Technologique / Immeuble Discovery
Route de l'Orme aux Merisiers RD 128 / 91190 Saint-Aubin, France

Acknowledgements

First of all, I would like to express my most sincere appreciation to Professor Jinbo Bai, under his supervision this work was done. His constant encouragement, guidance, suggestions and time were invaluable. He has instructed and helped me a lot in the past three years. I learned a lot from him: hard-working spirit, serious attitude towards research, etc.

I feel very grateful for the financial support from China Scholarship Council for the whole three years research. I also appreciate the help given by the Service de l'Education Ambassade de la République Populaire de Chine in France.

I would like to thank the members of the jury: Monsieur Alain Sylvestre and Monsieur Gilles Lubineau who had the difficult task to make a report on my manuscript, Mesdames Julie Diani, Claire Jean-Mistral; Messieurs Narayanaswami Ranganathan, Emmanuel Taine who made me the honor to examine my work.

Special gratitude is extended to Monsieur Le Gal Gilbert for fabricating the metallic moulds, Monsieur Nicolas Roubier for offering help in the mechanical measurements, Madam Françoise Garnier and Monsieur Thomas Reiss for the instruction of operating SEM. I would also like to thank Monsieur Francis Armand and Kervern Daniel for printing the posters for me and Monsieur Perrin Eric, Haghi-Ashtiani Paul and Professor David Bertrand who gave me a lot of help in experiment. I am also indebted to Madame Djebarri Farida, Konate Sokona. As well as all staffs of Lab.MSSMat, I would like to express my thanks for their assistance.

I also owe my sincere gratitude to my friends and my fellows who gave me their help and time accompanying me and I treasure the time we have spent together during the past three years in France: Delong He, Jinkai Yuan, Weikang Li, Salem Diana, Yang Ma, Ahlem Raies, Benhui Fan, Yu Liu, Xiaoxin Lu, Lynda Belkadi, Xiaofei Bai, Yang Liu, Yasmine EL Benna and Alizé Mousty.

My thanks go to Xin Wei, who gave me a number of encouragement and support, and my beloved parents for their loving consideration and great confidence in me all through these years. I am not a qualified son because I was always studying far away from home and I could not be by the side of my parents for all these years. My parents give me all their unselfish love, assistance, patience, confidence. I hope that I can make them proud of me and I will be able to spend more time with them in the future.

Thanks, Paris.

Table of Contents

Acronyms and Symbols

Acronyms

0D	0-Dimensional
1D	1-Dimensional
2D	2-Dimensional
3D	3-Dimensional
ABS	Acrylonitrile Butadiene Styrene
AFM	Atomic Force Microscopy
AR	Aspect Ratio
CB	Carbon Black
CCVD	Catalyst Chemical Vapor Deposition
CMPVA	Carboxymethyl Polyvinyl Alcohol
CNTs	Carbon Nanotubes
DE	Dielectric Elastomer
DMF	Dimethylformamide
DSC	Differential Scanning Calorimetry
EMI	Electromagnetic Interference
FTIR	Fourier Transform Infrared Spectroscopy
GCHs	Graphite Nanoplatelet-Carbon Nanotubes Hybrids
GF	Gauge Factor
GIC	Graphite Intercalate Compound
GNPs	Graphite Nanoplatelets
LDPE	Low Density Polyethylene
LLDPE	Linear Low Density Polyethylene
MWCNTs	Multi-Walled Carbon Nanotubes
MWS	Maxwell-Wagner-Sillars
PAN	Polyacrylonitrile
PC	Polycarbonate
PDMS	Polydimethylsilicone

PE	Polyethylene
PI	Polyimide
PMMA	Polymethyl Methacrylate
PP	Polypropylene
PR	Piezo-Resistive
PS	Polystyrene
PS	Pressure Sensitivity
PTC	Positive Temperature Co-Efficient
PVA	Polyvinyl Alcohol
PVC	Polyvinyl Chloride
PVDF	Polyvinylidene Fluoride
SEBS	Poly(Styrene-B-Ethybutylene-B-Styrene)
SEM	Scanning Electron Microscope
SWCNTs	Single-Walled Carbon Nanotubes
TEM	Transmission Electron Microscope
THF	Tetrahydrofurane
TIMs	Thermal Interface Materials
UHMWPE	Ultrahigh Molecular Weight Polyethylene
XRD	X-Ray Diffraction

Symbols

E	Electrical field
f_c	Percolation threshold
f_{CNT}	Carbon nanotubes concentration
f_{GNP}	Graphite nanoplatelets concentration
$f_{hybrids}$	Hybrids concentration
$Tan\delta$	Loss tangent
U_e	Energy density
vol.%	Volume fraction
wt.%	Weight fraction

ε_0	Dielectric permittivity of vacuum
ε_r	Relative dielectric permittivity
σ	Conductivity
σ_{AC}	Alternating current electrical conductivity
τ	Relaxation time
ω	Angular frequency

Résumé en français

En raison de leurs propriétés mécaniques, électriques et thermiques exceptionnelles, les nanotubes de carbone (NTC) ont reçu une importante attention mondiale. Les NTC ont un grand potentiel dans différents domaines d'applications tels que le stockage d'énergie et la microélectronique. Grâce à leur structure unidimensionnelle, leur important facteur d'aspect et leur faible densité, les NTC servent comme charges dans les composites. Par contre, en raison des fortes interactions entre eux, il est difficile de les disperser et de les aligner dans une matrice de polymère.

Il est connu qu'une bonne conception d'hybrides, constitués de NTC verticalement lignés sur des substrats, améliore de manière significative la dispersion de ces derniers dans la matrice. Ces hybrides sont préparés par le procédé de dépôt chimique en phase vapeur (CVD). Une fois, ces hybrides sont dispersés dans la matrice du composite cela conduit à une nette amélioration des propriétés multifonctionnelles de ce composite. Les substrats utilisés dans cette thèse sont les nanoplaquettes de graphite (NPG) pour donner des hybrides NPG-NTC que nous appellerons par la suite GCHs. Les GCHs ont l'avantage d'avoir une faible densité et une structure totalement conductrice qui améliore les propriétés diélectriques et électriques des composites.

Dans l'état de l'art, les relations entre l'organisation des GCHs et les conditions de synthèse par CVD et entre l'ajout des GCHs dans les composites et les réseaux conducteur interne dans les composites n'ont jamais été étudiées. Pour cela, dans cette thèse, nous allons soigneusement étudier et discuter ces problèmes mentionnés.

Dans le premier chapitre, nous présentons une revue générale de la structure, des propriétés, des applications et de la synthèse des NTC et des NPG. Nous présentons aussi les procédures de l'intégration des nanoparticules dans des matrices polymères et les méthodes de fonctionnalisation des NTC. Nous discutons aussi des états électriques et les caractéristiques (di)électriques des composites en fonction de la

quantité de la charge conductrice.

Le deuxième chapitre présente tout d'abord la synthèse des NTC sur les NPG par CVD. Ensuite, l'influence des paramètres de la CVD, la température, la composition du gaz et le temps de la réaction, ont été étudié. Les résultats qualitatifs et quantitatifs obtenus d'après les caractérisations des ces hybrides peuvent servir comme base de données pour l'intégration et l'influence des ces hybrides dans les composites.

Le troisième chapitre présente les composites binaires polyvinylidene fluoride/GCHs et leurs propriétés diélectriques qui sont nettement améliorées par rapport aux composites ternaires composés de polyvinylidene fluoride/NPG/NTC. Les composites obtenus par dispersion des GCHs dans la matrice à l'aide du procédé d'extrusion-injection, présentent un seuil de percolation fortement réduit (5,53 vol.%) et une stabilité thermique relativement élevée. Leurs propriétés diélectriques améliorées peuvent être attribuées à des réseaux sous forme de micro-condensateurs et le changement de la cristallinité de la matrice peut être attribué à la bonne conception des hybrides.

Le quatrième chapitre étudie les composites GCHs/polydiméthylsiloxane (PDMS) avec la haute performance piézo-résistive dans une large gamme de température. Le composite présente un seuil de percolation ultra-bas et une grande sensibilité piézo-résistive. En particulier, les autres améliorations des propriétés électriques obtenues dans les composites GCHs/PDMS par rapport à celles des composites à base de NTC/PDMS, de NPG/PDMS ou encore de NTC-NPG/PDMS. Les légers mouvements des doigts peuvent être détectés grâce à l'usage de ces films composites en tant que capteurs de mouvement.

Mots clés : Composites Polymère ; Nano/Micro Renforcement ; Propriétés Mécaniques ; Propriétés Electriques ; Piézorésistivité

General Introduction

Due to the outstanding mechanical, electrical and thermal properties, carbon nanotubes (CNTs) received worldwide attentions and intensive investigations in last decades. CNTs are greatly potential in applications such as energy storage and microelectronics. The one-dimensional structure, high aspect ratio and low density, promote CNTs serving as the excellent fillers in composites field. However, due to the strong interactions, CNTs are usually difficult to be dispersed and aligned in a polymer matrix.

Designing the CNTs construction reasonably is an effective way to ameliorate the dispersion states of CNTs in matrix. These specific hybrid constructions allowed CNTs arrays synthesized vertically onto the substrates through catalyst chemical vapor deposition method. These CNT arrays effectively overcome the problem of CNTs aggregation and promote the interconnection among CNTs. The considerable improvement of multi-functional properties of composites can be also achieved. Graphite nanoplatelets (GNPs) served as substrate make their synthesizing products-GNP-CNTs hybrids (GCHs) possess distinctive merits of all-carbon composition, totally-conductive coupling structure and the low intrinsic density. These GCHs constructions provide a particular improvement in the dielectric and electrical properties of composites. However, the relationship between GCHs organization and synthesizing conditions during CVD process and the influence of the addition of GCHs to internal conductive networks have not been reported in detail.

These mentioned issues will be investigated and discussed in this thesis, which is divided into four chapters:

The first chapter makes a general review of structures, properties, applications and synthesis of CNTs and GNP substrates, and the main procedures of fabricating composites and surface functionalization of CNTs. Moreover, a short introduction of the development of micro-nano hybrids applied to the functional composites is made. Most importantly, the developing electrical states and (di) electrical characteristics of

composites with ever-increasing conducting filler loading are reviewed in detail at the last part.

The second chapter discusses firstly the synthesis process through the CCVD approach and the relationship between CVD parameters and the corresponding construction of GCHs, where the temperature, gas composition and reaction time were controlled. The constructions CNT arrays are dependent on the synthesis conditions. Furthermore, the results obtained from analysis can provide a structural foundation for the huge application potential of GCHs constructions.

The third chapter introduces the poly(vinylidene fluoride)-based nanocomposites containing GCH particles, the dielectric properties of which are improved more greatly than the ternary composites loading equivalent mixture of GNPs and CNTs. The composites achieved by dispersing GCH particles into matrix using the mechanical melt-mixing process, showing a strongly reduced percolation threshold (5.53 vol.%) and the relatively high thermal stability. Their improved dielectric properties can be attributed to the formed microcapacitor networks and the change of crystalline formation of matrix, caused by well-designed CNT arrays constructions.

The fourth chapter investigates the advanced GCHs/ polydimethylsilicone (PDMS) composites with high piezo-resistive performance at wide temperature range. The synthesized GCHs can be well dispersed in the matrix through the mechanical blending process. The flexible composite shows an ultra-low percolation threshold (0.64 vol.%) and high piezo-resistive sensitivity (gauge factor ~10^3 and pressure sensitivity ~ 0.6 kPa^{-1}). Particularly, the much improvements of electrical properties achieved in GCHs/PDMS composites compared with composites filled with equivalent CNT, GNP or mixture of CNTs/GNPs. Slight motions of finger can be detected and distinguished accurately using the composites film as typical wearable sensor.

Key Words: Polymer Composites; Nano/Micro Hybrids; Mechanical Properties; Electrical Properties; Piezo-Resistivity

Chapter I

Carbon nanostructures and their functional effects in composites

1.1 Carbon nanotubes

1.1.1 Structures

24 years ago, Iijima reported their discovery of nanometer-size, needle-like carbon nanotubes (CNTs) with potential applications in microelectronic circuitry and microscopy.[1-2] Since then CNTs have developed as one of the most intensively investigated materials in recent decades. A number of outstanding intrinsic functionalities and surprising potential applications were excavated out.[3-4]

Generally, according to the different radial organizations, CNTs can be classified into two main types: single-walled carbon nanotubes (SWCNTs) and multi-walled carbon nanotubes (MWCNTs). The former consists of a cylindrical tube seamlessly wrapped by a graphene sheets, which is a single large molecular. While, the latter collects more concentric graphene cylinders can be considered as a mesoscale graphite system.[5] Both these two types of CNTs posses all carbon bonded in a hexagonal lattice except at their open ends. The schematic demonstrations and morphological characterization of SWCNTs and MWCNTs by transmission electron microscopy (TEM) are illustrated in Fig. 1-1. As shown in Fig.1-1c, the diameter of SWCNTs is typically around 1-1.4 nm. Due to the strong van der waals interactions among SWCNTs, the tightly packed SWCNTs bundles with the intertube distance is around 3.15 Å can be formed. In contrast with SWCNTs, the multi-walled counterpart with interlayer space and diameters are ~3.4 Å and several to hundred nanometers, respectively (see Fig.1-1d). In particular, the length of CNTs is able to attain in the

range from micrometers to centimeters. Owing to just the ultrahigh aspect ratio (axial length to radial diameter), CNTs are capable of showing their excellent intrinsic properties.

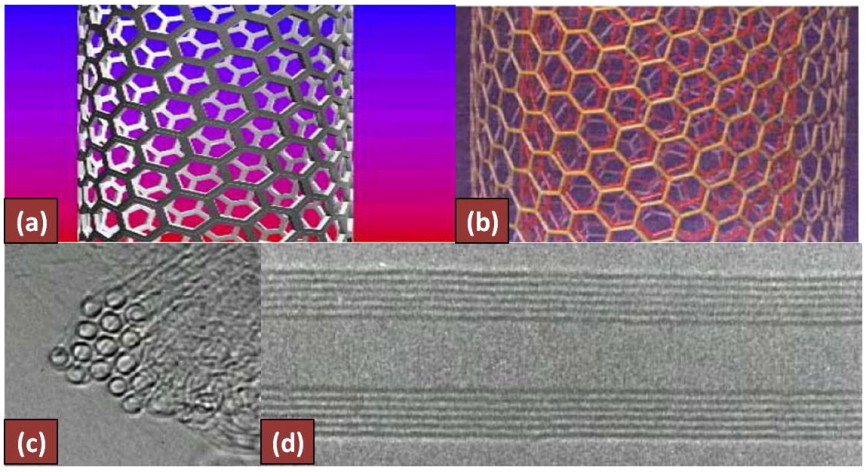

Fig.1-1 *Schematic diagram of (a) SWCNT and (b) MWCNT. TEM morphologies of (c) SWCNT and (d) MWCNT.[4]*

The different forms of atomic structures of SWCNTs can be described by the tube chirality (or helicity), which is defined by the chiral vector, namely, $\vec{C}_h = n\vec{a}_1 + m\vec{a}_2$, where the pair of integers (n, m) are the steps number along the unit vectors of the hexagonal lattice $\vec{a}_1$ and $\vec{a}_2$, respectively, as demonstrated in Fig. 1-2a.[6-7] In terms of amounts of coefficients (n, m), the orientation of carbon atoms around the nanotubes chirality are classified as three main categories: when n is equal to m, the arm chair structure; when n or m is equal to 0, the zigzag structure; all others (n, m) can be specified as chiral structure. Fig. 1-2b schematically illustrate these three structures of SWCNT, from left to right are armchair, zigzag and chiral structures, respectively. The various atomic structures can lead to that SWCNT showing the distinct natures. All armchair SWCNT are metallic with a empty band gap of 0 eV. SWCNTs with n-m=3k, where k is an intrger and is not equal to 0, are semimetallic with a small band gap on the order of a few meV. While, SWCNT with n-m $\neq$ 3k are semiconductors with a larger band gap on the order of ca. 0.18-1.8 eV, which is inversely dependent on the nanotubes diamaters.[8] Due to every single

MWCNT consists of several tubes and contains various of tube chiralities, their physical properties are difficult to pre-evaluate.

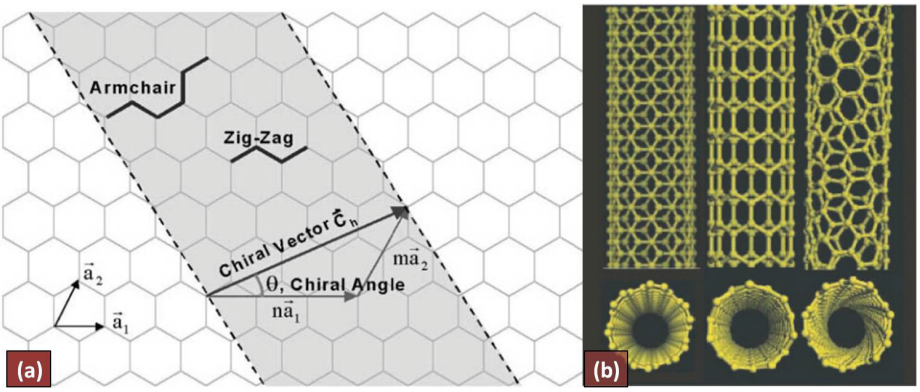

Fig.1-2 *(a) Schematic diagram showing the hexagonal sheet structure of CNT and (b) armchair, zigzag and chiral SWCNTs.[7, 9]*

1.1.2 Synthesis

In recent decades, SWCNTs and MWCNTs are most widely synthesized via three methods: electric arc discharge, laser ablation of carbon and chemical vapor deposition.[7] During these synthesis processes, carbon source, heat resource and catalyst precursor are considered as three necessary components.

The method of electric arc discharge utilizes two high-purity graphite rods placed end to end as the anode and cathode, a voltage source for providing a stable electric arc under a helium atmosphere (see the Fig1-3a). During the discharge process, the average temperature of the plasma regions between anode and cathode is as high as 4000 K.[10] The graphite anode can be vaporized into carbon atoms, which then deposit and concentrate onto the surface of the cathode or the wall of the internal cavity as the forms of nanotubes or other types of carbon. Particularly, the SWCNTs can be obtained by doping electrodes with a small quantity of metallic catalyst particles.[11-12]

Laser ablation is another way to synthesize fullerene and CNTs based on the high temperature physical vaporization mechanism. Fig.1-3b schematically depicts the reaction devise, where a laser beam is introduced and focused onto a graphite target

that doped with metallic catalytic. Nanotubes can be synthesized from the evaporated carbon under high temperature near 1200 ^{o}C and inert gas atmosphere.[13]

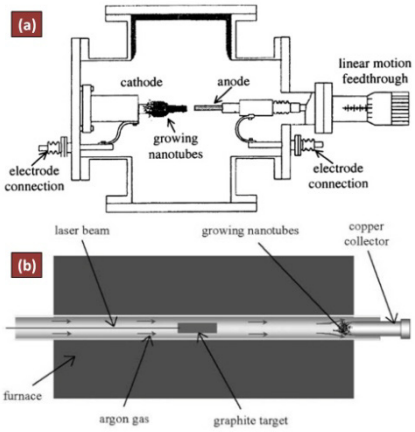

Fig.1-3 *Schematic illustration of (a) arc-discharge technique and (b) the laser ablation process.[11-12, 14]*

However, as a coin with opposite sides, CNTs produced by electric arc discharge with higher graphitization degree but complete following purification processes are necessary. As to the laser ablation process, although their products with high quality and purity, it is subjected to the low output-input ratio.[15] Furthermore, in order to make those superiorities of CNTs applied in composites, mass-production of CNTs becomes a critical affaire. Due to the relatively limited production, complex purification processes and the high cost of electric arc discharge and laser ablation processes, the gas-phase technology for CNTs growth has been considered as a promising method to provide large quantities of CNTs fillers to meet the demand of composites. Besides the larger productions, the as-synthesized CNTs are able to exhibit high purity, which can cut down the following purification processes effectively.

As one of the most representative gas-phase technology, the process of chemical vapor deposition (CVD) has been widely used in CNTs synthesis and intensively studied in recent decades. CVD is a general process, where gas phase molecules are able to be decomposed into reactive species under high temperature and inert gas

atmosphere. These decomposed atoms then deposit and aggregate, leading to the synthesized particles or film. CVD reactor configurations for CNTs growth mainly involve horizontal, vertical and barrel forms, from which the horizontal reactor is widely used in floating catalytic CVD process. The process of catalytic CVD is schematically shown in the Fig. 1-4.[16]

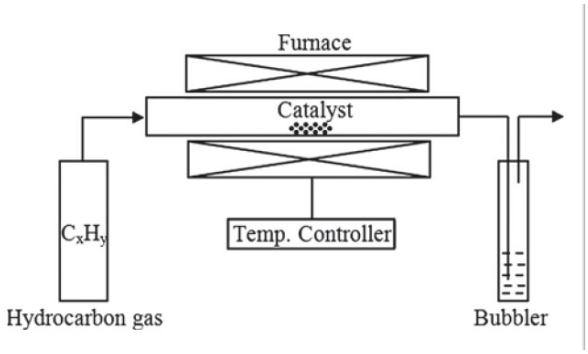

Fig.1-4 Schematic illustration of catalytic CVD process

Besides the mass-production that can be scaled-up into industrial, another outstanding superiority of CVD process concentrates on controlling the structure or architecture of CNTs. In fact, the construction and forms of synthesized CNTs, such as diameter, length, bundle density, can be well controlled by tuning experimental parameters during the synthesis process, such as the temperature, the type, concentration and composition of carbon sources and carrier gases, the type and structure of substrates, etc. Even the desired architecture of nanotubes synthesized on predetermined positions of a patterned substrate can be achieved by tuning growth parameters precisely.[17]

The history of catalytic CVD process traces back to the middle of the twentieth century, Radushkevich reported the tubular carbon filaments with diameter of 50-100 nm synthesized at the existence of iron catalyst and 600 ^{o}C.[17] They found that iron carbide firstly formed through dissoluting carbon in iron, which then provides a chance for carbon deposition over it and forming the graphene layers. Since then, the metal catalyst particles play an essential role in CNT growth. Metallic particles of iron, cobalt and nickel, the most common ones, possess excellent catalytic activity for CNT growth. Other metals, such as copper, gold, silver, platinum, served as catalyst in CNT

growth from various carbon source.[18-19] Recently, solid organometallocenes, such as ferrocene, cobaltocene, nickelocene, are widely used as catalysts for CNT growth as well. Compared to traditional metallic particles, the decomposition of carbon sources can be catalyzed more efficiently by metallic nanoparticles decomposed from these solid organometallocenes.[17] Particularly, the catalyst activity is not only dependent on the metal nature (various valence electrons configurations) but also the particle size. According to the "size-effect", under a certain size range, the diameter of CNTs prefer to increase with the enhanced catalyst particle size.[20-22]

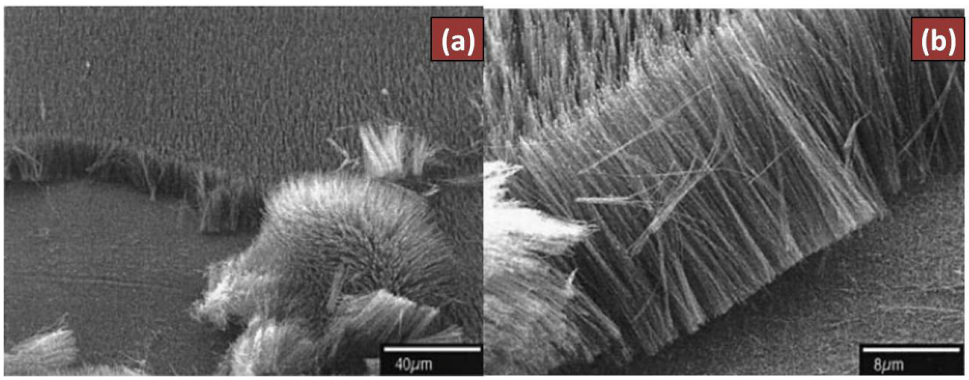

Fig.1-5 *SEM morphologies of straightness of MWCNTs grown on the glass through CVD.*

As another essential component in catalyst CVD process, carbon sources are capable of offering carbon atoms to synthesize CNT constantly. The carbon sources consists of various hydrocarbons can be specified into gas-state: carbon monoxide, acetylene, methane, ethylene and liquid-state: benzene, toluene, xylene, cyclohexane, etc.[23-30] At high temperature, the decomposition process of carbon source comprise the homogenous thermal decomposition in gas phase and typical catalytic decomposition on catalyst particles.[15] In very recent years, multi-carbon sources substituted for mono-carbon source were used for CNTs growth, in order to balance the reactivity under relatively wide synthesis temperature range.[31]

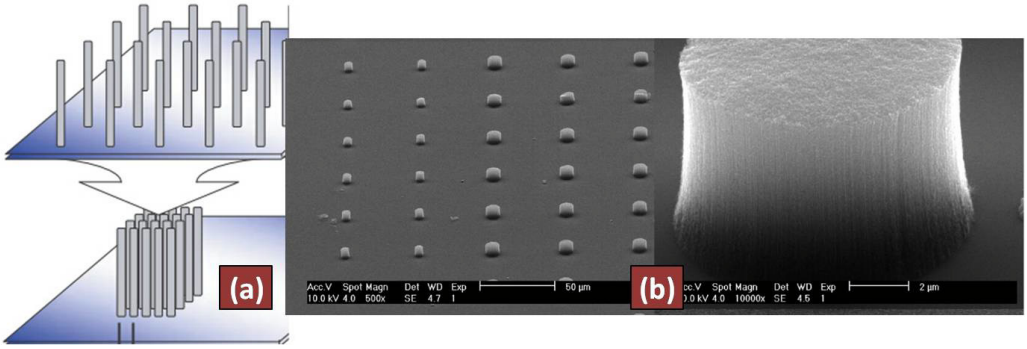

Fig.1-6 *SWCNT forests with ultra-high area density by controlling the CVD process*

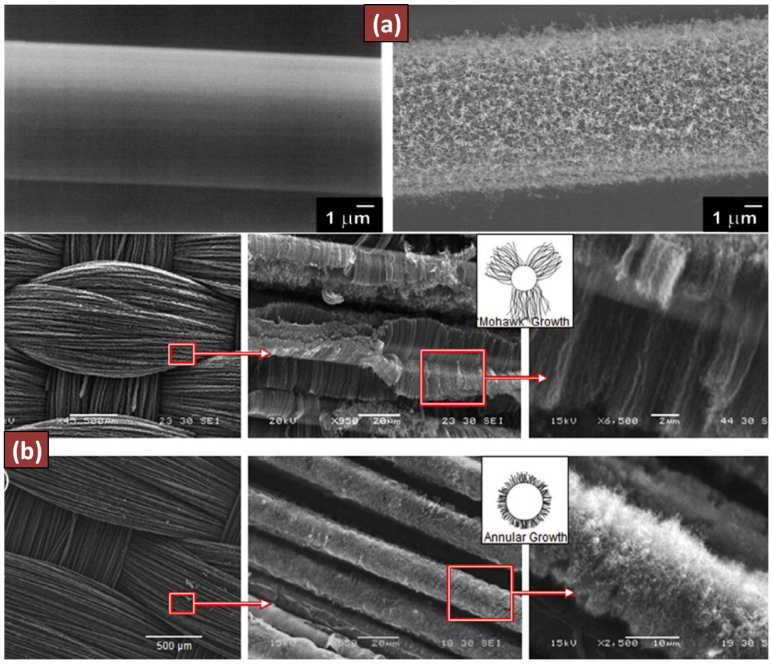

Fig.1-7 *SEM micrographs of (a) carbon fiber before and after CNTs growth and (b) Fibers in long or short CNTs fuzzy architecture before polymer infiltration.[5,6]*

A number of support materials can be applied as CVD substrates for CNTs growth, which is responsible for the various CNTs structures and constructions due to their different intrinsic natures. For example, vertically aligned CNTs forest can be typically synthesized on the large-area plat substrates. Ren et al. synthesized successfully large-scale well-aligned CNTs arrays on the nickel foils and glass at temperature below 700 ^{o}C, which is suitable for electron emission applications (see Fig.1-5).[32] Owing to the excellent electrical conductivity, CNTs forest is potential to replace traditional metals served as interconnects in integrated circuits and super-

capacitor electrodes only if the interconnect resistance can be reduced to the range be similar to the metal. Futaba et al. and Zhong et al achieved SWCNT forests with ultra-high area density as high as 8.3×10^{12} and 1.5×10^{13} tubes cm^{-2}, respectively, by controlling the CVD process (see Fig. 1-6).[33-34] Besides on the traditional quartz and glass substrates, CNTs can be successfully grown on the carbon fibers and fabrics using catalyst CVD process (see Fig.1-7).[35-36] After the CNTs growth, the specific surface areas of both carbon fibers and semi-conductor fabric were enhanced significantly, which would play a greatly positive role in reinforcing their composites. Veedu et al.[37] fabricated a 3D SiC micro-fibre fabric through growing MWCNTs on the surface of fabric.(see Fig. 1-8) Compared to the bulk fabric/epoxy composite, the 3D fabric/epoxy composites showed that the flexural modulus, strength and toughness increased by 105%, 240% and 524%, respectively. Gui et al.[38] presented a 3D architecture where CNTs were arranged into different morphologies and orientations using CVD method, of which the electrical and mechanical properties can be well controlled by tuning the structure and patterns of two distinctly different CNTs construction: sponge and array forms (see Fig.1-9).

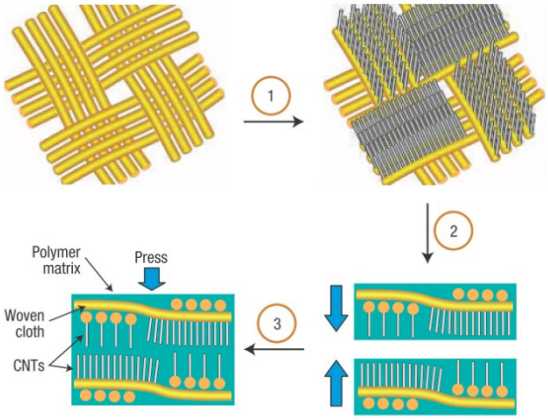

Fig.1-8 *Schematic illustration of a 3D SiC micro-fibre fabric through growing MWCNTs on the surface of fabric.[37]*

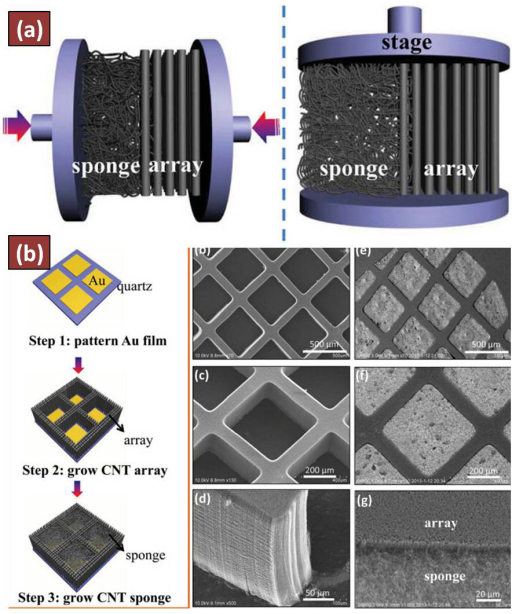

Fig.1-9 *Schematic illustration of (a) compression test and (b) fabrication of patterned parallel structures of three-dimensional CNT sponge-array architectures.[38]*

1.1.3 Properties and applications

In recent 20 years, hundreds of thousands of publications and patents concentrated on the investigation of the structure, synthesis, construction, intrinsic properties and application of CNTs and their composites. Owing to the unique electronic properties, a thermal conductivity in axial direction exceeds diamond and most materials, the superior mechanical properties with the ultrahigh stiffness and realized mass-production, CNTs are still considered as one of the most potential in numerous applications.

The elastic modulus of single CNT was carried out though observing and calculating the amplitude of CNTs oscillations measured by tunneling electronic microscopy (TEM), or bending the anchored CNTs using the tip of atomic force microscope (AFM) and recording the force exerted by the tube according to the displacement from the equilibrium position.[39-41]. Moreover, the nanotubes were attached between two opposing AFM tips and loaded under tension to measure the tension strength of CNTs.[42-43] Both the experimental and theoretical results gave

an elastic modulus and tension strength of individual WMCNTs around 1 TPa and 100 GPa, respectively, which is much stronger than any industrial fiber.[39, 44] As to the electrical properties, as mentioned before, the diameter and helicity of nanotube determines the nanotubes showing the metallic or semiconductor state, which is greatly responsible for the electrical performance. Four-probe measurements were generally applied to measure the electrical performance of CNTs. Results indicated that CNTs is able to carry current densities as high as $10^9 A \cdot cm^{-2}$,[33, 45] exhibiting the conductivity range from 10^2 to 10^6 $S \cdot cm^{-1}$. The wide conductivity distribution ascribes to that MWCNTs organized by various number of nanotubes with different chirality forms.[46-47] In addition, the highly anisotropic thermal conductivity of SWCNTs reach to 3500 $W \cdot m^{-1}K^{-1}$ which can be measured by the classic comparative method.[48-49] On the contrary, their thermal expansion is isotropic and usually negligible.[3]

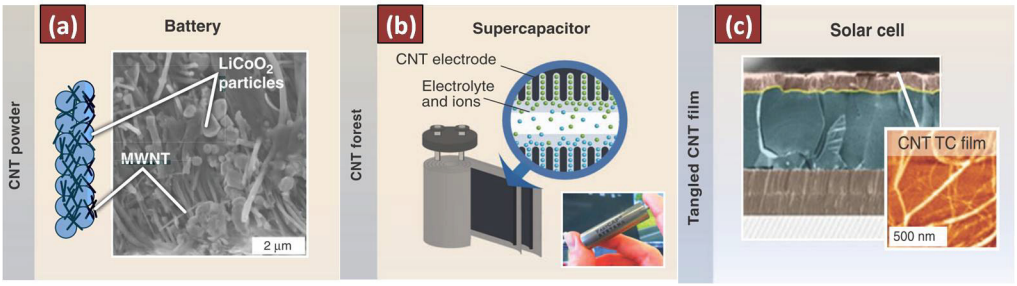

Fig.1-10 *Energy-related applications of CNTs.(a) Mixture of MWCNTs and functional particles for battery electrode. (b) CNTs forest apply to supercapacitor (c) Solar cell using a CNT-based transparent conductor.[50]*

Due to the mentioned intrinsic properties, there are a number of applications of CNTs have been investigated. Such as functional coating, transparent conducting films, CNTs-loading composites, energy storage, microelectronics, sensor and actuators and biotechnology, etc.[9] Some of them have been realized in products, others are under further amelioration, both which makes an advanced contribution to the CNTs development. In recent decades, due to the fast developing industry, the aggravating energy shortage becomes a critical issue. It is crucial to develop new, highly efficient and environmentally friendly energy generating, converting and

storage technology. Particularly, as shown in Fig.1-10, CNTs plays an important role in applications of energy storage. For example, loading a small quantity of CNTs into $LiCoO_2$ cathodes and graphite anodes can effectively increase the rate capability and cycle life of lithium ion batteries.[51-53] The usage of Pt in fuel cell can be reduced effectively even removed by employing CNTs as catalyst support.[54-55] For the organic solar cells, it is potential for CNTs to decrease the carrier recombination and increase resistance to photooxidation. Promisingly, transparent SWCNT electrodes would be incorporated in the prospective commercial photovoltaics. Supercapacitor possesses larger capacitances than traditional dielectric capacitors, and much faster charging rate, receiving wide and intensive attentions. The large capacitances are 180 and 102 $F \cdot g^{-1}$ can be achieved for supercapacitors with SWCNT and MWCNT electrodes, respectively, which is preferable for the applications require higher storage capacities, for instance, providing rapid acceleration for the hybrid vehicle.

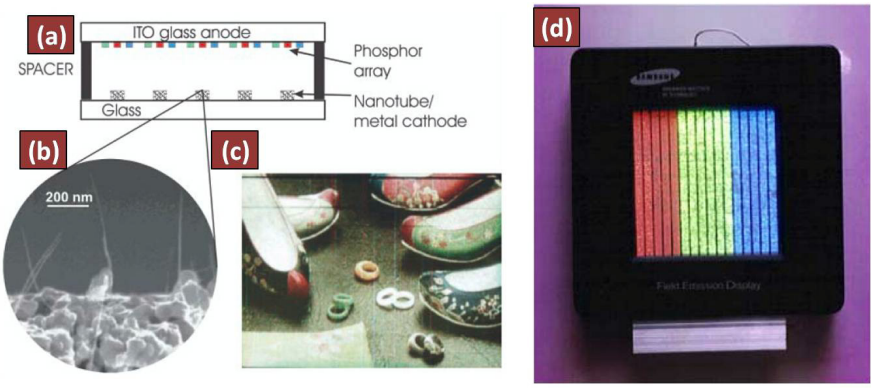

Fig.1-11 *(a) Schematic illustration of a flat panel display based on CNTs (b) SEM morphology of an electron emitter for a display (c) Photograph of a CNT field emission display made by Samsung (d).[9]*

In comparison with ordinary thermionic emission, the field emission electrons source is more advanced and efficient technology. Owing to their nanometer scale, structural integrity, electrical conductivity, and chemical stability, CNTs show a very low threshold electric filed and a great potential in electron emitters. In addition, CNTs endows the field-emitting devise with merits of stable emission and long lifetime.[56-57] One of the most practical applications is flat panel displays.

Compared to the liquid crystal displays, nanotubes are able to effectively reduce the power consumption, enhance brightness and response rate, and widen viewing angle and their operating temperature range.[4, 9]. Fig.1-11 present the some prototypes of nanotube-based field emission electron flat panel displays.[58]

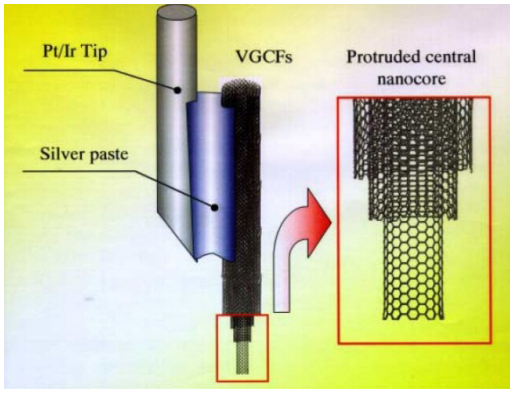

Fig.1-12 *The vapor grown carbon fiber (VGCF) provides a convenient and robust technique for mounting the MWCNT probe for the utilization in scanning probe instrument.[4]*

With advantages of high aspect ratio and excellent mechanical bending modulus, CNTs can make an indispensable contribution to the application as nanoprobes. These nanoprobes are competent in high resolution imaging, nano-lithography and nanoelectrodes. It is known that the single CNTs attached to the scanning probe instruments used for imaging tiny features (see Fig.1-12), while, a pair of CNTs positioned on an AFM tip, they can serve as a nano- tweezers to tune the positions of nanoscaled structures.[59-61] Moreover, CNTs that attached with certain functional groups by chemical modification can be used in molecular recognition, chemically sensitive imaging and local chemical patterning.

In general, CNTs with different structures can be well synthesized by controlling the experimental parameters of CVD process. Due to the chiral atomic structures, high aspect ratio and ultrahigh specific surface, CNTs exhibits outstanding overall properties and can be applied into numerous field. The investigation of incorporating CNTs dispersed in polymer matrices to form composite is another indispensable

aspect, which will be introduced in following sections.

1.2 Graphite nano-platelets

1.2.1 Structures and Properties

In comparison with the synthesized CNTs, Graphite is a naturally carbon material formed through stacking a number of graphene layers, which exists abundantly on earth. Graphite nanoplatelets (GNPs) are a kind of graphitic form in nano-scale, consisting of tens of stacked graphene multi-layers. The interlayer distance is a constant of ca. 0.34 nm.[62] Carbon atoms in a single GNPs layer are bonded covalently, while the stacked layers are bonded to each other through weak non-covalent Van der Waals interactions. Be different from natural graphite and single-layer graphene, GNPs possess the thickness varying from several to hundreds of nanometers, while their diameter in-plane usually in the microscale. Thus, compared with the high aspect ratio in axial direction of CNTs, distinctively, GNPs exhibit their intrinsic high aspect ratio in radial direction. The specific surface area of GNPs can reach to a theoretical value as high as 2630-2965 $m^2 \cdot g^{-1}$.[63] According to the various forming processes, such as intercalation, oxidization, heat treatment, microwave irradiation, and ultrasonication, etc. the thickness (layer number) and in-plane diameter can be well controlled.[64-67] Such large specific surface area and distinct two-dimensional(2D) reinforcing effect, making GNPs strongly potential in acting as functional fillers. In fact, the modulus and strength of graphene are reported as 1100 GPa and 125 GPa, respectively.[68]

Compared with the popular 2D structured nano clays, GNPs is superior and favorable due to their lower mass density and high electrical and thermal conductivities. In typical, the GNPs composed of multi-layer graphene, where, electronically, the *2p* orbitals can hybridize with *s* orbital to form three sp^2 orbitals. Then the energetically stable and localized σ-bonds can be formed with the three

closest-neighbor carbon atoms in the honeycomb lattice. Besides the electrons served as forming σ-bonds, the residual single valence electron occupies the $2p_z$ orbital. Therefore, the migration of $2p_z$ electrons provides a good electrical conductivity in the graphene plane.[69] It is noteworthy that the electricity is mainly conducted within the plan of graphene layers. Be similar with electrical behavior, The acoustic and thermal properties of graphite are highly anisotropic, since phonons propagate quickly along the graphene planes, but are slower to travel interlayer. In addition, GNPs with high-purity can be obtained from fruitful natural graphite resource by relatively facile approaches, rather than the rigorous conditions for synthesizing CNTs or carbon fiber, such as complex equipments, high cost and energy consumption.[69] This makes GNPs is competent to be used as the substitution of CNTs, applying in many fields.

1.2.2 Synthesis

For the natural graphite, there are two main differences between axial and in-plane directions. On one hand, in comparison with the interlayer distance in axial direction is 0.335 nm, the carbon atoms are arranged in a honeycomb lattice with space of 0.142 nm. On the other hand, the σ-bonds in the lattice plane is much stronger than the interlayer weak Van der Waals force. Thus, the larger lattice spacing and weaker bonding provide us a promising possibility to achieve GNPs by exfoliating natural graphite.[69]

Plenty of ways have been used for preparation of GNPs, among which the mechanical exfoliation and graphite-intercalation chemistry are most preferred. Because of the weak interlayer interaction, GNPs with different layer number can be obtained through mechanical milling and peeling off, the two main top-down processes of mechanical exfoliation. Mechanical milling takes advantage of drastic milling force to break the Van de Waals force, and consequently breaking up natural graphite to GNPs.[70] While, the technique of peeling off can be as simple as rubbing graphite against other matters or repeatedly peeling off graphite using adhesive tape,

or as precise as peeling graphite by manipulating AFM or STM tips. The formed graphitic sheets can be folded and tear via the fiction between tip and graphite surface.[71-72] However, the resulting GNPs prepared by these two methods have their own significant drawbacks: firstly, undesired large GNPs size and wide size distribution achieved; Secondly, the aim of mass-synthesis of GNPs is deeply astricted due to the low-productivity. However, these problems can be well overcome by the chemical graphite-intercalation approach.

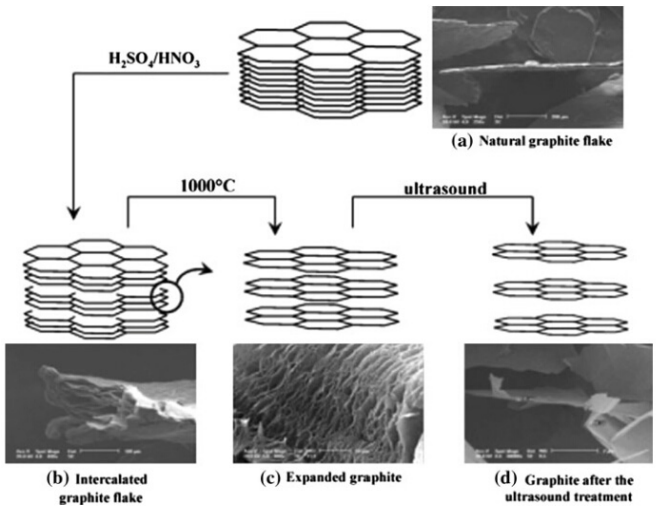

Fig.1-13 *Scheme of graphite structure modification after different treatments[62]*

The core principle of chemical graphite-intercalation is to fill into the natural graphite layers with certain chemicals which is capable of reacting and producing gas with a large volume or/and tremendous heat. The neighboring graphene layers then are separated by the high energy produced from gas expansion or/and heat (see Fig. 1-13). Thus the preparation of graphite intercalate compound (GIC) and expansion are two key steps of chemical ways. Acid is one of the most representative chemical agents for forming the GIC, where the natural graphite can be immersed in the concentrated/fumed sulfuric acid (H_2SO_4) solution with certain strong oxidants such as concentrated nitric acid (HNO_3), $KMnO_4$, H_2O_2, O_3, etc. and transformed into graphite intercalate compound through reactions.[73] Then, accompanying the generation of a great volume of gases of SO_2 and H_2O, these GICs are able to expand

violently under the ultrahigh temperature. Notably, this process is suggested to be taken in the nitrogen atmosphere, in order to keep the product-GNPs from being oxidized as far as possible. In addition, the alkali metals and compounds are also the effective agent for prepare GIC. Mark et al.[74] utilized the crystalline alkali compound KC_8 that formed by heating the mixture of graphite and potassium metal under vaccum at 200 ^oC as the intercalant. Then, the addition of ethanol solvates the potassium and produces the potassium ethoxide and abundant H_2, which effectively separates the graphite into GNPs with dozens of layers. Several other alkali metals well applied in graphite-intercalation as well. In addition to heat expansion, microwave irradiation and ultrasonication are usually used for providing high energy to expand GICs.[75-76] Viculis et al.[63] prepared the GNPs with ultra-low thickness: they reintercalated the acid-intercalated graphite using potassium or cesium at 200 ^oC, or the sodium-potassium alloy at room temperature, followed by the further separating processes of ethanol exfoliation and microwave irradiation drying.

In addition to these aforementioned conventional top-down routes, several other classic approaches are useful for the synthesis of GNPs. GNPs can be formed on certain metal surfaces by surface segregation of carbon atoms or decomposition of carbon-based molecules.[77] These reported metal substrates are Co, Ru, Ni, Rh, Pd, Pt and Cu, etc.[69] In the former method, the metal substrates are annealed in CO atmosphere or contact graphite directly, forming the carbon-containing metal substrates. Then GNPs can be achieved by annealing intermediate at high temperature, where carbon separates from the surface.[69] In the latter approach, firstly, covering carbon-containing molecules such as C_2H_2, C_2H_4, C_3H_6, CH_4, benzene and toluene etc. on the surface of metallic substrates at room temperature. Then anneal the carbon-covering metal at high temperature, leads to desorption of hydrogen atoms and the formation of GNPs on the metal surface. With the ever-fast development of electronics, the difficulty of transferring the produced ultrathin GNPs from metallic surface to the insulating substrates limits the method popularized in electronics. However, the way of growing GNPs onto the surface of semiconductors such as SiC

directly proves itself as a reasonable solution.[69]

Synthesis of free-standing GNPs is the typical bottom-up method to synthesize GNPs in a free-standing form, being similar with the synthesis of CNTs and carbon fiber. The methods are usually used for synthesizing CNTs such as the laser ablation and discharge can be also used for fabrication of GNPs through optimizing the temperature, current and hydrogen pressure.[78-80] It is worthy to note that CVD always plays an important role in controlling the growth of GNPs and other 2D carbon on substrates. For example, Shang et al.[81] synthesized the carbon nanoflakes on the Si(100) substrate with the thickness of less than 10-20 nm and a diameter of 300-600 nm using the hot filament CVD method. The size and density of GNPs are dependent on the reaction temperature.

1.2.3 Applications

Since 2004 graphene was discovered for the first time, this single layer 2D carbon structure with extraordinary intrinsic electrical conductivity (~6000S·cm^{-1}) and outstanding tensile strength (~1 TPa) attracted attentions of all over the world.[82-84] Particularly, the surprising milestone of 2010 Nobel Physics Prize was awarded for the preparation of graphene especially plays a critical role in pushing the investigation of graphene to a new high summit. However, there are lots of difficulties and challenges for the applications of graphene/polymer composites. Firstly, both the top-down and bottom-up processes are impossible to fabricate graphene in mass-production in short term, however, which is the basic requirement of composites. Secondly, due to the ultrahigh specific surface area, graphene layers extremely tend to form aggregations and stack layers. In fact, according to the coupling effect among graphene layers, the behavior of bulk graphite becomes dominant when the stack consists beyond 10 graphene layers. However, how to avoid aggregation and maintain the intrinsic superiorities of graphene is another imperative challenge. However, GNPs with relatively high aspect ratio, considerable physical, electrical and thermal

properties and especially, the low cost and ability of mass-production can be considered as not only the compromise between properties and practicability but also the optimal substitution of graphene as the 2D functional filler.

Firstly, due to the high aspect ratio, a GNP network can be formed in polymer matrix at a very low GNPs loading content. Meanwhile, the melt viscosity of mixture of GNPs and polymer will increase, which is influenced by the aspect ratio and the exfoliation degree of GNP.[85-86] Notably, compared with graphite in micro-scale, loading GNPs can provide a much higher melt viscosity of composite. However, owing to their self-lubricating property, GNP-loaded composites exhibit the lowest melt viscosity and best processibility in comparison with other carbon fillers at a certain loading content.[87]

Nano-particles usually have the high specific surface area, when loading it into a polymer matrix, the strong interfacial interaction benefit the load transfer within the composites. The high aspect ratio of GNP is different from that of CNT, which is able to provide a typical 2D reinforcement to composites. Thus, the anisotropic mechanical behavior of composites will be strongly influenced by dispersion and GNPs structures. The improvement of mechanical property is ascribed to that, on one hand, the relatively large 2D structures can tightly attract polymer chains and restrict their mobility, generating the formation of a stiffened interphase. On the other hand, when GNP network is formed in polymer matrix, the rigid backbone endows composites with increased modulus.[67] Cho et al.[88] modified carbon fiber/epoxy composites by loading a small amount of GNPs into system. Compared with the bulk composite, the addition of 5 wt.% GNPs gave rise to the increase of in-plane shear modulus, strength and compressive strength by 17%, 11% and 16%, respectively. Mark et al.[74] loaded 4 wt.% GNPs into PAN solution, the composite nanofibers prepared via electrospinning showed a double normalized young's modulus. However, opposite reinforcing effects have been also reported, such as the strength decrease or firstly increase to a critical loading content, then drops down with the increasing GNP loading.[89-91] These decrease could be explained by inducing many stress

concentration sites and weak interface caused by the ineffective dispersion. Thus, it is necessary to develop preparation approaches of optimizing the GNPs dispersion and intercalation of molecular chains into layer-stacked structures.[92]

As mentioned before, the GNPs with excellent in-plane electrical conductivity are capable of endowing their composites with pronouncedly improved electrical conductivity. The percolation threshold range of GNP/polymer composites is generally higher than that of polymer-based composites using CNTs as filler. When the internal GNP conducting network constructed, namely beyond the percolation threshold, the electrical conductivity of GNP/polymer composites would be independent on the loading content and maintain at the stable level of around 10^{-3} $S \cdot cm^{-1}$.[73] Taking advantages of the temperature and pressure dependence of electrical conductivity of composites, some interesting smart materials and sensors can be achieved. Yu et al.[93] studied the temperature-dependent electrical resistance of GNP/carboxymethyl polyvinyl alcohol (CMPVA) composites, where there was a significant transition between positive and negative temperature coefficient effect at 70 ^{o}C as demarcation point. The unusual results could be explained by thermal expansion of matrix destroyed the conducting network and the increasing thermal disturbance of conducting charges. Moreover, in terms of piezoresistive applications, Chen et al.[94] reported a GNPs/silicone rubber composite, which exhibited a percolation threshold as low as 1.36 vol.% and an ultrasensitive positive piezoresistive behavior under the finger-pressure range (0.3-0.7 MPa) The detailed discussion of piezoresistive behavior will be introduced in section 1.4.

Dielectric permittivity is an important physical parameter to evaluate the capability of the electrical energy storage of materials. According to the percolation theory, the permittivity of composites will exhibit a giant enhancement when the internal conducting network is close to be constructed. GNPs with their high aspect ratio and electrical conductivity are able to effectively increase the permittivity of composite at a relatively low loading content. Be similar to other properties, the dielectric permittivity is also influenced by the degree of exfoliation of GNPs. Xu et

al.[95] prepared a GNP/PMMA composites through in situ polymerization. Their percolation threshold at room temperature was about 1 wt.% GNP loading content, much lower than that of the conventional graphite loaded counterpart. For most pure polymers the intrinsic permittivity is under a low level. Since poly (vinylidenfluorid) (PVDF) possesses relatively high permittivity about 10 at room temperature, it is considered as the most promising host dielectric material. Li et al.[96] fabricated the GNP/PVDF composite using solution mixing followed by compression molding. A large permittivity of 173 and low loss tangent of 0.65 were obtained at 1kHz in the GNP content closed to the threshold (2.4 wt.%). With the similar process, He et al.[97] integrated acid-intercalation exfoliated GNPs with PVDF to form nanocomposites. Their permittivity as high as 200 and 2700 could be achieved near the threshold(1.01 vol.%) at 1k and 100 Hz, respectively, which is 20 and 270 times higher than that of pure PVDF. Furthermore, under a higher GNPs loading content, the composites are potential to application of microwave absorber and electromagnetic interference shielding.[98-99]

Phonons propagate fast along the graphene planes but are slower to travel interlayer, leading to a highly anisotropic thermal property of graphite. GNPs possess a high thermal conductivity and are able to shear this advantage to polymer matrix, in order to form composites with improved thermal conductivity. Generally, the thermal conductivity of composite lies on not only the aspect ratio and loading content of GNPs, but also the interface and contact thermal resistance between filler and matrix. Particularly, it is reported that few-layer GNPs have similar aspect ratio to SWCNTs but a double increase in thermal conductivity when loaded in an epoxy-based composite.[100] With the development of miniaturizing electronics, the undesired heat energy dissipation between heat source and circuit board becomes a bothersome problem. Thus, thermal interface materials (TIMs) are born at the right moment and received intensive progress. Current TIMs consist of polymers or greases loaded with thermally conducting particles. The traditional fillers include silver, alumina or silica, which can obtain the required thermal conductivity only at very high loading content

(~70%).[101] Yu et al.[101] found that the GNPs with 4 layer offered a more than 3000% increase of thermal conductivity in comparison with neat epoxy, at the loading content as low as 25 vol.%. Similar enhancements of thermal conductivity of GNPs/polymer composites which aim to be more suitable for the TIMs applications have been widely investigated.[102-106] Besides the thermal conducting property, GNPs are usually used in amelioration of the thermal stability of polymer composites. Generally, thermal stability mainly involves physically thermal expansion and chemically thermal degradation/decomposition. For the former, the large 2D layer structure of GNPs can effectively restrain the thermal expansion of polymer molecules, making GNPs as an efficient dimensional stabilizer.[107-108] With regard to the letter, GNPs are able to act as an excellent flame retardant to delay the onset temperature of thermal degradation or decomposition. Especially, only 5 wt.% GNPs leaded to the increase of onset temperature of composites about 45 ^{o}C, 35 ^{o}C and 24 ^{o}C in comparison with pure PVA, PMMA and Nylon-6, respectively.[67, 109-110]

In general, thanks to their merits of 2D multi-layered construction, high aspect ratio, low cost and availability of mass-production, which strongly encourages GNPs to be the optimal substitution of graphene and employed as an useful filler in composites. In fact, most functional properties of composites are dependent on dispersion and the exfoliation degree of GNPs. In order to make a further progress in the improvement of overall performances of GNPs/polymer composites, the reasonable surface modifications and synergetic utilization of multiform carbon fillers could be the potential strategies.

1.3 Carbon nanotubes in polymer matrices

1.3.1 Processing methods

As mentioned in previous sections, CNTs exhibit dramatic intrinsic properties. Dispersing CNTs into various polymer matrices to form structural composites, which

benefits to make a great use of the advantage of two phases and further widen their applicable range. In fact, CNTs served as not only the effective reinforcing agent, but also the excellent functional filler, endowing composites with surprisingly improving performances. Generally, the ordinary polymers can be divided into mainly two types: thermosetting polymers and thermoplastic polymers. The former is a prepolymer material that can cure irreversibly induced by heat, chemical reaction or specific irradiation, such as majority of vulcanized rubbers and resins. In contrast, the latter can be processed and molded repeatedly above a specific temperature, such as majority of plastics: polyethylene (PE), polypropylene (PP), polystyrene (PS), polyvinyl chloride (PVC), PVDF, etc. Therefore, in order to obtain the better dispersion of CNTs in different polymer matrices, choosing an appropriate processing method is important.

1.3.1.1 Dispersing CNTs into thermosetting polymers

Due to the high specific surface area and Van der Waals interactions, the undesired stable bundles are easily formed by CNTs. These bundles are greatly difficult to be separated and dispersed uniformly in a polymer matrix. For thermosetting polymers, in order to keep CNTs from re-agglomerating during the curing process, sufficient energy should be provided to the dispersion of CNTs in the liquid prepolymer state. Several processing approaches can be applied to disperse CNTs, such as mechanical calendaring, ball milling, high speed stirring, and ultrasonication.

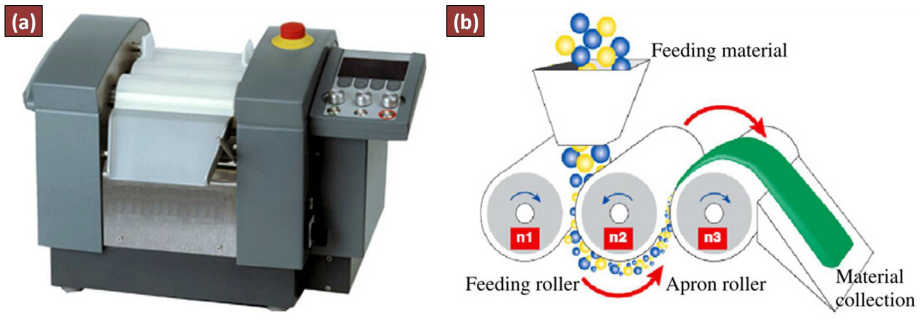

Fig.1-14 *(a) Commercial three roll mills machine and (b) its working mechanism[111]*

The calendaring mixing involves a two- or three-roll mill, where the series of rolls show a different rotating speed with a constant geometric progression and the opposing rotating directions between adjacent rolls. The narrow gaps between rollers can be adjusted from 500 to 5 μm (depends on the machine types), driving the separation of CNTs bundles and formation of homogenous dispersion with a relatively narrow size-distribution. This differential speed system is able to generate high shear force for well dispersing CNTs into the thermosetting polymers. Fig.1-14 demonstrates a commercial three-roll mill (a) and its schematic operating mechanism (b). Be different from the mechanical melt-mixing process, the calendaring mixing always carries out at or around room temperature. The gap width between rollers, rolling speed and mixing time are considered as three key factors to determine dispersing effect. Particularly, the sheer force applied to the pre-composites is positively dependent on the rolling speed, but inversely dependent on the nip width. Thostenson et al.[112] intensively investigated the influence of mixing degree of CNTs/epoxy controlled by nip width to final dispersion morphologically. The result showed that the improving dispersion with the decreasing nip width. In addition, the calendaring mixing process is preferably suitable for the liquid pre-polymer with a certain viscosity, especially, for the room temperature vulcanized silicone and epoxy resin.

In-situ polymerization is another efficient processing way to achieve relatively uniform dispersion of CNT in a thermosetting polymer. Mixing CNTs and monomers firstly with or without solvent, then with enhancing temperature and adding additives, composites are formed by polymerizing monomers at the presence of uniformly dispersed CNTs. Particularly, in situ polymerization is specific to fabricate composites with insoluble and thermally unstable polymers.[113] A number of composites loading CNTs were reported prepared through in situ polymerization, such as polymethyl methacrylate (PMMA)/SWCNTs composites,[114] CNT/Polyurethane(PU)

composites,[115] poly (2,5-benzoxazole)/MWCNTs composites with significantly improved dielectric permittivity,[116] polyimide (PI)/SWCNTs composites with 10-fold enhanced electrical conductivity,[117] the same system obtained a quite low percolation threshold (around 0.05 wt.%) and high piezoresistive stress coefficient of 1.52×10^{-3} MPa $^{-1}$,[118] etc. In situ polymerization with its distinct mixing process can significantly promote the interfacial interaction between CNTs fillers and polymer matrices, endowing composites with excellent functionalities. It is worthy to note that in situ polymerization is also useful to help certain thermoplastic polymers that are difficult to be dissolved and process in melt to form composites.

Solution mixing is another frequently-used approach for fabricating thermosetting polymer/CNTs composites. In this method, CNTs particles are dispersed and the pre-polymer matrix is dissolved in the specific solvent. The mixture mixed by mechanical stirring, magnetic agitation or sonication at room or appropriate temperature. For example, Lahiff et al.[119] prepared a elaborate structure through the solution mixing: a polydimethylsiloxane(PDMS) was spincoated on the top of CNTs forest that synthesized via CVD on patterned substrates, which could illustrate distinct functional performance. Because of solution mixing is more utilized for preparing thermoplastic-based composites, the detailed discussion will be made in next section.

1.3.1.2 Dispersing CNTs into thermoplastic polymers

A majority of thermoplastic polymers can be used as structural and engineering materials, thus, homogeneously dispersed CNTs can make a positive contribution to the expanded reinforcement effect and functional applications.

As mentioned before, CNTs can be dispersed in solvent as the form of colloidal suspension, which benefits to fabricate CNTs-loaded composites through in-situ polymerization and solution mixing process. In the way of solution mixing, the CNT/polymer composites is formed by evaporating the solvent, which could be the most effective way to fabricate composites films with an ultralow thickness in

comparison with other ordinary processing methods. Moreover, compared to melt mixing (will be introduced later), the solution processing should be a good alternative to prepare composites with high filler loading. The viscosity of the mixture can be tuned by adjusting the quantity of solvent. However, due to the strong intermolecular Van der Waals interactions as well, the way of simply stirring CNTs in a solvent is hard to obtain the desired dispersion. In order to ameliorate the condition, it is better to use the high power ultrasonic irradiation for cooperating, which is an effective tool in breaking CNTs aggregates and entanglements.[113] Utilizing this way, CNTs were widely reported being well dispersed in various thermoplastic polymers: PVA,[120] acrylonitrile butadiene styrene (ABS),[121] ultrahigh molecular weight polyethylene (UHMWPE),[122] PU,[123-124] and PS.[125] In addition, PVDF is a semi-crystalline thermoplastic polymer with the strong electronegativity structure, exhibiting a relatively high dielectric permittivity. PVDF served as potential energy storage material, can be completely dissolved in dimethylformamide(DMF) solvent. A plenty of PVDF/CNTs composites were fabricated through solution mixing process to obtain lower percolation threshold and higher dielectric performance.[126-128]

Although the solution mixing process exhibits plenty of aforementioned advantages, a large quantity of toxic solvents have to be used just for dissolving the polymer and dispersing fillers, such as toluene, chloroform, tetrahydrofurane (THF), DMF, etc. On one hand, these toxic and carcinogenic solvents would be totally discharged into external circumstance in the form of vapor, which is harmful to both body health and ecological environment. On the other hand, due to the large consumption of high cost chemical solvents, it is difficult for solution mixing to realizing mass-products in industrial in a short term.

Melt-mixing is a good answer to solve these problems, which is a practical and useful method for fabricating almost all the thermoplastic polymers, particularly, with advantages of simple, fast, massive production and high standardization degree. In the melt process, polymer matrices become soft, viscous and processable under a high temperature that over melting temperature (T_m). CNTs can be mechanically dispersed

into a polymer matrix using the twin screw extruders or compounders.[129] The high shear force during the melt-mixing process is capable of breaking the original CNTs aggregates and promoting a better dispersion. For example, Dang et al.[130-131] dispersing CNTs, carbon black (CB) and their mixture into thermoplastic polymer matrices, such as PVDF and UHMWPE to prepare the composites through the melt-mixing process using a Haake rheometer. The results showed the stable dispersion of nanofillers and the significant positive temperature co-efficient (PTC) effect. Zhang et al.[132] fabricated nylon-6 based composites loading 1 wt.% MWCNTs as reinforcing agent by the method of melt mixing using a Brabender twin-screw mixer, which exhibit a improved dispersion and mechanical properties. With the same processing method, Bocchini et al.[133] prepared a MWCNTs/linear low density polyethylene (LLDPE) composites, where the thermal and oxidative degradation of composites was delayed significantly ascribed to the homogeneous dispersion of CNTs. In our group, Yuan et al.[134] prepared the MWCNTs/PVDF nano-composites via melt-mixing using a twin-screw micro-compounder. The Raman result showed the interfacial interaction layer between PVDF and MWCNTs was formed, giving rise to a giant dielectric permittivity as high as 3800, while, the conductivity was maintained in low level. Besides the morphological methods, the XRD test can be also a useful tool to evaluate the CNTs dispersion in polymer matrices.[135]. In addition, a number of CNTs/thermoplastics composites were successfully fabricated using this method and studied intensively, such as polycarbonate (PC),[136-137] PMMA,[138-140] PI,[141] HDPE,[142] PP[143] and polyoxymethylene,[144] etc.

In summary, for both thermosetting and thermoplastic polymers, there are various processing methods can be selected in fabricating the CNTs filled nano-composites. However, every processing method likes a double-edge sword. It is important to choose an appropriate processing method with overall consideration of the polymer type and property, the desired functional property, environmental effect, time-consumption and cost. Due to the advantages of high repeatability, reliable processing capability and free contamination, two types of mechanical mixing process:

calendar mixing and melt mixing were selected to be utilized in our experiment.

1.3.2 Performances and applications

Appropriate mixing and molding process is able to disperse CNTs into various polymer matrices, providing composites infinitely splendid possible. CNTs must be proud of its large specific surface area and extraordinary intrinsic mechanical properties, which makes CNTs as the brilliant star in reinforcing polymer-based nanocomposites. Owing to high Van der Waals effect, a tight bonding and entanglement between matrix and CNTs can be formed. When adding load onto composites, the interface can provide a good interfacial load transfer from low-modulus matrix to high-modulus CNTs. Thus, CNTs/polymers with improved stiffness, strength, and toughness are potential to load-bearing applications.[145] For example, the epoxy resin showed 6% and 23% enhancement in stiffness and fracture toughness, respectively, by loading just 1 wt.% MWCNT, especially, without deteriorating other mechanical properties.[146] Generally, the improvement are dependent on CNTs diameter, aspect ratio, alignment, dispersion effect and interfacial interaction with matrix.[50] These CNT-reinforced composites are widely used in sporting accessories, such as tennis or badminton racket, golf club and bicycle frames. Moreover, their potential in the aerospace and aviation technology leads to the reduced weight and energy consumption, while enhanced strength.

With the feature of unusually high thermal conductivity, CNTs is considered as one of the best fillers to thermal conductive composites. The thermal conductivity of CNTs is dominated by atomic vibration or phonons.[147] Nanocomposites with high thermal conductivity are competent to be applied in thermal interface materials, heat sinks, print circuit boards, power electronics, electric motors and generators, heat exchangers, etc. Compared to the high enhancement of electrical conducting, due to the existence of high thermal resistance between CNTs, the thermal conductivity of composites shows only moderate enhancement.[147] Biercuk et al.[148] increased

successfully the thermal conductivity by 125% through loading 1 wt.% raw SWCNT into the epoxy matrix. When the SWCNT content increased to 3 wt.%, the enhancement of thermal conductivity was as high as 300% at room temperature.[149] In addition, because of MWCNTs is possible to modify the rheological property of composite via hindering the flux of degradation products, which is effective to delay the heat degradation of composites and be used as a flame-retardant additive to plastics. For example, Ge et al.[150] reported that with addition of 5 wt.% MWCNTs, the PAN-based composite exhibited a surprising 24 ^{o}C shift in onset decomposition temperature in comparison with pure PAN. Compared to ordinary halogenated flame retardant, the CNTs alternative with less harm to environment is greatly potential to be commercialized.[151]

As mentioned before, both SWCNTs and MWCNTs exhibit high electrical conductivities, making them provide composites with various electrical functionalities. Plenty of applications are being realizing for these conducting composites, such as electrostatic dissipating filters, conducting adhesives, electrostatic painting of mirror housings, electromagnetic interference (EMI) shielding, fuel lines printable circuit wiring, etc.[9] Especially, as the electrically conducting components in polymer composites is the first realized main application in commercial with regard to MWCNTs.[9] For example, composites with randomly distributed MWCNTs at 10 wt.% loading exhibited the electrical conductivity as high as 10^4 S m^{-1}.[152] According to the classic percolation theory, composites experience a transformation form insulation state to conducting state, when the conducting CNTs content beyond the percolation threshold. In order to augment electrical conductivity while maintain the flexibility of polymer matrix as far as possible, how to reduce the percolation threshold is the crucial issue for conducing composites. A number of investigations indicated that the percolation threshold of CNT loading composites were dependent on the aspect ratio, alignment, dispersion, modification of CNTs, matrix types, processing method, quenching, etc.[149, 153-157] When electromagnetic radiation travels in the conducting medium, its power and amplitude could be dumped significantly. In fact, a

large dielectric loss can be achieved under the filler content far beyond the percolation threshold, where the light-weight CNTs/polymer composites are the reasonable choice of EMI shielding materials.[158-159] Yang et al.[160] reported that their MWCNTs/PP composites showed a considerably higher shielding effectiveness than carbon nano-fibers counterpart. Furthermore, piezo-resistive (PR) materials allow applied pressure to be quantified through corresponding electrical resistance changes, have drawn great interests for their applications in many fields, such as finger sensing, artificial-skin and wearable electronic devices. CNTs with its 1-dimensional high aspect ratio structure were widely reported as functional fillers serving in the PR materials.[161-164] It is noteworthy that the piezo-resistive sensitivity is inversely dependent on the aspect ratio of CNTs.[165]

It is worth to note that there are a number of potential applications for composites with low content of CNTs which is insufficient to form the internal conducting network. Dielectric elastomer(DE) is one of the most representative applications, which can deform when stimulated by an electrical field are an attractive branch of electroactive polymers.[280] DEs can be potentially applied as emulational robots, haptic displays, and Braille devices, artificial muscles for orthotics and tunable optical lens.[166-169] Their actuation property is proportional to the dielectric permittivity, which increases substantially when CNTs content close to threshold, according to the classical percolation theory. Kim et al.[170] prepared the poly(styrene-b-ethybutylene-b-styrene)(SEBS)/SWCNTs nanocomposite films, which exhibits higher dielectric permittivity and actuation strain than SEBS/CB composites. Besides the loading component, CNTs also served as the electrode material in DE studies. Pei et al.[171-172] utilized SWCNTs as compliant electrodes of DE actuator, reducing the probability of terminal failure caused by defects significantly. Moreover, further combined SWCNTs with dielectric oil can achieve larger than 150% area strain of acrylic film and suppress the corona discharge. In addition, one of the promising applications of CNTs is to collect passively component diagnostic data and to provide signals that prevent and control component failures, which is an important

feature for future aircraft and spacecraft.[173-174] For the CNTs/polymer conducting composites, the deformation or damage evolution under loading can be monitored by their in situ electrical resistance change.[174-178]

1.3.3 Surface modification

As discussed before, CNTs employed as an effective reinforcing agent and excellent functional filler for polymer composites. However, on one hand, due to intrinsic strong Van der Waals interactions, CNTs usually exist as the form of bundles that are difficult to be dispersed and aligned in a polymer matrix. These CNT bundles give rise to not only the anisotropic properties but also the formation of hard spots in mechanical and electrical, which is fatal to the stability and service lifetime of composites. On the other hand, owing to the aromatic nature of the bond, the carbon atoms on CNTs walls are relatively stable, providing CNTs with the inert feature. Thus, their interaction with polymer matrix is mainly by the typical physical absorption, namely, Van der Waals interactions. Thus, the continuing efforts have been made to modify the surface properties of CNTs and adjust the interfacial conditions, in order to guarantee the proper dispersion and appropriate interfacial adhesion between CNTs and polymer matrix. These methods can be mainly divided into chemical functionalization, doping and interfacial modification in physical.

Chemical functionalization is the general approaches of attaching functional groups and molecules onto the carbon end or the sidewalls of CNTs covalently. The direct covalent functionalization at siderwall gives rise to a conversion from sp^2 to sp^3 hybridization and a simultaneous loss of π-conjugation system on graphene layer. Almost all the chemical functionalizations proceed on chemically reactive sites which originated from defects. Defect sites can exist in various forms, such as the open ends, holes in the sidewalls, pentagon, heptagon irregularities in the hexagon graphene framework.[111] The oxidizing method is the dominating way to create the defects on the CNTs, where several strong oxidants can be used as effective defects creator, such

as HNO_3, H_2SO_4, H_2O_2, $KMnO_4$, ozone and reactive plasma.[179-185] These created defective sites are able to attach covalently with the carbonoxylic acid or hydroxyl groups, making CNTs easily converted into other functional groups and highly reactive for further chemical reactions. The degree of functionalization is roughly dependent on the time and processing procedures during oxidation reaction and the oxidability of acid.[186-187] Besides the oxidation reactions, the fluorination and cycloaddition process have been employed for bonding fluorine atoms or other functional groups onto sidewalls of CNTs.[188] Particularly, the fluorine atoms can be successfully substituted by amino, alkyl and hydroxyl groups.[189-190] The chemically functionalized CNTs are rich in polar groups, leading to strong interfacial bonds with many polymer matrices, further endowing their composites with improved mechanical and functional properties. The relevant processes of chemical functionalization are summarized in the Fig.1-15.

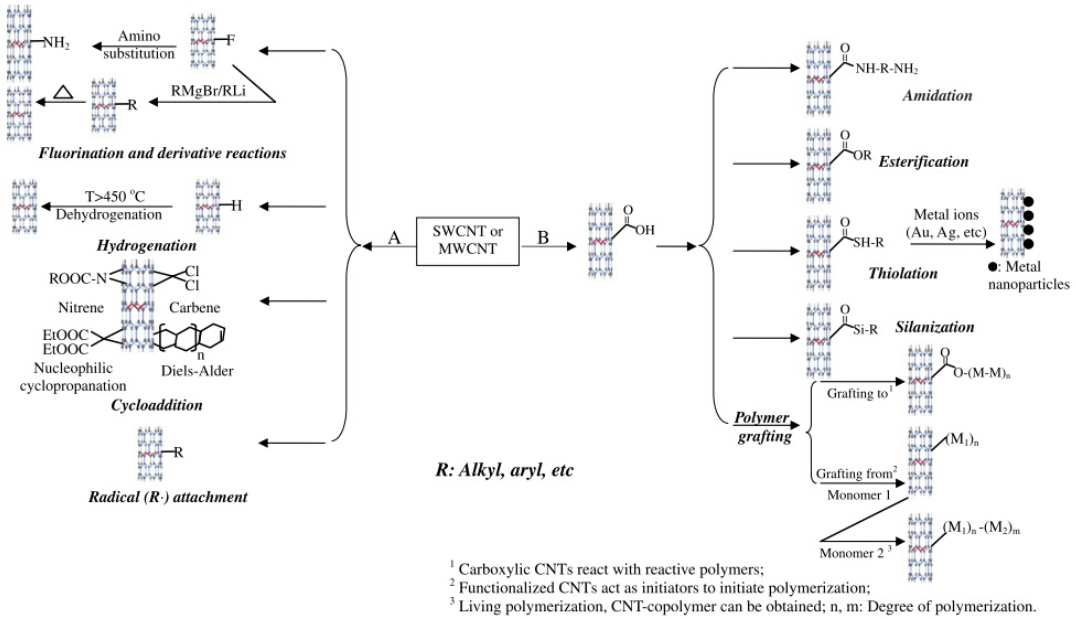

Fig.1-15 *Strategies for covalent functionalization of CNTs (A: direct sidewall functionalization; B:defect functionalization) [111]*

In order to further improve the interaction between functionalized CNTs and polymer molecules, "grafting to" and "grafting from" are the two main methods employed for processing CNTs/polymer composites. The former method involves

bonding as-prepared polymer molecules with reactive functional groups onto the functionalized CNTs via chemical reactions, which is limited by the relatively small grafting fraction and the depressed reactivity of polymer that result from steric hindrance.[191]While, the latter is based on the polymer is grafted to the CNTs surface via in-situ polymerization of monomers in presence of reactive functionalized CNTs and CNT supported initiators.[113] In this case, the grafting density can be significantly enhanced. Thus, pre-functionalizing CNTs is an effective way to promote the dispersing effect during in situ polymerization process. Hu et al.[192], fabricated PI-based composite loading the acyl group grafted MWCNTs via in situ polymerization, where CNTs can be uniformly dispersed in polymer matrix.

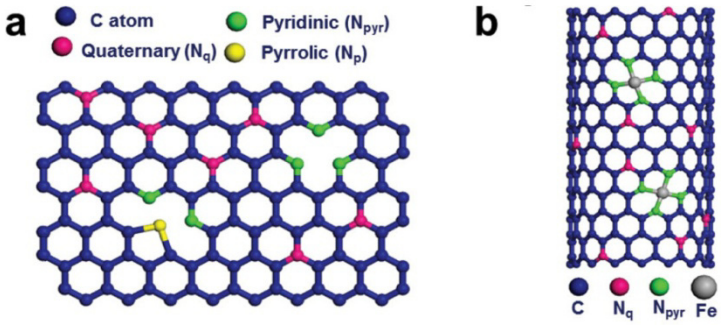

Fig.1-16 *N-doping of CNTs and graphene. (a) possible configurations of N-doping and (b) Fe-N4 complex hybridized CNT.[193]*

For precisely controlling the electronic structures and properties to meet the demand of various applications, substitutional doping of heteroatoms in the graphitic lattice has been considered as an efficient and robust approach.[193-195] In this method, the atomic scale structures, surface energy, chemical reactivity and mechanical properties of CNTs can be modified. Compared to the other elements with larger atomic size, boron(B) and nitrogen (N) which possess the small mismatch in atomic sizes are the most popular doping elements.[193] Fig.1-16 illustrates schematically the B-and N-doping of CNTs. During the doping process, there is a competition between C=C and C-heteroatom bonding, which is strongly dependent on the synthesis temperature. A moderate temperature is preferable to benefit the formation of C-heteroatom bonds.[196] Compared to the initial CNTs, dramatic

changes in structure can be exhibited in doped-CNTs, such as bamboo-like features, branching and knee-like bending can be obtained by N-, S- and B-doping, respectively.[197-199] Due to the high charge density and tunable surface charge state of heteroatom-doped CNTs, it has been proved with enhanced chemical reactivity.[200-201] For example, it is found that the N-doped sites can be utilized not only as initiator for polymer molecular chain growth, but also for direct deposition of various ceramics, metals and polymers at CNTs surfaces.[202-203] These core/shell nano-structures with particular polarization behaviors are highly potential for the high performance composites. In addition, beyond the limitation of several elements, recently, charge-transfer doping is a novel method for various kinds of dopants transfer charges to CNTs, for instance, gas molecules, organic/organometallic molecules, polymers, metals and metal oxides.[193] Kong et al.[204] studied the charge-transfer doping of SWCNTs by NO_2 and NH_3, applied for gas sensing successfully.

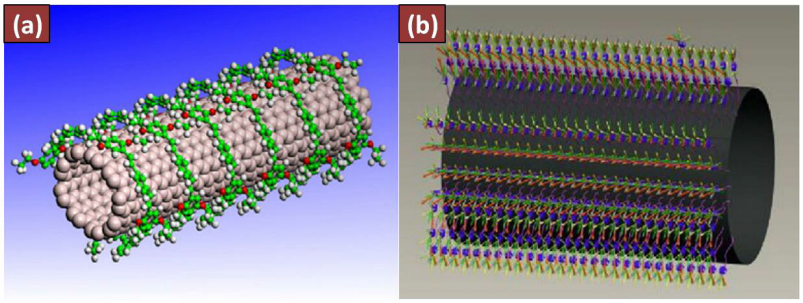

Fig.1-17 *Schematics of CNT functionalization using non-covalent methods. (a) polymer wrapping and (b) surfactant adsorption.[111]*

Physical functionalization is a non-covalent method for tuning the interfacial properties of CNTs, which can effectively improve the solubility and processability without sacrificing the physical properties of CNTs. Polymer wrapping process is one of the representatives. Through the Van der Waals interactions and π-π stacking between CNTs and polymer chains containing aromatic rings, polymer wrap around the CNTs to form supermolecular complexes of CNTs[111](see Fig.1-17a).

Surfactants play a important role in functionalizing CNTs. CNTs can be well dispersed in water in the presence of anionic, cationic and non-ionic surfactants(see Fig.1-17b) [111]. The interaction between the surfactants and CNTs can be influenced by the nature of the surfactants, such as the alkyl chain length, functional group size and charge.[111] Barrau et al.[205] ameliorated the dispersion of CNTs in an epoxy matrix by utilizing the amphiphilic palmitic acid as the surfactant. The hydrophobic part of palmitic acid is absorbed onto the CNTs, while the electrostatic repulsions between CNTs induced by hydrophilic groups play an important role in keeping them from aggregation.

1.3.4 Construction design- micro-nano hybrids structures

Functionalization of CNTs can effectively improve both the CNTs dispersion in polymer matrices and interaction between phases. However, aforementioned methods have undesired drawbacks as well. During the chemical functionalization reactions, CNTs are strongly possible to be fragmented into smaller pieces through the powerful ultrasonication process, which is fatal to the intrinsic mechanical properties of CNTs, and meanwhile induces the increased dielectric percolation threshold. In addition, both methods of chemical functionalization and heteroatom doping are usually accompanied by defect formation in graphic structures. The transformation of bonding hybridization from sp^2 to sp^3 leads to the oxygenated sites becoming local carrier-scattering site, reducing the carrier mobility and disrupting the π conjugation. Particularly, the π conjugation dominates the transport ability of electrons and phonons, which are responsible for the electrical and thermal conductions of CNTs, respectively.[111].The utilizations of concentrated acids or strong oxidants also result in the environmental pollution.

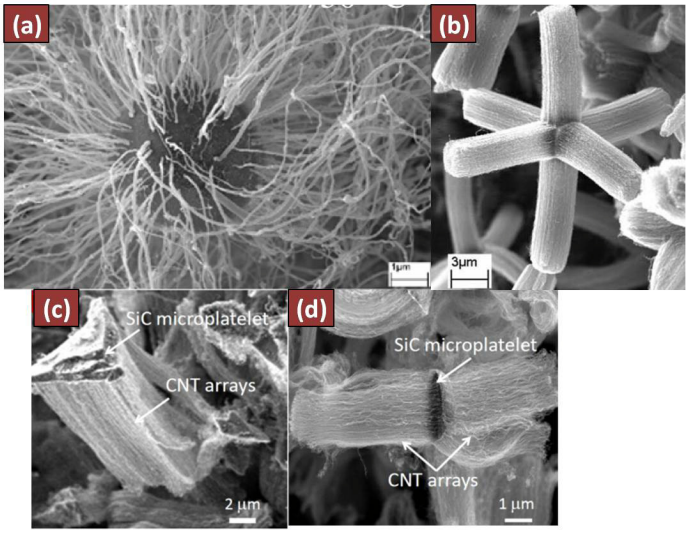

Fig.1-18 *SEM morphologies of (a) the urchin-like and (b) the six-branch structure of Al_2O_3- MWCNTs hybrid constructions. (c) "single-direction" and (d) "two-direction" SiC-CNT hybrid.[31, 206]*

Besides approaches of optimizing the surface composition of CNTs and the processing mode, very recently, the dispersion states of CNTs in matrix are capable of being ameliorated significantly by designing the CNTs construction reasonably. These specific constructions allowed CNTs arrays synthesized vertically on to the micro-scaled substrates, forming CNTs-based hybrid constructions. In our recent research, the well-organized micro-nano hybrid constructions obtained by synthesizing CNTs on semi-conducting substrates micro-SiC, micro-spherical Al_2O_3 through the floating catalyst CVD process.[31, 207-211] Fig.1-18 presents the morphological images of typical SiC-CNTs hybrids and Al_2O_3-CNTs hybrids constructions. Since the relationship among hybrids organization, experimental parameters during CVD synthesis and substrate types have been intensively investigated, these micro-nano hybrid constructions exhibited outstanding ability in improving the various functional properties of composites.

The aligned CNTs of the hybrids can improve the interfacial properties between substrates and the matrix, leading to a significant mechanical reinforcement to composites. Ci et al.[207] prepared a SiC-CNTs hybrids/epoxy composite with a 23.5% increase of Young's modulus in comparison with neat epoxy. Li et al.[212] compared

the mechanical performances of epoxy-based composites loading Al_2O_3-CNTs hybrids with different aspect ratio of grown CNTs. Although both the mechanical elastic modulus and tension strength of composite firstly increased then decreased with the enhancing aspect ratios, the tension modulus and strength increased by more than 8% and 14%, respectively, compared to neat epoxy. Besides the reinforcing effect in mechanical, micro-nano hybrid constructions also make positive contribution to the thermal property. Bozlar et al.[213] reported the Al_2O_3-CNTs hybrids/epoxy composites achieved a predicted thermal conductivity at the very low filler content, where aligned CNT arrays are able to effectively reduce the number of thermal contact resistances between CNTs.

Hybrid micro-architectures play a positive role in keep CNTs from forming aggregations. Thus, both interfacial area and polarization between fillers and matrices can be effectively enhanced, which benefits the reduction of dielectric percolation threshold. Yuan et al.[214] fabricated a SiC-CNTs hybrids/PVDF composite, where a large dielectric permittivity before percolation and a low real percolation threshold were obtained as more than 800 at 100Hz and 1.47 vol.%, respectively. Li et al.[211] found the PVDF-based composites loading “single-direction” SiC-CNTs hybrids possessed lower percolation threshold than loading “multi-direction” counterpart. As mentioned before, the application in in-situ sensing is a very useful field in aerospace field. However, CNTs hybrids with their particular construction are capable of forming the internal conducting network, in order to detect structural failures and give back the corresponding response. Li et al.[212, 215-216] studied the in situ sensing properties of epoxy and glass fabric reinforced epoxy-based composites with various micro-nano hybrids, which are strongly dependent on the CNT aspect ratio, substrate types and hybrid constructions.

1.4 The conductive network construction of composites

Setting the percolation threshold as the watershed, polymer-based composites

can be divided into two aspects of pre- and post-percolation. The former exhibits the insulating or semi-conducting feature, which is potential to applications of dielectric capacitors and energy storage. While owing to its formed electrically conducting network, the latter shows the typical behaviors of conductors and makes a great contribution to functional conducting composites. Because of the dielectric and electrical conductive performance of composites are the most important issues to be investigated in this thesis, it is deeply necessary to make a detailed theoretical background before studying them.

1.4.1 Pre-percolation: dielectric composites

1.4.1.1 Polarization and relaxation

Dielectric property is one of the most frequently investigated properties for composites in the pre-percolation region. Generally, the dielectric permittivity is a frequency-dependent complex physical quantity.

$$\varepsilon^*(\omega) = \varepsilon'(\omega) - j\varepsilon''(\omega) \tag{1-1}$$

where ω is angular frequency, the real $\varepsilon'(\omega)$ and imaginary part $\varepsilon''(\omega)$ is related to the dielectric permittivity and loss, respectively. $\varepsilon'(\omega)$ is usually denoted as ε_r which is responsible for evaluating the relative electrical energy storage of a material, in comparison with the permittivity in vaccum (ε_0 =8.854 pF·m^{-1}). The frequency-dependent heat energy dissipation induced by alternative electrical field are usually characterized by the loss tangent ($\tan\delta(\omega)$).

$$\tan\delta(\omega) = \varepsilon''(\omega)/\varepsilon'(\omega) \tag{1-2}$$

When an external electric field goes through a dielectric, internal charges are polarized to form an equivalent internal electrical field to resist and balance the external one. The process of separating positive/negative charges from the balance state and the forming the electric dipole moments is the so-called polarization. Typically, the polarization of dielectrics mainly includes electron polarization, ionic

polarization, dipole polarization and interfacial polymerization. These four dominant polarization forms are schematically demonstrated in Fig. 1-18.[217]

(a) Electron polarization As shown in Fig. 1-19a, for each neutral atom, the cores of the rounding electron cloud with negative charges and their central atomic nucleus that possessing positive charges coincide and without presenting the electric dipole moment. However, under the influence of external electrical field, electron cloud would deform and form a tiny electric dipole moment. This is the electron polarization, typically, which carries out in any materials and can be observed at ultrahigh frequency range (10^{14}-10^{16} Hz).

(b) Ionic polarization The ionic polarization generally exists in the ionic crystals such as NaBr, KCl and NaCl which composed of equal kations and anions. When adding the external electrical field to crystal, the kations and anions are able to move along the electrical field and break the initial chained-arrangement. Meantime, the electric dipole moment also changes from 0 to certain values (see Fig.1-19b) The ionic polarization usually takes place at high-frequency level around 10^{12} Hz.

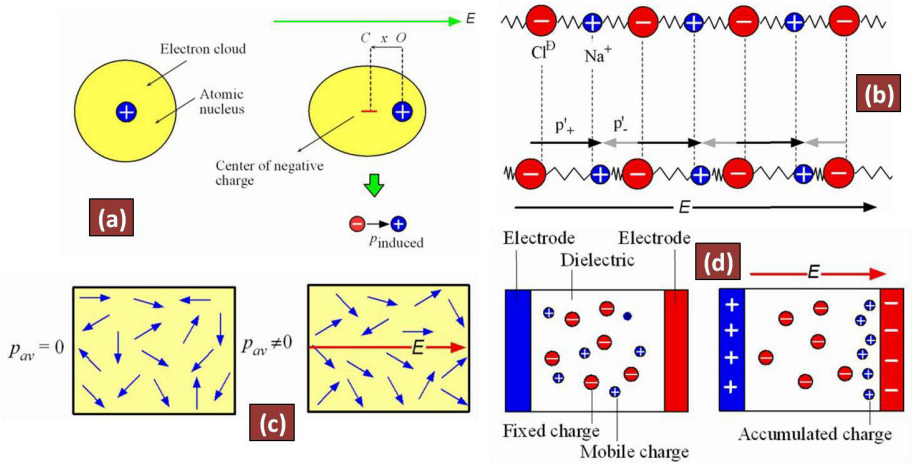

Fig.1-19 *Electrical mechanism of (a) electron, (b) ionic, (c) dipole and (d) interfacial polarization.[217]*

(c) Dipole polarization Some molecules possess the intrinsic permanent electric dipole such as HCl, which shows a randomly orientation induced by thermal excitation effect (see Fig.1-19c). However, when applying an external electric field, these permanent dipoles tend to arrange themselves and form dipole moments along

the direction of electric field. This polarization caused by dipole orientation occurs at the lower frequency range (~ 10^6 Hz) and presents stronger temperature-dependency in comparison with electron and ionic polarization.[218]

(d) Interfacial polarization Charges accumulate on the interfaces of heterogeneous materials or the different regions of homogenous material, leading to the interfacial polarization.[219-220] As shown in Fig.1-19d, more opposite charges will be attracted to electrodes by accumulated ones. Due to the permittivity is positively associated with the electric charge at a constant input electrical field, the increasing charges give rise to an enhancement of permittivity. It is worth to note that the interfacial polarization plays a dominating role in improve permittivity of polymer-based composites, the multi-phase heterogeneous materials. In fact, a majority of approaches of augmenting permittivity of composites are based on enhancing the interfacial polarization by adjusting interfacial structure or increasing interface, such as functionalizing surfaces of nanoparticles in chemical or physical, improving filler dispersion through various processing procedures, avoiding the CNTs aggregation by construction design, etc. In additional, it is inevitable to include various mobile charges such as electrons, holes, ion vacancies, which could make contributions to the interfacial polarization as well. This kind of polarization can be characterized at low frequency region, ranging from 10^{-2} to 10^2 Hz.

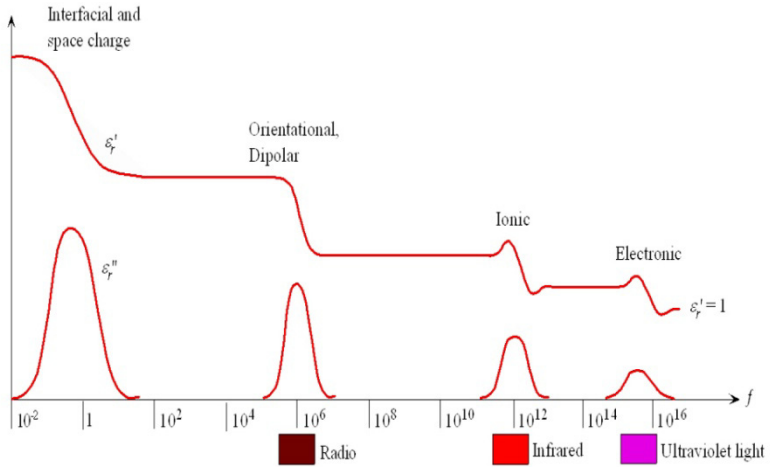

Fig.1-20 *The frequency dependence of imaginary and real parts of the dielectric permittivity.[217]*

The dielectric relaxation is the transformation process from one to another equilibrium state (polarized/non-polarized), where the relaxation time is an important parameter to determine the dielectric loss. Take the dipole polarization as an example, dipoles in dielectrics always keep adjusting their orientations with the alternating electric field. The dielectric relaxation can be inhibited by the thermal excitation and trop short relaxation time, where in both cases dipoles would orientate randomly rather than consistently following the electric field direction. Thus, the dielectric behavior of composite is dependent on not only the frequency of alternating electric field, but also the temperature, according to the thermal excitation and time-temperature equivalence. Fig.1-20 illustrates the frequency-dependent features of complex dielectric permittivity.

1.4.1.2 Theoretical models

A majority of materials consist of more than one component or phase, particularly, the multi-phased composites. In fact, due to a number of real effects need to be involved, it is very tough to achieve a precise calculation of permittivity of composites. Since the middle of last century, several dielectric models were discovered and then improved by more and more subsequent studies. Although these models can make a positive contribution to the prediction of permittivity of composites, they are still limited by the narrow applicable range.

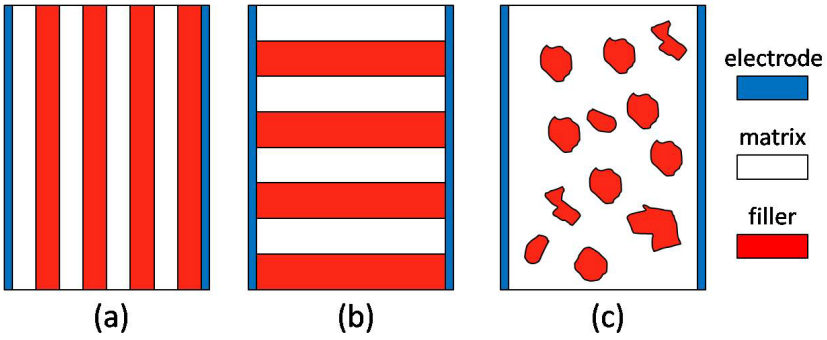

Fig.1-21 *Distribution of the two phases in heterogeneous composites.*

(a) The simple boundary model. For any two-phase composite, the lower and

upper bound of permittivity $\varepsilon_{c,min}$ and $\varepsilon_{c,max}$ are denoted by a series and parallel model, respectively.

$$\varepsilon_{c,\min} = \frac{\varepsilon_m \varepsilon_f}{\varepsilon_m \phi_f + \varepsilon_f \phi_m} \tag{1-3}$$

$$\varepsilon_{c,\max} = \varepsilon_m \phi_m + \varepsilon_f \phi_f \tag{1-4}$$

where ε_m, ε_f are the permittivity of matrix and loaded filler, respectively; ϕ_m and ϕ_f are the volume fraction of matrix and filler in composite, respectively. Typically, $\phi_m + \phi_f = 1$. In fact, Equ.1-3 and 1-4 provide two bounds for the dielectric permittivity ε_c of composites in any given physical system: $\varepsilon_{c,min} \leqslant \varepsilon_c \leqslant \varepsilon_{c,max}$. The mentioned mixing models with series and parallel are shown in Fig.1-21a and b. However, the real distribution of two phases is much more complex than these ideal models (see Fig.1-21c)

(b) Maxwell-Garnett model. When spherical fillers are distributed into a continuous matrix phase, the permittivity of composites can be calculated out via Maxwell-Garnett formula.[221-222]

$$\frac{\varepsilon_c - \varepsilon_m}{\varepsilon_c + 2\varepsilon_m} = \phi_f \frac{\varepsilon_f - \varepsilon_m}{\varepsilon_f + 2\varepsilon_m} \tag{1-5}$$

Maxwell-Garnett model is typically suitable for the spherical particles. However, in order to better estimate the permittivity of real composite, the model should be modified by considering the geometry of dispersed particles. Thus, the modified model with taking into a depolarization factor which concerns to the deviation from sphericity was developed.[223]

$$\varepsilon_c = \varepsilon_m \left[1 + \frac{\varepsilon_f \left(\varepsilon_f - \varepsilon_m \right)}{A\left(1 - \phi_f\right)\left(\varepsilon_f - \varepsilon_m\right) + \varepsilon_m} \right] \text{ for } \phi_f < 0.1 \tag{1-6}$$

Where A signify the depolarization.[224] Maxwell-Garnett model has widened its applicable range by giving up considering the resistivity of two phases. However, when the conducting fillers are loaded in composite with an increasing fraction, the significant transition from insulator to conductor gives rise to that the simulating results have relatively large deviation from the real values.

(c) Bruggeman model

Aforementioned transition of conducting state can be simulated by the Bruggeman effective-medium model.[225-227] When fill spherical particles into dielectric matrix, the permittivity of composite acts up to the following formulas.

$$\frac{\varepsilon_f - \varepsilon_c}{\varepsilon_c^{1/3}} = \frac{(1-\phi_f)(\varepsilon_f - \varepsilon_m)}{\varepsilon_m^{1/3}} \tag{1-7}$$

The Bruggeman model defines the spherical particles should possess a homogenous ambience. However, practically, those particles would contact to each other when the percolation takes place. The model cannot involve the interaction of inter-particles, thus, can only be used at the loading content below the threshold. With consideration of the interaction of particles, the Bruggeman model can be modified into Jaysundere-Smith equation:

$$\varepsilon = \phi_f \frac{\varepsilon_f \phi_f - \varepsilon_m \phi_m [3\varepsilon_f / (\varepsilon_m + 2\varepsilon_f)] \times [1 + 3\phi_m (\varepsilon_m - \varepsilon_f)/(\varepsilon_m + 2\varepsilon_f)]}{\phi_f + \phi_m [3\varepsilon_f / (\varepsilon_m + 2\varepsilon_f)] \times [1 + 3\phi_m (\varepsilon_m - \varepsilon_f)/(\varepsilon_m + 2\varepsilon_f)]} \tag{1-8}$$

This equation served in estimating the permittivity of composites filled with a small quantity of spherical conducting particles.

(d) Lichtenecker rule

In distinctively, Lichtenecker rule is an empirical equation deduced from experimental results directly.

$$\varepsilon_c^n = \phi_m \varepsilon_m^n + \phi_f \varepsilon_f^n \tag{1-9}$$

where the parameter *n* obtained from the experiments, which varies from -1 to 1. Each value of *n* corresponds to a micro-structure of composite. Particularly, n equals to -1 and 1, the extreme value, corresponding to the mentioned series and parallel model, respectively. Although it is not very clear about the applicable range of this model even nowadays, it is suitable for fitting permittivity of various heterogeneous materials. It is maybe explanted by the compromise of series and parallel extreme conditions.

1.4.1.3 Maxwell-Wagner-Sillars effect and Micro-capacitor model

When loading conducting particles into insulating polymer matrix, the permittivity of composites shows a giant enhancement. This enhancement usually takes place at the filler-loading content closed to percolation threshold. Recently, the Maxwell-Wagner-Sillars effect and micro-capacitor model have been considered as two reasonable models to provide explanation to the enhancement.

According to Maxwell electromagnetic field theory, when a current flows through the interface between two dielectric materials with different relaxation times τ (τ is the ratio of the permittivity ε and the conductivity σ), electric charge q_s can be accumulated at this interface.[228] This is the Maxwell-Wagner-Sillars effect. Due to the relaxation time of polymer is about several orders of magnitude longer than conducting carbon nano-particles, charges can easily accumulated at the interface of insulating and conducting phase, giving rise to an improved interfacial polarization and dielectric permittivity. Dang et al.[127] prepared a trifluorophenyl(TFP)-funtionalized MWCNTs/PVDF composite, displaying a giant dielectric permittivity as high as 8000 at 100 Hz. Due to the strong interaction between TFP-MWCNTs and PVDF matrix by F groups enriched in the interface, the nomadic charges were blocked at internal interface. Both the large π-orbital of MWCNTs that endows large domains with nomadic electrons and F groups with strong electronegativity plays an important role in reinforcing the Maxwell-Wagner-Sillars effect. Similar reinforcing effect can be also found in Yuan's work.[134]

It is known that conducing particles with the loading content near threshold are isolated by thin dielectric polymer layers to form a heterogeneous percolative system, which could provide a dielectric with outstanding features of energy storage.[229] It can be explained by employing the microcapacitor model: each adjacent conducting particles are served as a local micro-capacitor, where the fillers are considered as two electrodes and the very thin polymer matrix layer in between as the dielectric. With the increasing content and aspect ratio of conducting fillers, the interajacent dielectric layers become thinner and thinner. Thus, each microcapacitor contributes a dramatic

large capacitance. Each filler is not confined to be applied as the electrode of only one micro-capacitor, while, countless conducing fillers as the shearing electrodes forms a network of local capacitors. This capacitor-network is responsible for the achieved giant permittivity and intensity of local electric field when conducting fillers are extremely close to each other near threshold. The improved intensity of the local electric field drives the migration and accumulation of the charge carriers in interfaces, promoting the Maxwell-Wagner-Sillars effect and further improving the permittivity of composites.[230] Simoes et al.[231] developed the capacitor model numerically, which was able to well explain the anomalous decrease of permittivity above the percolation threshold by the formation and destruction of micro-capacitor networks. Both 1D CNTs and 2D disk-shaped GNPs with high aspect ratio are promising electrodes for separating polymer matrix into a great number of thin layers as dielectrics, leading to a micro-capacitor network.[134, 232] Thus, it is worth to note that the dielectric permittivity is strongly dependent on the dispersion and distribution of conducting particles, giving rise to the considerable variations of electrical properties.

1.4.1.4 Challenges

Dielectric material is the promising candidate for energy conversion and storage systems. Compared with traditional batteries, capacitors that based on dielectrics have much higher charge/discharge speed, but cannot hold much energy. The energy density (U_e) of a dielectric material is related to its dielectric permittivity (ε_r) and the applied electrical field (E).

$$U_e = \frac{1}{2}\varepsilon_r \varepsilon_0 E^2 \tag{1-10}$$

Therefore, to improve the energy density of a dielectric capacitor, it is reasonable to increase the dielectric permittivity and dielectric strength (the minimum electric field responsible for the dielectric breakdown) simultaneously. Ceramics with high permittivity play effective roles in increasing permittivity of composites. However,

the effective increase can only take place under high loading content, where the weak interfacial interaction and undesired pores make the flexibility and continuity of composite, the distinctive superiority of polymer matrix, deteriorated quickly. In terms of conducting particles filled composites, conducting network formed at the percolation threshold, where the high leakage current is capable of running through the materials, leading to a dielectric breakdown. Due to the dielectric breakdown is irreversibly fatal to performance and applicability, to improve dielectric strength of percolative nanocomposites is the key challenges in long term.

1.4.2 Percolation behavior

1.4.2.1 Principle and theoretical models

Percolation theory was firstly proposed as a mathematic issue, aiming at the study of influences caused by the variation of interconnecting degree of each component in a huge and disordered system.[233] It was then employed to explain various physical phenomena, due to its distinctive characteristic of making a connection between micro-structures and macro-properties of heterogenous materials.

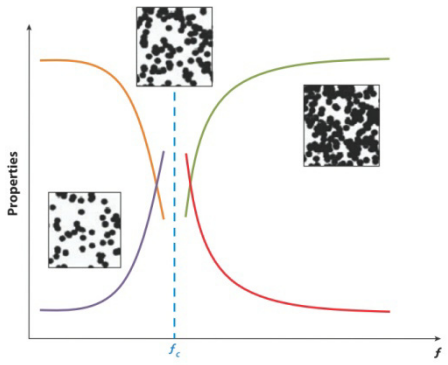

Fig.1-22 *Schematic of nonlinear changes in the properties of composites neat the percolation threshold. The insets demonstrate the geometric phase transistion of conducting fillers.[233]*

With regard to the dielectric percolation, as shown in Fig.1-22, at low filler

loading concentration, conducting particles are separated from each other by the insulating polymer matrix which dominates the electrical properties of composites. With the increasing loading content, adjacent particles form into local clusters. Ever-increasing clusters connect to each other and construct a 3D conducing network at a critical filler loading, leading to a dramatic enhancement of electrical conductivity and the transformation from insulator to conductor. Particularly, this critical loading is the percolation threshold f_c, which is allowed to be estimated theoretically by the classical percolation power laws.[126, 233]

(1) For the conducting filler content (f_{filler}) is close to but below f_c, the conductivity of composite (σ_c) follows the law:

$$\sigma_c \propto \left(f_c - f_{filler}\right)^{-s} \tag{1-11}$$

Where s is critical exponent which depends on the dimension of fillers, for example, s = 1.1-1.3 or 0.7-1.0 for fillers with 2D or 3D constructions, respectively.

(2) For the condition of $f_{filler} > f_c$, the conductive fillers construct a continuous percolating path throughout the polymer matrix. σ_c of composite is determined by the following equation:

$$\sigma_c \propto \left(f_{filler} - f_c\right)^{t} \tag{1-12}$$

Where the critical exponent t is also related to the dimension of fillers, t =1.1-1.3 for 2D fillers; t=1.6-2.0 for 3D fillers.

(3) For the extreme condition, the filler loading is very close to f_c, namely, $|f_{filler} - f_c| \rightarrow 0$, σ_c of composite is described as:

$$\sigma \propto \omega^{u} \tag{1-13}$$

Where $\omega = 2\pi\nu$, ν is the frequency, $u = t / (s+t)$ is the corresponding critical exponent.

In similar, not only the σ_c increases over several orders of magnitudes, but the permittivity exhibits a giant enhancement at the percolation threshold, which diverges as follows.

$$\varepsilon_c' \propto \left(f_c - f_{filler}\right)^{-s'} \quad \text{for } f_{filler} < f_c \tag{1-13}$$

Where s' is a critical exponent of approximately 1. Notably, this is not always

observed in practical continuous systems.[126]

1.4.2.2 Influential factors to percolation threshold

The percolation threshold of a composite is significantly influenced by the dispersion, aspect ratio, shape and interface condition of conducting fillers. The dispersion and distribution of conducting fillers within the polymer matrix served determinate role in influencing the f_c. Take CNTs as an example, inferior dispersion and distribution can be achieved by insufficient or unreasonable mixing process. The entangled CNTs bundles or locally concentrated CNTs aggregations are highly possible to form a local conducting path, leading to the unauthentic f_c and dielectric strength. In addition, the f_c of same composite can be verified by different mixing process, molding method, and with or without post-treatment. Yuan et al.[134] fabricated a CNTs/PVDF composite through melt-mixing with f_c of ~10 vol.% which is much higher than that of composites prepared by solution mixing. It is explained by that the high temperature and shear force break CNTs into smaller tubes in some ways, giving rise to a higher f_c. For a multi-phase (more than two phases) composite filled with spherical conducting fillers, its f_c is determined by the ration between the particle size of the major and minor phase. For instance, a very low f_c of 0.095 was obtained from the Ni/ferrite/polymer composite, which resulted from the small Ni particles were forced into the gaps between larger ferrite particles.[ncw10R8]

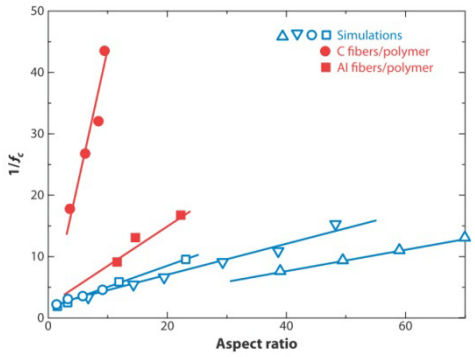

Fig.1-23 *Dependence of the percolation threshold on the aspect ratio of the fillers in composistes filled with randomly oriented fibers.[233]*

Compared to spherical particles, ellipsoidal fillers can reduce the f_c of composite into a low level, because the ellipsoidal fillers form an interconnection more easily. The aspect ratio of filler is another dominating factor in determining f_c. As shown in Fig.1-23, plenty of simulating and experimental results have proven that the f_c reduces with the increasing aspect ratio.[234-235] No matter CNTs with high aspect ratio in axial or GNP and graphene with high aspect ratio in radial, which can provide their composites a sharp change in conductivity and permittivity at very low f_c.[157, 236] Furthermore, due to the size effect, the f_c reduction is related to the difference of nanotubes length, implying that the f_c can be effectively reduced by adding a small quantity of longer CNTs. In fact, the hybrid nanofiller system with two or three different aspect ratios leads to better properties of composites, especially, the electrical properties. Thanks to this synergetic effect, the hybrid conducting filler of CNTs and GNPs filled composites exhibited a dramatically enhanced electric conductivity at low loading levels in comparison with GNPs or CNTs singly filled composite.[237-238] Fig.1-24 presents the synergetic effect of CB, GNP and CNT three-phase filler system.[239]

When the spheroid filler particles are oriented under electric field or polarization, which is able to form the anisotropic microstructure of composite. In this case, the different f_c observed along the direction parallel or perpendicular to the filler. For example, CNTs that aligned in the in-plane direction were loaded into a polymer matrix, the difference of f_c along the two orthogonal plane could reach to one order of magnitude.[233]

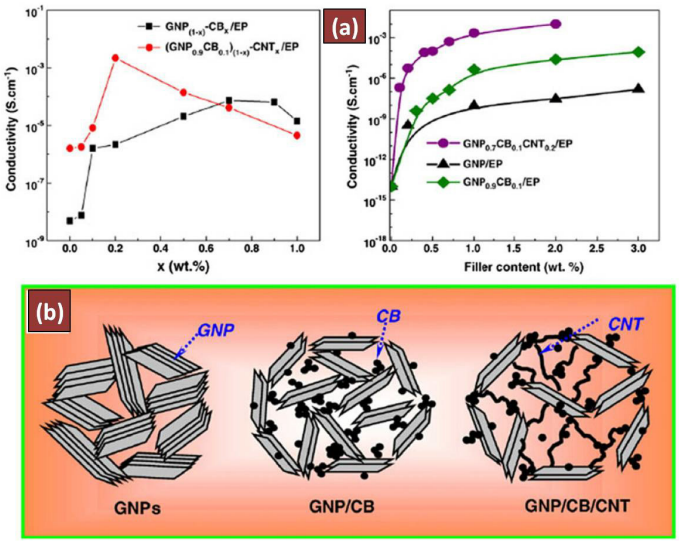

Fig.1-24 *(a) The electrical conductivity of multi-formed conducting particles filled composites. (b) Schematic illustration of the synergetic effect of GNPs, CB and CNTs.*

In addition, the f_c of composite is determined by not only characteristics of fillers, but also the features of polymer matrix such as viscosity, polarity and degree of polarization, and the interfacial interaction between fillers and matrix. Generally, the influence of matrix features to f_c concentrates on that matrix hinders the uniform distribution of fillers, which results in a higher f_c. This problem can be ameliorated by utilizing immiscible multi-phase polymer matrices to some extents.[233] Moreover, several strategies have been used for tuning the interface between filler and matrix, such as chemical surface functionalization and core-shell constructions. The electrical conductivities of fillers and the contact rate between adjacent fillers can be adjusted by controlling the composition and thickness of these additional intermediate layers. Thus, with aims of suppressing the dielectric loss, improving the dielectric strength and widening the compositional window, these strategies are promising way to tune f_c of composite.[230]

1.4.3 Post-percolation: conducting composites

1.4.3.1 Ohmic contact and Tunneling theory

The percolation means the internal conducting network has been constructed. However, what kind of interaction that between conducing particles plays a dominating role in inducing the formation of network, how the leakage current is generated and transferred, which will be introduced in following part.

Ohmic contact is one of the most common interconnecting methods, where conducting particles contact to each other directly through overlapping. For instance, both the electrical interconnection between single CNTs of CNTs bundle and interlayer interconnection of GNPs can be considered as the ohmic contact in electrical. Although the individual CNT has the electrical conductivity as high as in the order of 10^4-10^7 $S \cdot m^{-1}$, the ohmic contact resistances between CNTs cannot be ignored.[240] In particular, the ohmic contact resistance between crossed metal/metal-type or semiconducting/semiconducting- type SWCNTs was measured as 100-400 kΩ, which is close to the theoretical level varied from 100kΩ to 3.4MΩ.[241-242] When conducting fillers are dispersed into a polymer matrix, the ohmic contact would also take place in composites. On one hand, in the local aggregation of conducting fillers caused by inhomogeneous dispersion. On the other hand, the probability of ohmic contact is positively related to the filler loading content when beyond f_c.

In comparison with the ohmic contact, the inter-particle tunneling effect is preferably considered as the dominant mechanism of interconnecting conducting fillers to form the conducting network. It is worth to note that the tunneling effect make a connections between particles in electrical rather than geometrical. When conducting fillers are dispersed in a matrix, they can be separated by the thin and insulating matrix layers. According to the micro-capacitor model, a large local electric field generated between two conducing fillers. If the intermediate layer with a very low thickness cannot withstand the ever-increasing local electric field, a short circuit occurs and induces large leakage current, which is the tunneling effect.[243-244] In

fact, there is a competition between Coulomb blockade and tunneling between neighboring conducting particles. According to the tunneling model, the inter-particle tunneling conductivity (σ_{tun}) can be described as:[245]

$$\sigma_{tun} \propto \exp\left(-\frac{l-2b}{d}\right) \tag{1-14}$$

Where l is the centre to centre spacing of the particles, b and d are the radius of the particles and the typical tunneling range, respectively. For the CNTs/polymer composite, the maximum tunneling distance is calculated about 1.8nm.[240] In fact, the (l-$2b$) represents the real distance between the edges of particles, which is determined by the filler loading content. The conductivity of composite increases exponentially, due to the sharply decreased value of (l-$2b$) nearby the percolation threshold. With further increasing filler loading leads to the $l \rightarrow 2b$, the intermediate insulating matrix layer becomes ultra-thin, not only plenty of tunneling current but more and more quasi-ohmic contacts occurs, where a stable conducting network is established. Simmons et al.[246] also gave an approximate estimation of the tunneling resistance (R_{tun}) between two neighboring CNTs:

$$R_{tun} = \frac{V}{AJ} = \frac{h^2 d}{Ae^2\sqrt{2m\lambda}} \exp\left(\frac{4\pi d}{h}\sqrt{2m\lambda}\right) \tag{1-15}$$

Where V is the electrical potential difference, J the tunneling current density, e the quantum of electricity, m the mass of electron, h the Planck's constant, d the distance between CNTs, λ the height of barrier, and A the cross-sectional area of tunnel. According to this estimation, Hu et al. [huning08] simulated and achieved a negative correlation between tunneling conductivity and distance between CNTs under different λ values (see Fig.1-25).

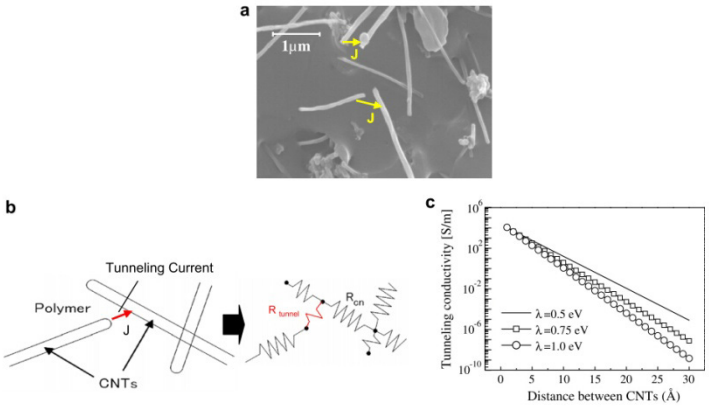

Fig.1-25 *Modeling of tunneling effect in the resistor network.[247]*

In addition, the tunneling between only closest adjacent particles is taken into account, which could be responsible for the nonuniversality of critical exponents of percolation power laws.[248] For example, some abnormally large t of 5~10 have been reported in percolative composites.[233, 249]

1.4.3.2 Piezo-resistive behaviors

At the critical loading content that region beyond the threshold and before the stable conducting network established, composites exhibit the fantastic piezo-resistive feature. The PR behavior is an important functional property of composites and greatly potential to numerious intresting applications. In fact, the PR effect is a competition between destruction and constuction of internal conducting network under the additional pressure. The formed internal conductive network reconstructs itself synchronizedly with external applied pressure, showing a measurable electric resistance deviation. According to the classical tenneling theory, Zhang et al.[250] calculated the total electrical resistance R of composite as follow:

$$R = R_{tun}\left(\frac{L}{N}\right) \tag{1-16}$$

Where L and N is the number if particles forming a single conducting path and the number of conductive paths, respectively. Integrating the eqn.1-14 and eqn.1-15, R of

composite changes exponentially with the inter-particle spacing. However, the spacing can be adjusted by not only the filler loading contet, but also the applied deformation. Particularly, the external pressure and deformation are able to orientate the conductive particles along a certain direction and vary the inter-particle distance, leading to the corresponding resistance changes and a difference of resistance changing types in various directions (see Fig.1-26[154, 251-252]). According to the same or reverse response of the resistance of composite with the increasing external pressure, the PR behavior can be devided into two main types: positive PR behavior and negative PR behavior. The PR bahavior is dependent on the applying type of external pressure and the shape of conductive particles. Generally, uniaxial tension leads to a typical positive PR behavior, while applying uniaxial compression to composite filled conductive particles with low aspect ratio (such as low structure CB and metallic powder) or high aspect ratio (such as high structure CB, CNTs, GNPs and graphene) gives rise to the typical negative or positive PR behavor, respectively.[165, 253]

Sensitivity, coherency and repeatability are main three factors to evaluate the PR behavior of a composite. Firstly, high PR sensitivity requires composites to exhibit a large resistance change when responded to a small pressure stimulis, which is the substantial functional property of PR composites. In recent decades, with the ever-improving PR sensitivity, PR composites are potential to be applied into ultra-precise sensing system. According to the influence form of applied external loading, the sensitivity of PR composites can be evaluated effectively by the gauge factor (GF) and pressure sensitivity (PS), respectively, which is typically applied in the strain or pressure sensors. It is generally confirmed that the PR sensitivity of composites attains the maximal value at the filler content beyond and just over the threshold, due to the just established unstable internal conducting network. In this case, a small pressure may not influence the inter-particle distance of micro-capacitor structures but is sufficient to induce a relatively significant impact to the total conducting network, leading to a obvious PR properties. Be contrary to the effect of conducting filler

aspect ratio to percolation shreshold, composites with lower aspect ratio of conducing filler that more easily orientate along applied loads show higher PR sensitivities. In addition, the threshold value and flexibility of polymer matrix also play important roles in determining the PR sensitivities. Composites become no more soft under high conducting filler loadings. The strong strenthening effect originated from nanoparticles significantly enhances the elastic modulus and make composites hard to deform and realize PR property under external loading.

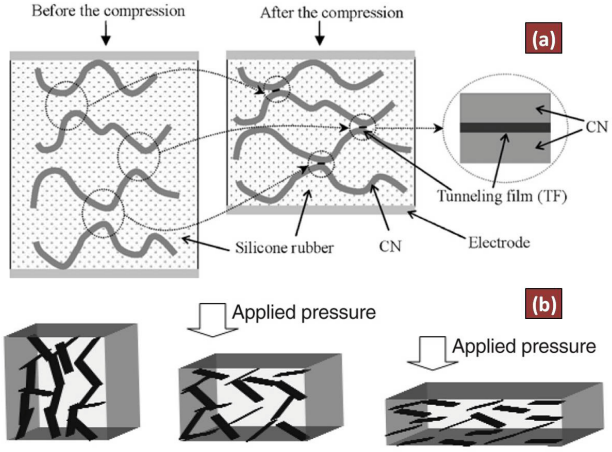

Fig.1-26 *Schematic models for the change of internal conducting network of composites consist of (a) CNTs and (b) GNPs.[94, 252]*

Good coherency means composites have a relatively short relaxation time, the change of electrical resistance can well match the varying applied loading. In fact, due to the intrinsic viscoelastic feature of polymers, the delay between deformation and electric resistance change is inevitable, which is influenced by testing temperature, loading-unloading frequency, degree of crosslinking, etc. In order to achieve a better coherency as far as possible, it is neccessary for composites to have good interadhesion between filler and matrix and an excellent elasticity. Moreover, the PR tests taken at the Hooke region show better coherency in comparison with that at plastic region. The repeatability is a dominanting property served to evaluate the stability, life-time and applicability of PR composites. Owing to the viscoelastic characteristic of macromolecular, both the stress relaxation and sweeping effect probably lead to a reduction of electric resistance changing amptitude and PR

sensitivity after a long-tern operation. Furthermore, the continous loading-unloading cycles are able to modify permanently the structure of the conductive networks, resulting in a irreversible impact to PR sensitivity.

In addition, designing a PR device properly also benefits to improve the integrated sensitivity as high as possible. Pang et al.[254] proposed an amazaing ultraflexible device composed of linterlocking pillars for detecting multiple stimuli such as compression, shear and torsion forces (see Fig.1-27). Although the device is conceptual now, the surprising strategy is suffient to provide a broader space for the develepment of PR composites.

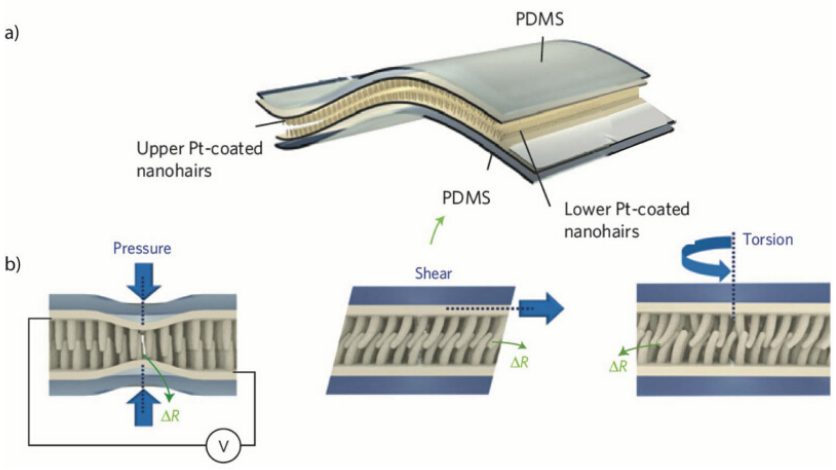

Fig.1-27 *Conceptual images of the device composed of interlocking pillars used for detecting multiple stimuli.[254]*

1.4.3.3 Applications and Perspectives

Due to the typical mechanical-electrical response, PR composites are promising candidates for various sensors. According to the flexibility of host polymer, PR composites are potential to apply in “hard” or “soft” sensor. For the former, PR composites consist of conducting particles and a hard polymer matrix, such as epoxy and thermoplastics. These functional composites with high elastic modulus have been widely used in the in-situ fractures sensing in aerospace field, which has been introduced in detail in section 1.3.2. For the latter, the host polymers of composite are mainly flexible elastomers, including traditional rubbers, silicone rubber and

flexibility-controlled PU, etc. With merits of high flexibility, sensitivity and relatively wide operating temperature range, elastomers-based PR composites have drawn great interests for their applications in many fields, such as artificial-skin, finger sensing and wearable electronic devices.[255-256].

For the “soft” PR composites, their PR properties are strongly influenced by the intrinsic features of polymer matrix and conducting particles. Firstly, in order to apply to the artificial skin, the polymer matrix should be provided with the characteristic of human skin: mechanically compliant and stretchable. In recent years, PDMS with its advantages of chemical inertness, temperature-insensitivity over a wide range, biocompatibility, transparency and tunable mechanical properties has overwhelmingly been applied as the polymer matrix or substrates for the fabrication of PR composites.[257] Moreover, the aspect ratio of conducting particles can not only determine the type of PR behavior as mentioned before, but also be responsible for the final PR properties of composites. In fact, nanoparticles endow polymer with both the electrical functionality and the mechanical strengthening. A composite filled by high aspect ratio fillers exhibits a lower percolation threshold and more flexible mechanical property, but its internal conductive network is not easy to orientate and deform under external loads. However, the counterpart with low aspect ratio also leads to an awkward dilemma between the ability of high orientation and deformation of conductive network and reinforced mechanical property. Thus, how to choose the reasonable filler which is capable of making a balance among various properties of composite such as high PR sensitivity, low percolation threshold and moderate mechanical strengthening is still a challenge.

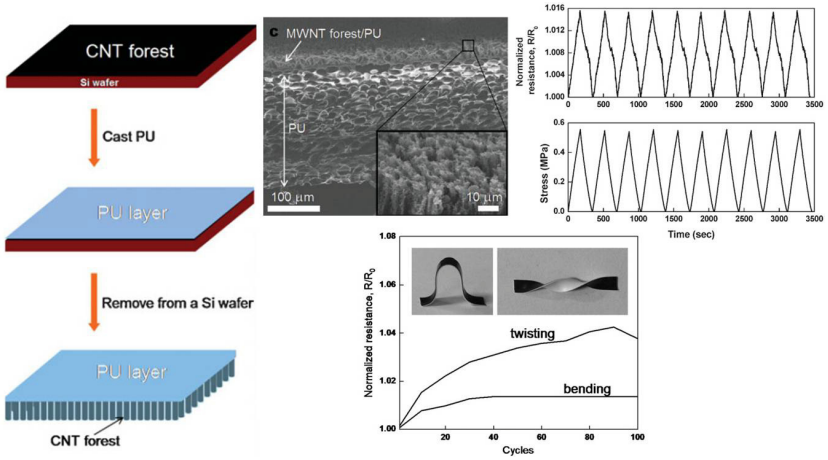

Fig.1-28 *Schematic diagram of the preparation of CNT forest/PU composite sheet and its piezoresistive properties under multiple deformation.[258]*

A number of CNTs filled PR composites have been introduced before. The CNTs networks offer a relatively uniform performance and are compatible with conventional lithography and printing techniques.[259] However, the general problem of CNTs dispersion is adverse to the improvement of PR property as well. Chemical functionalization is an effective approach to separate aggregations and ameliorate dispersion of CNTs. Be distinct from dielectric property, the PR performance of composite could suffer negative influences through this method, due to the restraining effect to tunneling current and intrinsic electrical conductivity by additional functional groups at the interface. To overcome these problems, reasonable design of CNTs construction and conductive network is a promising approach to optimize PR property of composites. Kim et al.[258] prepared the highly elastic and electrically conducting composite sheets through infiltration of MWCNTs forests with PU binder, which exhibited the repeatable PR property under deformation strain up to 40%(see Fig.1-28). The CNTs construction controlling is also one of the core points of this thesis and will be discussed detailedly in Chapter III.

1.5 Conclusions

This chapter provides a general review on the structure, synthesis and properties of CNTs and GNPs, and their applications in polymer-based composites, particularly the utilization in dielectric and piezoresistive composites. CNTs and GNPs with their distinct structure and intrinsic properties endow polymer matrices with a number of amazing functional properties. Nevertheless, there is a large elevating space for the development of these carbon-filled composites.

Due to the typical sp^2 hybrids structure, CNTs have an excellent intrinsic electrical conductivity. When loading CNTs into polymer matrices, the formed nanocomposites that integrating the advantages of both CNTs and polymers have greatly improved electrical properties, particularly, their applications are strongly expended in comparison with CNTs. However, due to the nano-scale size and high aspect ratio, CNTs are easily frizzy and form aggregations when mixed into host polymer, which is a long-standing challenge since the first day of development of CNTs/polymer composites. The dispersion and distribution of CNTs are able to be improved to some extent by choosing an appropriate mixing process. The strategy of traditional mixing processes cooperated with ultrasonication technology leads to a better dispersion. However, the processing modes are tightly dependent on intrinsic features of polymer matrices, and a majority of them cannot be scaled into mass-production. Chemical functionalization to CNTs is considered as another approach to ameliorate the dispersion state, which modifies the interfacial structure and interaction between filler and matrix. The additional interface plays a complex role in influencing the electrical property of composites, such as improve interfacial polarization. However, definitely, the electrical conduction between CNTs is inevitably weakened by this way.

In recent, the dispersion of CNTs is capable of being ameliorated effectively by designing the CNTs construction reasonably. These specific constructions allowed CNTs arrays synthesized vertically on to the micro-scaled substrates, forming CNTs-based hybrid constructions. Different substrates give rise to the distinctive CNTs constructions and electrical characteristics, among which electrically conducting

GNPs as substrate material benefits to the formation of unique completely-conducting CNTs hybrid construction. These CNTs arrays construction can be synthesized through CCVD process. However, the experimental parameters of CCVD process play dominating roles in determining the organization, aspect ratio and electrical properties of synthesized CNTs arrays. According to the microcapacitor model and MWS effect, a number of microcapacitors can be formed by distributing CNTs and intermediate insulating polymer layer, leading to a significant enhancement of permittivity of composite. The CNTs arrays served as natural microcapacitors is able to overcome the frizzy entanglements effectively and increase permittivity of composites. These hybrids with their distinctive conducting multi-branch constructions make the tunneling effect and ohmic contact more easily, leading to the relatively low threshold values. Furthermore, the conductive network consist of CNTs hybrids is more sensitive to external stimuli because these conducting fillers acted as the typical “concentrators”.

In this thesis, we will discuss in detail these issues, aiming to find the relationship between synthesizing parameters and hybrids organization, develop and optimize the CNT-based polymer composites in the view of the electrical energy storage and piezo-resistive sensing.

Chapter II

Synthesis and characterizations of CNTs-based micro-nano hybrids

2.1 Introduction

Due to their excellent intrinsic properties, CNTs served as one of the most representative functional nano-fillers in composites field during current 20 years. These intrinsic properties include their one-dimensional structure in nanometer-scale, high aspect ratio, low bulk density and the outstanding mechanical, thermal and electrical functionalities. When loading CNTs into polymer matrices, randomly dispersing CNTs are capable of endowing their composites with surprisingly enhanced mechanical modulus, dielectric performance, thermal and electrical conductivities.[9, 48, 50, 147, 260-261]

However, as two sides of a coin, the typical high aspect ratio of CNTs makes it easily frizzy and results in the undesired aggregation in polymer matrices as reported in numerous experiments. As to the mechanical performance, on one hand, the agglomeration of CNTs existed in the polymer matrix could give rise to the significant reduction of effective interface between CNTs and matrix, which is detrimental to mechanical reinforcement effect of CNTs to composites. On the other hand, CNTs aggregations result in the inhomogeneous dispersion and distribution, inducing the formation of mechanical weak region. In addition, as to the electrical performance, achieved significant contact resistance, weaken interfacial polarization and strongly reduced breakdown strength ascribed to CNTs aggregation could be fatal to the dielectric and electrical properties of composites.[111]

Therefore, recently, the synthesis of CNTs on the micrometer-sized particles has

been proved as a significant way to ameliorate the CNTs aggregation and to improve multifunctional properties of composites. Be different from other CNT−semiconducting substrate hybrid structures, the special coupling micro-architecture consisting of CNTs and GNPs were synthesized. GNP-CNTs hybrids (GCHs) served as the distinctive conductive filler with features of all-carbon composition, in particular coupling structure and low intrinsic density.[31, 208-209, 211, 262]

In this chapter, we present firstly the synthesis process through the approach of catalyst chemical vapor disposition (CCVD). After a series of processes of carbon source decomposition and carbon atoms redisposition, numerous CNTs can be well grown and vertically aligned onto the surfaces of GNP substrates, forming the special structure. Secondly, in order to investigate the relationship between the CVD synthesis conditions and the corresponding construction of GCHs, several key parameters during the CVD synthesis are selected and tuned such as: the temperature, gas composition and reaction time during the CVD synthesis are tuned. In fact, the constructions of achieved synthesized products are strongly dependent on the synthesis conditions. In addition, the results obtained from qualitative characterization provide a structural foundation for the huge applicable potential of GCHs constructions. The foundation also leads us to further intensively study the multi-functional contributions to different composites made by these particular features of GCHs in chapters III and IV.

2.2 Experimental

2.2.1 Materials

Main materials involved in this study are listed in Table 2-1.

Table 2-1*. Information of main materials used in this experiment*

Material	Molecular formula	Physical states	Purity	Notes
Xylene	C_8H_{10}	Liquid	98.5+%	Assay, isomers plus ehtylbenzene, Alfa Aesar
Ferrocene	$Fe(C_5H_5)_2$	Solid	99%	Alfa Aesar
Argon	Ar	Gas		Carrier gas
Hydrogen	H_2	Gas		Carrier gas
Acetylene	C_2H_2	Gas		Carbon source
GNP particles		Solid		Hundreds of nm in thickness; <5um in diameter, Xiamen K-Nano Co.

2.2.2 Floating CCVD equipment and process

The GCHs constructions were synthesized by using floating CCVD process in a horizontal quartz tube (length and inner diameter are 1100 mm and 45 mm, respectively), as schematically depicted in Fig. 2-1. The as-received GNP particles were homogeneously dispersed on the surface of a rectangular quartz plate (3×50 cm^2), which was then placed at the center region of the reactor. The CVD reactor was then heated to a given temperature (ranging from 550 to 850 ^oC) by an electric resistance furnace (60 cm long) under the gas-mixture atmosphere of argon and hydrogen. The gas flow rate was controlled by electronic mass flow meters (Bronkhorst, France). After keeping the temperature reactor stable about 10 minutes, ferrocene dissolved in xylene at a concentration of 0.05 g ml^{-1} was injected in the reactor by a syringe system and carried on the stable reaction region by the carrier gases (Ar + H_2) in the form of spray. When the catalyst solution started to be injected, the acetylene was conveyed into the reactor at the same time. The CNT growth time was controlled at a given value (ranging from 5 to 40 min). After the reaction, the furnace was cooled down under carrier gases atmosphere. The total gas flow rate during the whole process was kept at 1L min^{-1}.

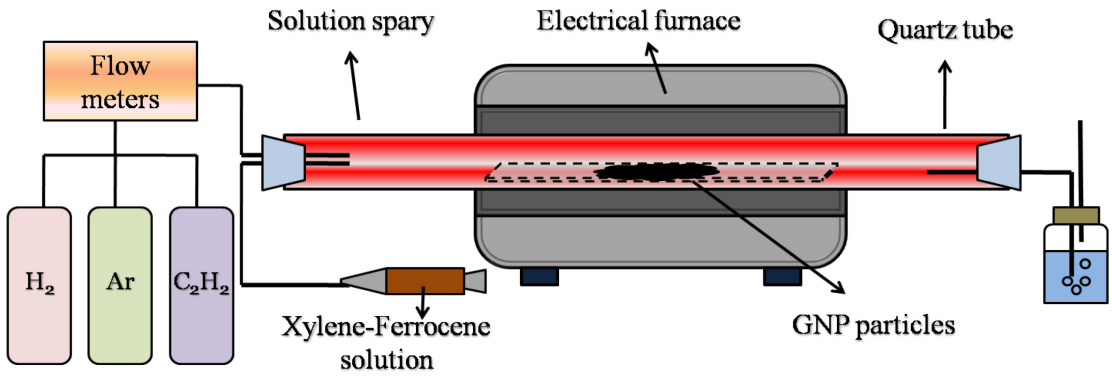

Fig.2-1 *schematic illustration of CVD synthesis system for the preparation of GCH particles.*

2.2.3 Characterization methods

The as-synthesized GCH particles were characterized by the following methods and equipments: Scanning electron microscope (SEM, ZEISS LEO 1530 Gemini) and the Transmission electron microscope (TEM, Titan) were used to observe the morphology of GCHs. X-ray diffraction (XRD) patterns of GCHs was measured on XRD detector ((BRUKER D2 PHASER with X Flash 430). The thermal property of GCHs was characterized by the simultaneous thermal analyzer (NETZSCH STA 449 F3 Jupiter). Raman spectrometer (Horiba, Labram, Simple monochromateur, laser He-Ne (632.8 nm)).

2.3 Influences of CVD parameters to GNP-CNTs hybrids structures

In order to achieve the hybrids construction of GCHs, there are two main reactions carried out during the floating CCVD procedure, namely, the decomposition of carbon source and the decomposition and re-agglomeration of catalyst precursor. Both mentioned reactions can be strongly influenced by synthesizing conditions, which finally determines the synthesized CNTs arrays morphology and the hybrid

organization. In this study, we firstly investigated the effects to final hybrids constructions resulted from three crucial experimental parameters: temperature, hydrogen ratio and synthesis time.

2.3.1 Temperature

The GCHs constructions synthesized by floating CCVD process at constant hydrogen ratio (H_2/Ar=0.3:0.7 L·min^{-1}) and moderate time (10 min) with different temperature ranging from 550 ^{o}C to 850 ^{o}C are shown in Fig. 2-2. The construction morphology of GCHs synthesized at 550 ^{o}C, 650 ^{o}C, 750 ^{o}C and 850 ^{o}C are demonstrated in Figs. 2-2 a-b, c-d, e-f and g-h, respectively. It is clearly seen that at the low synthesis temperature (550 ^{o}C), a relatively small quantity of CNTs is grown onto substrates with widely distributed diameters. Notably, be similar to the as-received original GNP particles, the multi-layered formation is well maintained after the reaction. However, with the reaction temperature reaches to 650 ^{o}C, majority of synthesized CNT arrays are well grown and perpendicularly aligned onto surfaces of individual GNP substrates, forming a series of complete GCHs construction. When the reaction temperature increased higher than 750 ^{o}C, the length of grown CNTs array enhances significantly. However, accompanied with a reduction of CNT arrays area number density could be clearly observed, especially, for the sample of 850 ^{o}C.

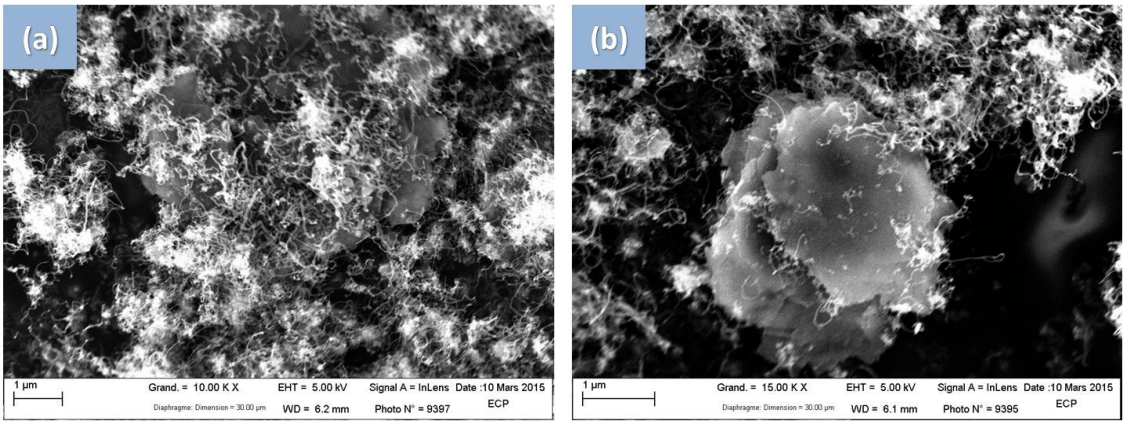

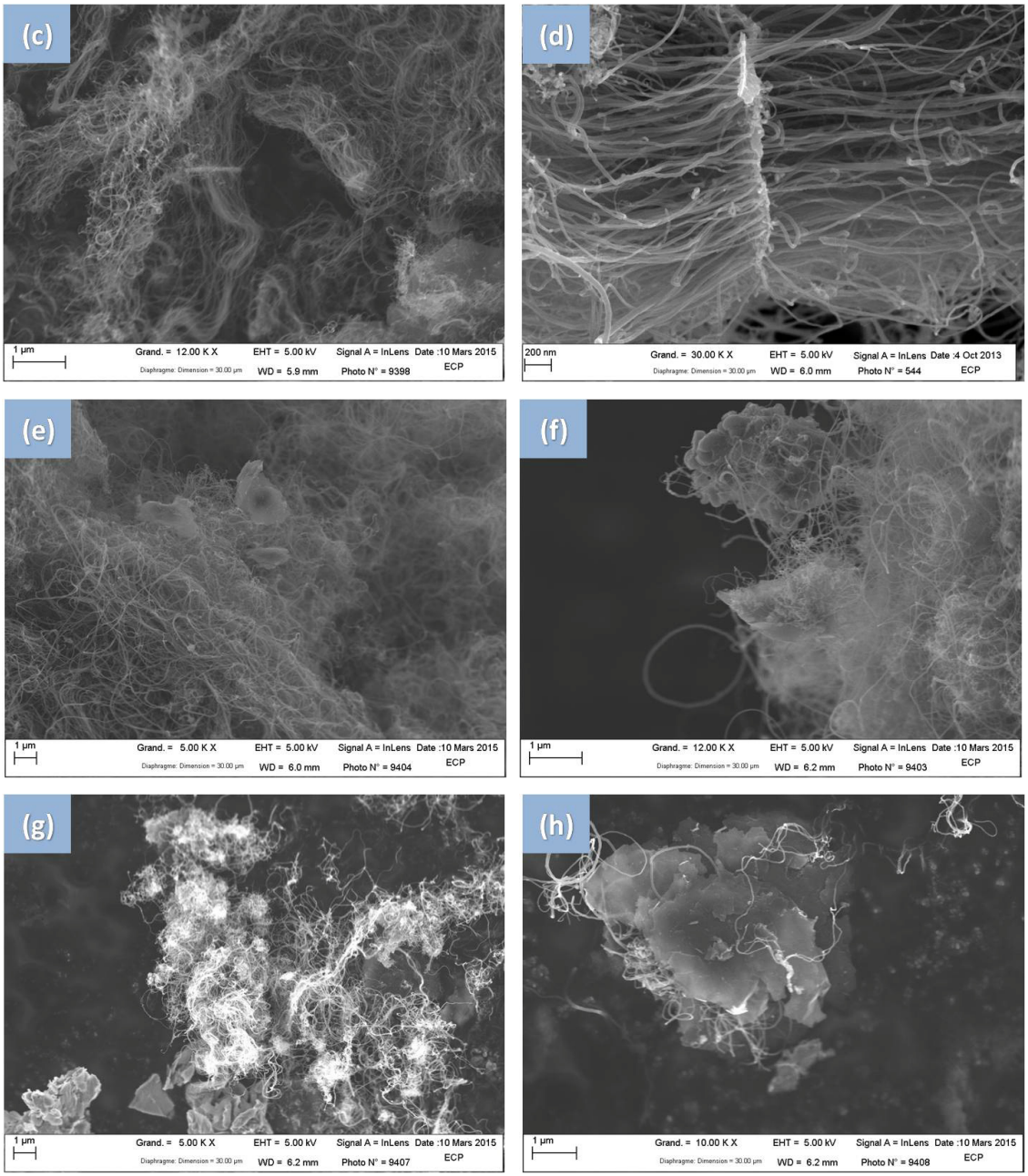

Fig.2-2 *SEM morphology of GCHs constructions synthesized by floating CCVD process at different temperature. (a),(b) 550 ^{o}C; (c),(d) 650 ^{o}C; (e),(f) 750 ^{o}C; (g),(h) 850 ^{o}C.*

It is known that the decomposition of catalyst precursor prefer to occur on the substrate surface rather than in the gas atmosphere at low temperature. The interaction between substrate and reactants reduces the activation energy of the decomposition reactions, which provides a positive circumstance for the CNT nucleation.[31] At the reaction temperature of 550 ^{o}C, on one hand, the energy in the reactor is insufficient

to separate stacked GNPs into individual ones, the CNTs could be locally grown onto the surface of the original GNPs layer. On the other hand, due to the high decomposition temperature of xylene, only few amount of xylene is decomposed, resulting in that the growth of CNT arrays is inhibited by the low concentration of carbon atoms.[31, 208-209, 262] However, when the reaction temperature increased to 650 ^{o}C, the previous multi-layered GNPs are exfoliated into a number of individual GNP structures. These flexible platforms benefit to the deposition of catalyst and the formation of complete "multi-directions" GCH constructions. In fact, the CNTs are synthesized by a series of complex process that carbon atoms are dissolved, diffused and precipitated under the function of catalyst particles. The dissolving and diffusion rates increase with temperature. When the reaction temperature increased higher than 750 ^{o}C, the carbon concentration is too high and the dissolving effect becomes absolutely dominant. Therefore, the carbon atoms accumulate on the substrate surface as amorphous carbon, terminating the growth of CNTs.[17]

2.3.2 Hydrogen ratio

Fig. 2-3 showed the morphology of GNP-CNTs organization synthesized at constant temperature of 650 ^{o}C and reaction time of 10 min, with different hydrogen ratios to total gas rate ranging from 0 % to 30 % (the H_2/Ar from 0 to 0.3/0.7 L·min^{-1}). Hydrogen served as one of the carrier gases, playing an important role in tuning the construction of CVD products and controlling the decomposition of catalyst precursors and carbon sources.[263] As shown in Fig.2-3a and b, distinctively, a number of "sticks" with much larger diameter than traditional CNTs grafted onto the GNP substrate, which was synthesized through CCVD process without H_2. These unusual constructions can be observed in detail from the TEM image (see the Fig. 2-4). Compared to CNTs, these "sticks" with diameter of larger than 100 nm do not display the typical tube-structure of CNTs. Thus, it could be confirmed that these "sticks" composed of amorphous carbon. In fact, hydrogen can make significant

contribution to protect the iron catalysts from being coated by accumulating amorphous carbon, in order to promote the active lifetime of the catalyst.[264-265] Noteworthily, from the coexistence between CNTs and amorphous carbon sticks is shown in Fig.2-3c and d to few amorphous carbon stick can be observed in Fig.2-3e-h, indicating that the formation of amorphous carbon sticks is suppressed effectively with the increasing hydrogen ratio.

Additionally, except for amorphous carbon sticks, the mean length of CNTs reduces gradually with the enhancing hydrogen ratio. However, their diameter maintains relatively stable range. Thus the aspect ratio of CNT arrays exhibits a negative trend with the increase of hydrogen ratio.

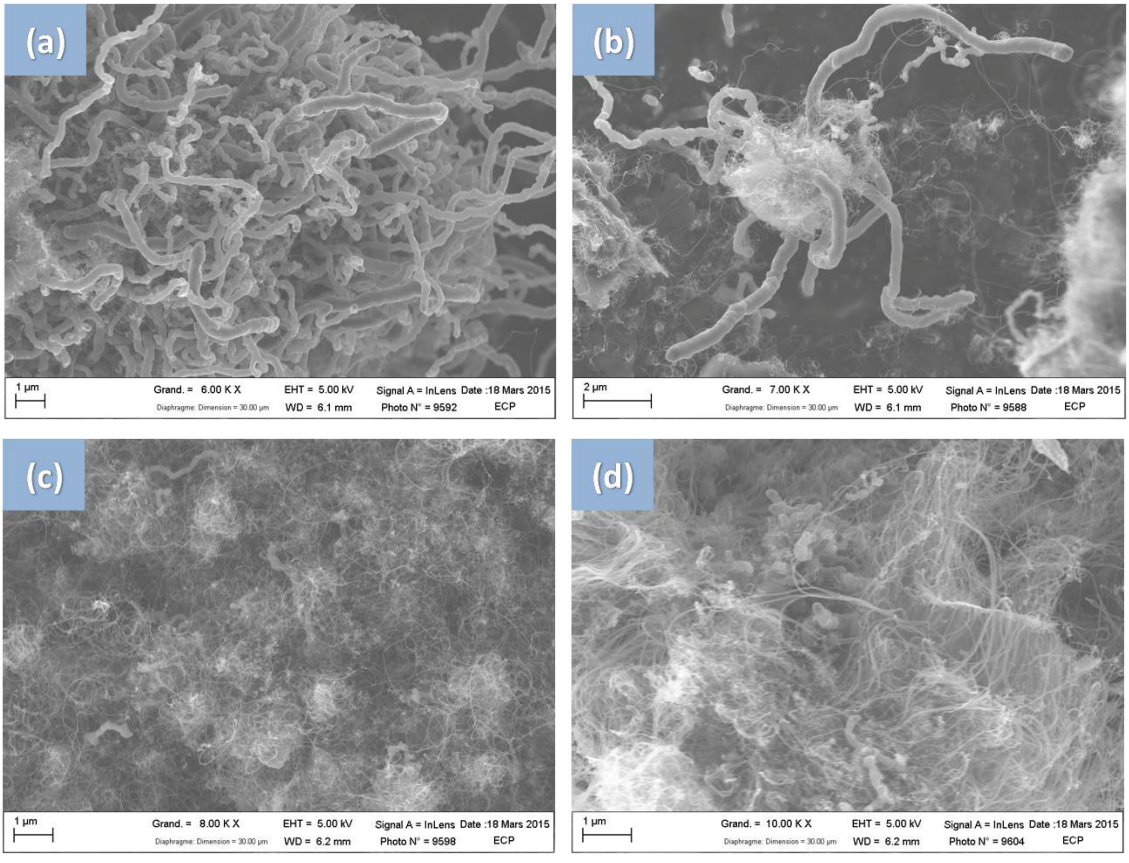

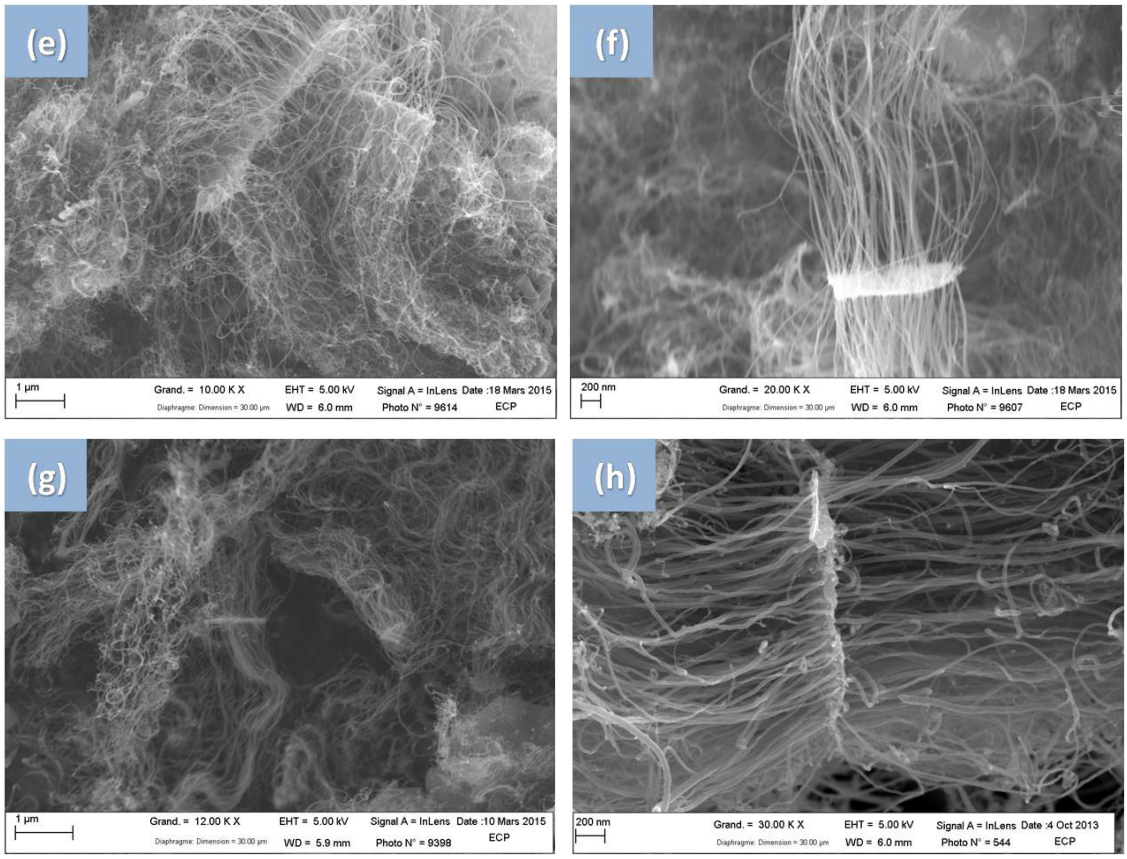

Fig.2-3 *SEM morphology of GCHs constructions synthesized by floating CCVD process at different hydrogen ratio to total carrier gas rate: (a),(b) 0%; (c),(d) 10%; (e),(f) 20%; (g),(h) 30%.*

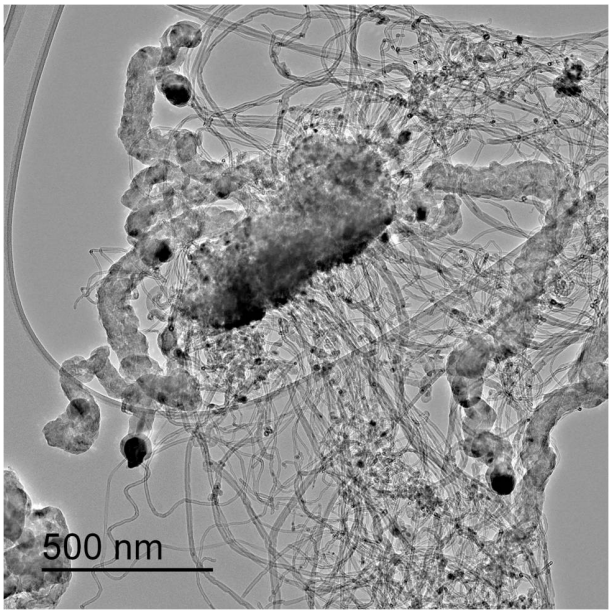

Fig. 2-4 *TEM morphology of "stick" composed of amorphous carbon.*

2.3.3 Reaction time

The evolution of GCH particles at different growth times ranging from 5 min to 40 min has been shown in Fig. 2-5. The CCVD synthesis operated at the constant temperature as 650 ^{o}C and hydrogen ratio to total gases of 30%. It is noted that under selected conditions the "two-directional" construction of GCHs was well maintained from a short reaction time (5 min) to a longer one (40 min).

Fig. 2-6 illustrated the relationship between the average length of synthesized CNTs and different reaction time. According to the linear fitting, it is found that the length of synthesized CNT arrays quasi-linearly enhances with the reaction time, the corresponding slope=0.22.

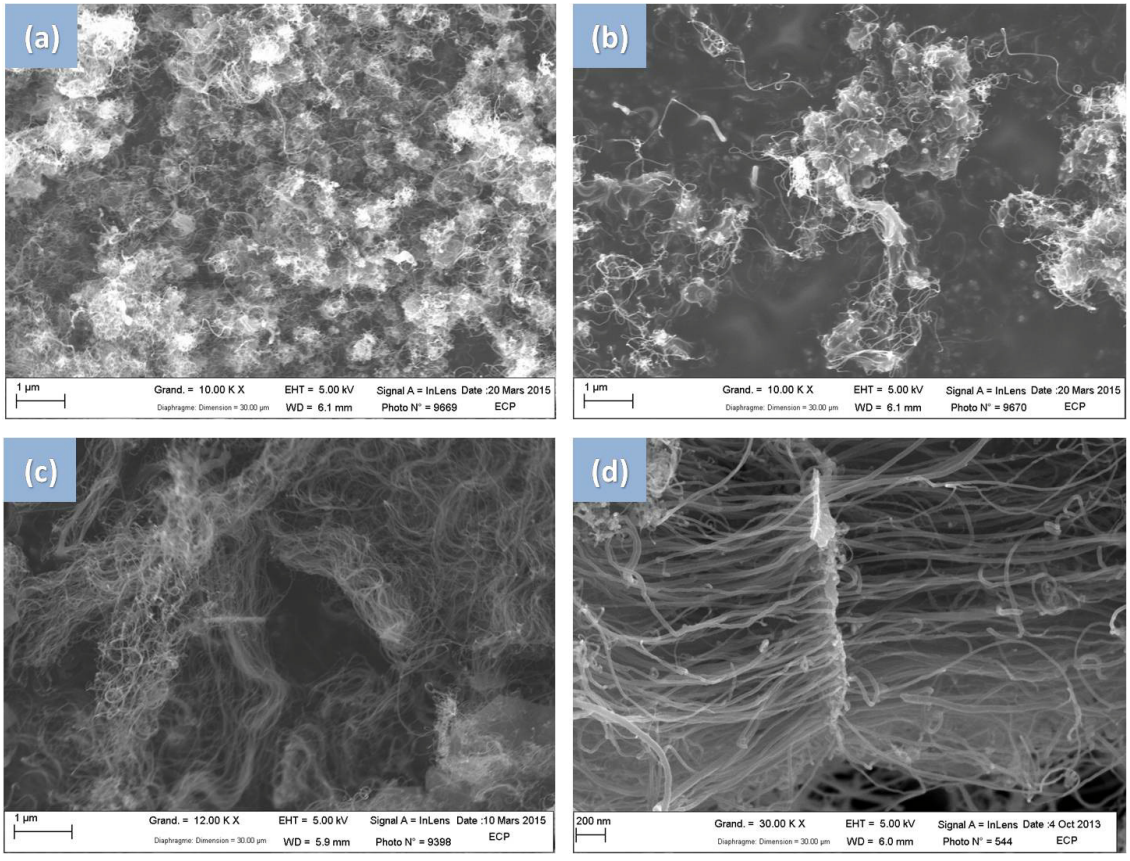

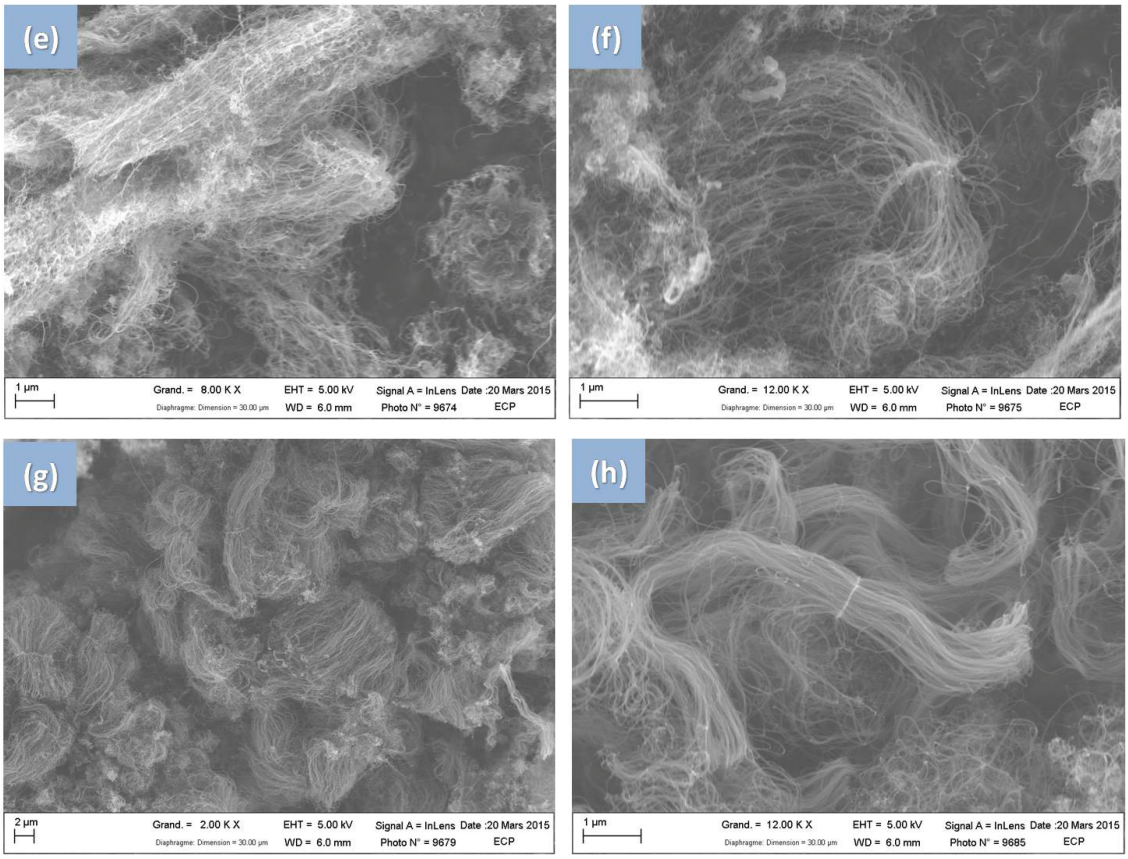

Fig.2-5 *SEM morphology of GCHs constructions synthesized by floating CCVD process with different reaction time: (a),(b) 5 min; (c),(d) 10 min; (e),(f) 20 min; (g),(h) 40 min.*

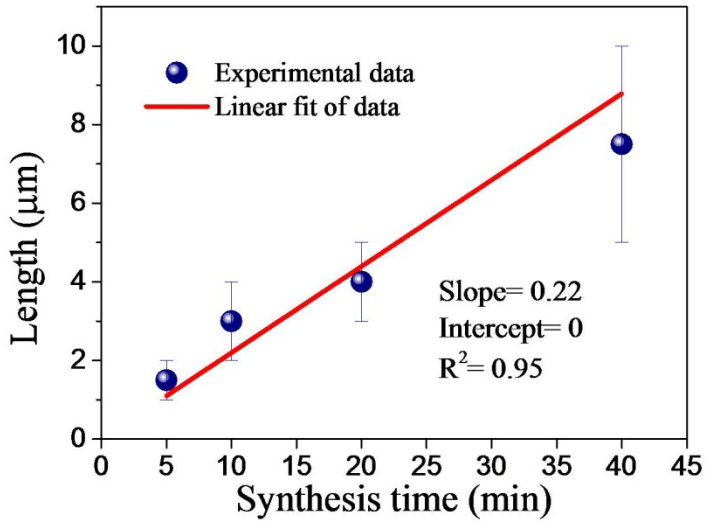

Fig. 2-6 The relationship between the average length of synthesized CNTs and different reaction time.

2.4 The qualitative analysis of the product of CVD synthesis: GNP-CNTs hybrids

As mentioned before, the electrical performance of composites is strongly dependent on the aspect ratio of CNTs. According to the construction morphology comparison by tuning three important experimental parameters, the GCH construction with synthesis conditions as temperature, hydrogen ratio and reaction time of 650 ^{o}C, 30%, and 10 min, respectively, was selected as the typical functional filler of composites in following studies. In fact, this typical GCH construction exhibited moderate length and aspect ratio of CNT arrays, which could not only avoid the CNT arrays entanglement in polymer matrix, but also keep CNT arrays without being detached from GNP substrates of a certain sort when experiencing the processing procedure. In this study, we make several necessary characterizations and analysis based on this typical GCH construction, in order to make a qualitative foundation for better understanding those interesting performance improvements of composites endowed by GCHs.

2.4.1 Composition of GCHs and byproducts from CVD synthesis

The catalyst is one of the most important factors in the floating-catalyst CVD process. What kind of residual byproducts could be formed from CCVD process, and whether these byproducts can affect the performance of composites should be well studied. In this experiment, the ferrocene ($Fe(C_5H_5)_2$) powders that used as the catalyst were dissolved into the xylene solvent. The solution was injected into the active region in the furnace, in order to drive the carbon hybrid structure to be synthesized. A series of complex chemical reactions react in the furnace, which can be found in detail in our previous work.[209-210, 266] Generally, the catalyst reacts according to an integrate formula:

$$\mathrm{Fe}(\mathrm{C_5H_5})_2 + H_2 \Rightarrow Fe + 2C_5H_6 \qquad (2\text{-}1)$$

Due to the whole synthesis taken place under the Ar atmosphere, it can be concluded that the iron is the residual production of the catalyst. Fig.2-7 provides the XRD patterns of ferrocene powders, GCHs and iron.[267-268] From the XRD patterns, none of typical peak of ferrocene can be noticed obviously in the curve of GCHs, indicating that the catalyst was decomposed completely and with little residue in the synthesized production. Moreover, it is clearly observed that there are three typical peaks in the XRD pattern of iron: 44.64°, 64.98° and 82.28°. Especially, the peak observed at 44.64° in the GCHs pattern verifies that the iron as the production of catalyst exist in the GCHs particles.

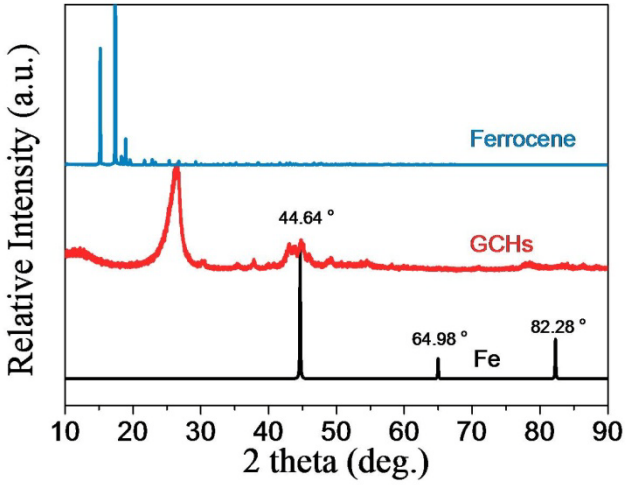

Fig. 2-7 *XRD patterns ferrocene, GCHs and GCHs.*

The quantity of iron can be evaluated using TGA (see Fig.2-8a). It is noticed that the content of iron (iron oxides) in the total production is 5 wt.%. After calculating, the concentration of residual iron in the sample that GCHs/PDMS composite would be lower than 0.1 vol.%. In addition, the by-product particles with diameter and length around 8 nm and 20 nm, respectively, could be clearly observed in TEM image (see Fig. 2-8b). Most of them are found that positing in the inner tubes of synthesized CNTs, which could make little contribution to the formation of conductive network. Therefore, it is concluded that the influence of the by-product of catalyst to electrical performance of composite can be ignored.

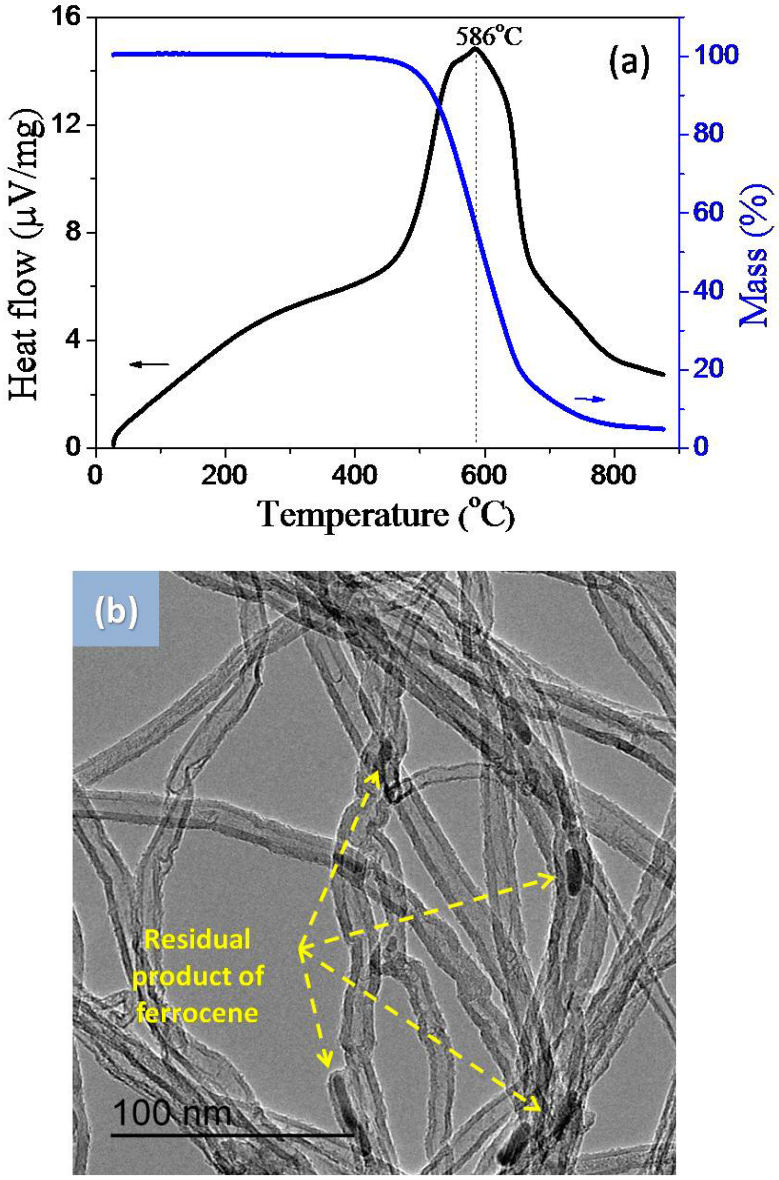

Fig. 2-8 *(a)The TGA and DSC curves of the typical GCH construction, (b) the by-product of catalyst observed from TEM image.*

Besides the few concentration of metallic catalyst, it is known that the CNTs/GNP mass ratio is not only a critical issue to evaluate the composition of GCHs construction, but also an important parameter to influence the structure of hybrids and the inner conductive network in polymer matrix. Although the way of TGA is generally used for measuring the mass ratio of most CNTs-based hybrids,[214, 269] it is difficult to distinguish the CNTs and GNP by the loss mass, due to the complete-

carbon based backbone. From the DSC/TGA result, there is only one heat flow peak can be found at 586 ^{o}C in the whole testing temperature range. The peak is integrated by the thermal decomposition of both CNTs and GNP substrates. Indeed, in this experiment, the mass ratio of CNTs/GNP substrate is achieved by comparing the weight of GNPs substrate before and after CVD synthesis. The mean mass ratio of CNTs and GNP substrate of 5 synthesized GCHs is calculated as 1.09, which is similar to the result of relevant report.[262] However, in consideration of the influence of metallic catalyst, the real mass ratio is calculated as 0.99/1. Therefore, the mass ratio of CNTs and GNP substrate is approximated at 1 in our work.

2.4.2 Structural characterization

In general, the structure of carbon walls with axial and internal cavity is considered as the typical feature to confirm the CNTs structure. The high resolution TEM characterization of synthesized GCHs and CNTs obtained can be seen in Fig.2-9. The structure of carbon multi-wall and internal cavity can be observed from the TEM image of single CNT, which in accordance with the report of our previous research.[31]

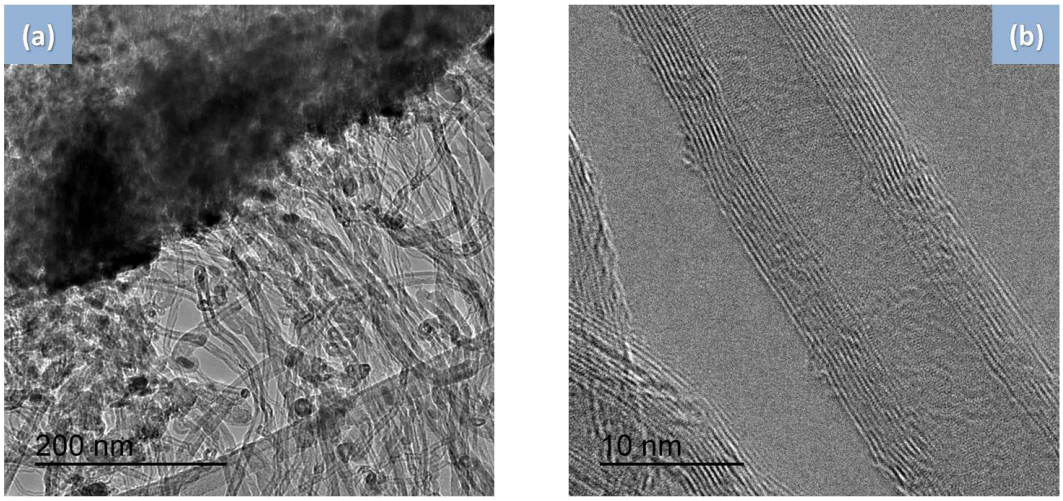

Fig. 2-9 *(a)Typical TEM image of the part of GCHs (b) High-resolution TEM image of synthesized CNT with detailed displayed structure.*

In addition, Raman spectroscopy is a useful approach to evaluate the structure of CNTs. Usually, there are two main vibrational modes, G (around 1580 cm^{-1}) and D bands (around 1330 cm^{-1}) are exhibited in the Raman spectral region. The former corresponds to the graphite mode G-band and associates with the orders sp^2 hybridized carbon network. The latter is corresponds the defect mode D-band and related to local defects that originate from structural imperfections. The relative intensity ratio of the D- and G-bands (I_D /I_G) is used to evaluate the nanostructure of CNTs. The Raman spectrum of the GNPs substrate and GCHs are shown in Fig.2-10a. In order to remove the influence of GNP substrate to GCHs during the Raman characterization, the Raman data of the CNTs that synthesized on the quartz using the same CVD process is also shown in Fig.2-10a.

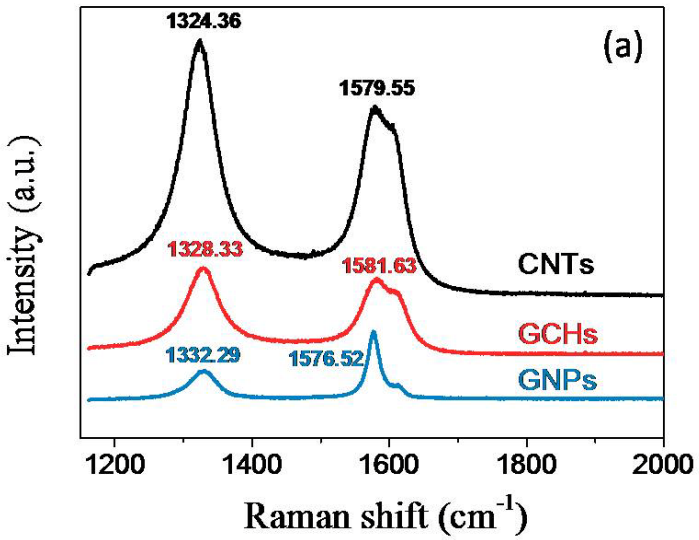

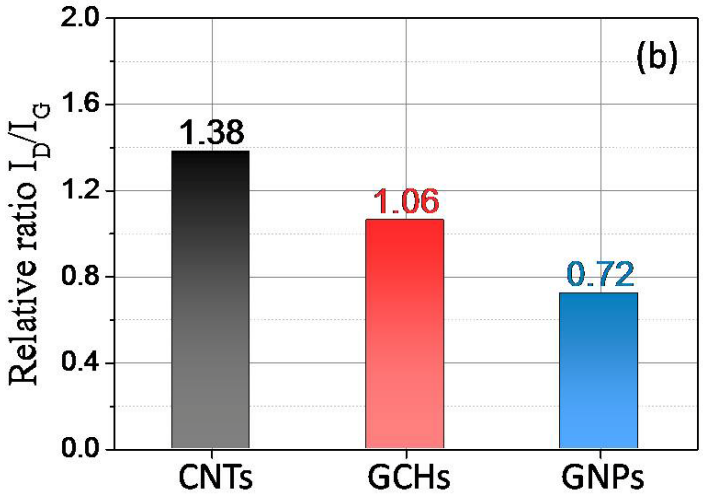

Fig. 2-10 *(a) Raman spectra of CNTs (black), GCHs (red) and GNPs (blue). (b) The relative intensity ratio of D- and G-band (I_D/I_G) of CNTs, GCHs and GNPs*

Besides the characterization of HRTEM, the typical peak positions of CNTs from Raman characterization are able to confirm that the synthesized nanostructures on the GNPs substrate can be identified as carbon nanotubes as well.[270-271] However, the relative intensity ratio of D- and G-band of GCHs and CNTs is 1.06 and 1.38, respectively, which indicates that there are some defects and structural imperfections exit in the carbon crystal lattice (see Fig.2-10b). In fact, the controllable CVD synthesis and hybrids production optimization will be one aspect of our next research.

2.4.3 Thermal exfoliating effect

As mentioned before, the thermal exfoliating effect plays an impertant role in determining the construction of GCHs. GNPs substrates with the structure of multi-natural flake graphite sheets are demonstrated in Fig.2-11a and b, showing an average thickness of hundreds of nanometers and diameter of 1-4 μm, respectively. Fig.2-12c and d clearly illustrate the 1D-2D coupling structure of the synthesized GCHs, where the length and diameter of those vertically-aligned CNTs are 2-4 μm and 15-20 nm,

respectively. Particularly, In order to prepare the TEM sample, the GCHs particles were dispersed into ethanol via ultrasonic procedure. Fig.2-11e demonstrates that the relatively completed hybrid construction can be achieved from TEM characterization, implying that the inter-cohesion between CNT arrays and GNP substrate is relatively stable.

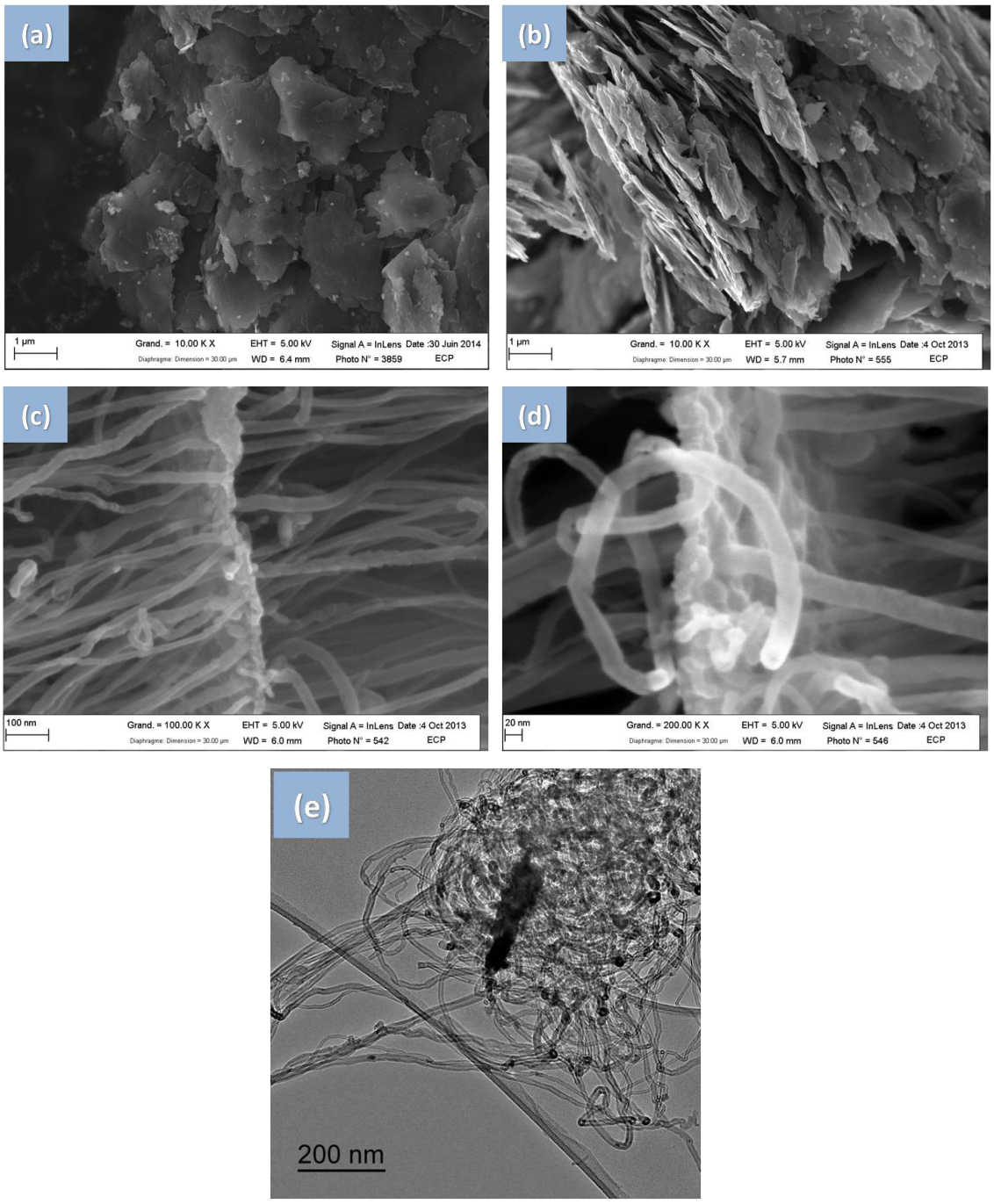

Fig.2-11 *Typical morphological characterization of (a and b) The structure of as-*

recieved GNPs with multi-layer stacked construction; (c and d) The construction of GCHs particles with individual GNP layer as substrate; (e) The construction of GCH particle using TEM.

It is noteworthy that all CNT clusters were observed to grow perpendicularly onto the surfaces of individual GNP (its thickness is less than 20 nm) rather than those of GNPs aggregate (natural state). In fact, during the CVD synthesis process of GCHs, the high temperature in furnace was used for not only offering required energy for chemical reaction, but also accompanying a thermal exfoliation effect which separates the original GNPs aggregates into a number of much thinner individual GNP layers.

In order to futher investigate the thermal exfoliating effect of GNPs, Fig.2-12 provides the X-ray diffraction (XRD) patterns of CNTs, GNPs aggregate and the GNP-CNTs hybrid. From GNPs to GCHs, the strong peak around 26.46^{o} dropped significantly, indicating the inter-layer distance of exfoliated GNP substrate kept constant, but the exfoliation degree of GNPs aggregate enhanced. However, the sharp peaks 44^{o} and 54.3^{o} of GNPs aggregate became gradual, which is in accordance with typical peaks of CNTs, suggesting that CNTs clusters were grown onto the surface of GNP substrate.

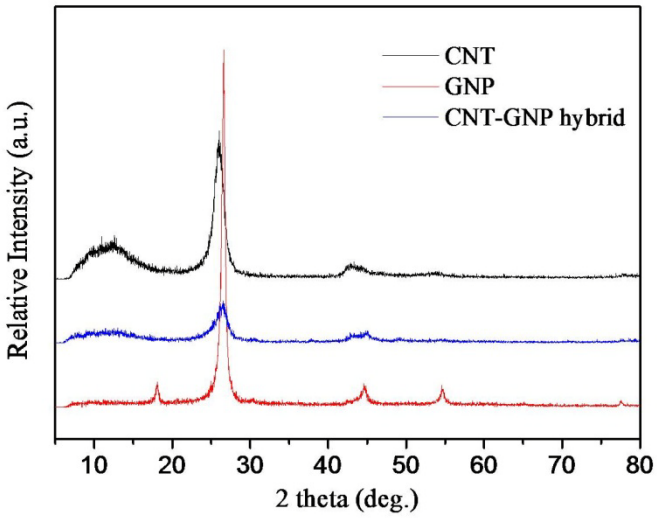

Fig.2-12 *The X-ray diffraction patterns of CNTs, GNPs aggregate and the GCHs*

Thus, due to the particular thermal exfoliating effect, both the specific surface area of fillers and the interfical area between fillers and polymer matrix can be increased effectively. Several notable properties of composite are well endowed by this special structure, which will be introduced in detail in following chapters.

2.5 Conclusions

Well-organized GNP-CNTs hybrid constructions were synthesized through floating CCVD process. The grown CNT arrays vertically aligned on the surface of two-dimensional GNP substrates without any pretreatment. The construction of GNP-CNTs hybrids can be controlled by tuning experimental conditions. The effects of three important parameters: temperature, hydrogen ratio and reaction time on the organization of CNTs on GNP substrates were discussed in detail.

At low temperature, on one hand, the energy in the reactor is insufficient to separate stacked GNPs into individual ones. On the other hand, few amount of xylene is decomposed, resulting in that the growth of CNT arrays are inhibited by the low concentration of carbon atoms. However, when the synthesis temperature is high, carbon atoms accumulate on the substrate surface as amorphous carbon, terminating the growth of CNTs. Therefore, the synthesizing temperature is around 650 ^{o}C that benefits the formation of GCH constructions. In addition, hydrogen plays a necessary role in determining the construction of synthesized product. With the increasing hydrogen ratio, the diameter of CNTs maintained in a stable range, while their length and corresponding aspect ratio showed a gradual reduction. Moreover, the mean length of synthesized CNT arrays quasi-linearly enhances with the reaction time, particularly, their corresponding slope was linearly fitted as 0.22.

The GCH construction with the mass ratio of CNTs and GNP substrate approximated at 1, synthesized through temperature, hydrogen ratio and reaction time

of 650 ^{o}C, 30%, and 10 min, respectively, was selected as the typical functional filler of composites in following studies. During the synthesizing process, the catalyst ferrocene can be transformed into a very few quantity of iron (oxide) particles finally, most of which are embedded in the inner tube of CNTs. Thus, influence to electrical performance of composite resulted from catalyst byproduct can be ignored. The grown CNTs of the typical GCHs construction exhibited a legible carbon multi-wall and internal cavity structure, making a structural foundation for the following functionality investigation of composites. The thermal exfoliating effect make a great contribution to exfoliate the original multi-layered GNPs into a number of individual-layered ones. It could give rise to the significant enhancement of both the specific surface area of fillers and the interficial area between fillers and polymer matrix.

GCHs with distinct features of all-carbon composition, largely-improved specific surface area, totally-conductive structure and low intrinsic density, are greatly potential to endow their composites with surprising multi-functional performances.

Chapter III

The dielectric behavior of GNP-CNTs hybrids/PVDF composites

3.1 Introduction

As an indispensable component of electroactive smart materials, Poly (vinylidene fluoride) (PVDF) with merits of excellent intrinsic dielectric and piezoelectric behaviors has been received intensive attention. Due to the distinct electronegativity of fluorine atoms and the strong electrical dipole moment of PVDF chains, PVDF is potential to be applied as smart sensors, micro-actuators and especially, dielectric capacitors. In recent years, to meet the demand of low driving electrical field, miniaturization and high portability of electronics, developing the novel dielectrics possess both high dielectric permittivity and flexibility becomes an important challenge.[126-127, 272-274]

Although pure PVDF polymer shows relatively high permittivity (ε'~10) compared with other engineering plastics, it is insufficient to achieve the prospective of energy storage devices. In order to solve this problem, recently, PVDF-based composites with improved ε' were obtained through the approaches that loading high-permittivity nano-ceramics or conducting nano-particles into PVDF matrix, which has been widely reported. However, for the ceramics-loading composites, their effectively improved ε' achieved only under the massive ceramic loading content, where their flexibility and electroactive functionality would deteriorate sharply. Particularly, the enhanced ε' of conducting filler-loading counterpart can be mainly ascribed to the percolation theory. Both the conductivity and ε' of composite are capable of displaying a dramatic increase when the conducting phase content adjoins to the

critical value-percolation threshold (f_c).[126-127]

Carbon nanotubes (CNTs) are considered as the milestone-style functional filler for the nano-composites field. Nevertheless, as a coin with two sides, when loaded in the polymer matrix, it is inevitable for these distinctive one-dimensional structures with high aspect ratio to aggregate into together easily. The CNTs aggregation can not only reduce the effective interfacial area and polarization between CNTs and polymer matrix greatly, but also drive the local electrical weak points formed. It results in the decline of both ε' and electrical breakdown strength, which is fatal to energy storage performance of materials. Thus, how to improve the dispersion and distribution of CNTs in polymer matrix is always a hot issue that attracted intensive investigation.

Surface-modification to CNTs is one of effective ways to ameliorate the dispersion in polymer matrix. However, to make a reasonable balance among CNTs dispersion, the electrical properties of conducting filler and the percolation threshold still needs further systematical study. In addition, the processing method is one of key issues to control the dispersion state of nano-fillers. Compared with the widely utilized solution-mixing method, the melt-mixing process has been proven as another efficient way to obtain the stable dispersion. The high temperature and shear force during the melt-mixing process are able to promote interactions in molecular lever between nano-fillers and polymer matrix. The achieved stable dispersion state and the solvent-pollution free processing procedure make the approach of melt-mixing, realistically, suitable for the industrial mass-production.

In this chapter, we present the advanced electrical conducting construction/PVDF composites with both improved dielectric performance and decreased percolation threshold, fabricated through the melt-mixing process using a lab-scale twin screw micro-compounder. The GNP-CNTs hybrids (GCHs) particles with vertically-aligned CNT arrays construction served as typical functional filler were well synthesized through CCVD approach. Be distinguished from common Al_2O_3-CNTs and SiC-CNTs hybrids using semi-conducting particle as substrates, the conducting GNPs served as substrate for growth of CNTs arrays could endow their

product with several distinctive merits of all-carbon composition, totally-conductive coupling structure and, especially, the low intrinsic density. The individual GNP substrates acted as a number of wire concentrators are able to conduct every single CNT that grafting on them. The melt-mixing process without the abuse of chemical solvent plays crucial roles in ameliorating the filler dispersion and promoting the interaction between GCHs and polymer matrix. Compared to their general counterpart of the PVDF-based ternary composites loading by the simple mixture of GNPs and CNTs with equivalent conducting phase concentration, the GCHs/PVDF binary composites show a remarkably low percolation threshold and relatively superior thermal stability. A comprehensive analysis is performed to investigate the dielectric property and percolation behavior of GCHs/PVDF binary composites, indicating that the strategy of reducing f_c though reasonably designing conducing filler construction is feasible. The GCHs/PVDF composites are potential to be applied as embedded capacitors with high performance.

3.2 Experimental

3.2.1 Materials and sample preparation

Graphite nanoplatelets with the thickness and diameter of 1-5 μm and hundreds nm, respectively, were offered by Xiamen K-Nano Graphene Technology Co. The commercial MWCNTs provided by Shenzhen Nanotech Port Co. (China). Their length and diameter were about 5-15 um and 20-40 nm, respectively. Semicrystalline polymer PVDF (Kynar 761, Arkema Group, France) was chosen as the electro-active polymer matrix in our experiment.

The GCHs particles were synthesized using a floating-catalyst CVD method, which is in accordance with the processing procedures mentioned in Chapter II. By controlling the synthesis duration and temperature as 10 min and 650 ^{o}C, respectively, the hybrid construction with the CNT/GNP mass ratio approximated to 1 was

obtained. The GCHs/PVDF binary nanocomposites and GNPs/CNTs/PVDF ternary nonocomposites were prepared using one-step melt blending, where nanofillers with hybrid volume fraction ranging from 0 to 10 vol.% were dispersed into the PVDF matrix at the melt state. The mechanical blending was carried out using a twin-screw micro-compounder (Micro 5 cm^3 Twin Screw Compounder, DSM) at 200 ^oC (upper), 210 ^oC (middle) and 220 ^oC (bottom) in Ar atmosphere. A long blending time (40 min) and a low blending shearing rate (40 rpm) were selected for not only protecting hybrid construction from being damaged as much as possible, but also obtaining a good dispersion as well. The resulting composites with a thickness of 1.5 mm were prepared through injection molding (Micro 5 cm^3 Injection Molder, DSM) under a pressure at 1.6 MPa for 1 min, the temperature of mold was 60 ^oC.

3.2.2 GNP-CNTs hybrids/PVDF composite characterizations

Scanning electron microscope (ZEISS LEO 1530 Gemini) was used to observe the morphology of the fillers and the fractured surfaces of GCHs/PVDF binary nanocomposites and GNPs/CNTs/PVDF ternary nonocomposites. Transmission electron microscope (TEM, Titan) was utilized to observe the morphology of GCHs. X-ray diffraction (XRD) patterns of the fillers and composites were measured on XRD detector ((Bruker D2 PHASER with X Flash 430). Fourier transform infrared spectroscopy (FTIR, Bruker Tensor 27) was employed to record the wave numbers. The dielectric properties were characterized as a function of frequency (from 10 Hz to 10 MHz) using an impedance analyzer (Solartron 1260). The temperature-dependent dielectric performance were characterized as a function of frequency (from 1 kHz to 10 MHz) and temperature (from -50 ^oC to 150 ^oC) using an impedance analyzer (Agilent 4294A) and supporting temperature chamber (Espec SU-261). Before the dielectric characterization, silver paste was coated on the sample as the electrodes to reduce the contact resistance.

3.3 Results and discussion

3.3.1 Composition of PVDF-based binary and ternary composites

In order to illustrate the distinctive dielectric performance of GCHs/PVDF binary composite endowed by the special contribution of GCHs particles reasonably, GNPs/CNTs/PVDF ternary composite were prepared. The weight ratio between individual GNPs phase and CNTs phase are well controlled as 1, being in accordance with that of GCHs particles. Fig.3-1 schematically illustrates the internal construction of binary and ternary composites. The concentrations for each component in GCHs/PVDF binary and GNPs/CNTs/PVDF ternary composites were shown in detail in Table 3-1. Since, the B-n and T-n will be used for referring to GCHs/PVDF binary and GNPs/CNTs/PVDF ternary composites with the weight fraction of total conducting phase n%, respectively.

Table.3-1 *Concentrations for each component of conducting phase(s) in the GCHs/PVDF binary composites and GNPs/CNTs/PVDF ternary composites.*

	GCHs	GNPs		CNTs		Total conductive phase	
	(wt.%)	(wt.%)	(vol.%)	(wt.%)	(vol.%)	(wt.%)	(vol.%)
GCHs/PVDF Binary composites							
B-1.7	1.7					1.7	1.42
B-4	4					4	3.38
B-6	6					6	5.09
B-6.5	6.5					6.5	5.52
B-7	7					7	5.95
B-8	8					8	6.81
B-8.5	8.5					8.5	7.24
B-9	9					9	7.67
B-10	10					10	8.54
GNPs/CNTs/PVDF Ternary composites							

T-2	1	0.79	1	0.89	2	1.69
T-4	2	1.59	2	1.79	4	3.38
T-6	3	2.40	3	2.70	6	5.09
T-6.5	3.25	2.60	3.25	2.92	6.5	5.52
T-8	4	3.20	4	3.61	8	6.81
T-10	8	4.02	8	4.52	10	8.54

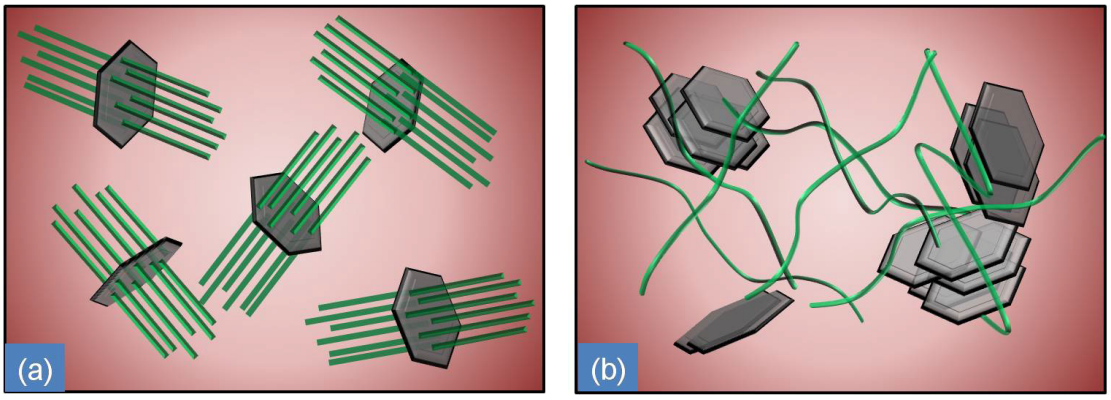

Fig.3-1 *Schematic illustration of the difference between (a) GCHs/PVDF binary composites and (b) GNPs/CNTs/PVDF ternary composites*

3.3.2 SEM morphologies of PVDF-based binary and ternary composites

The main fabrication process of GCHs/PVDF composites has been mentioned in the experimental section. Fig.3-2a demonstrates the morphological feature of graphite nanoplatelets (GNPs) which served in this work not only as the substrate materials of GCH particles during the CCVD process, but also the independent component in ternary composites. These multi-layered carbon structures with thickness of hundreds of nanometers and diameter of 1-4 μm, offer adequately large platforms for both the deposition of catalyst particles and the growth of CNT arrays. CNTs as another independent conducting phase in ternary composites with length and diameter of 3-5 μm and 15-20 nm, respectively, existed in the form of frizzy entanglement (See Fig. 3-2b).

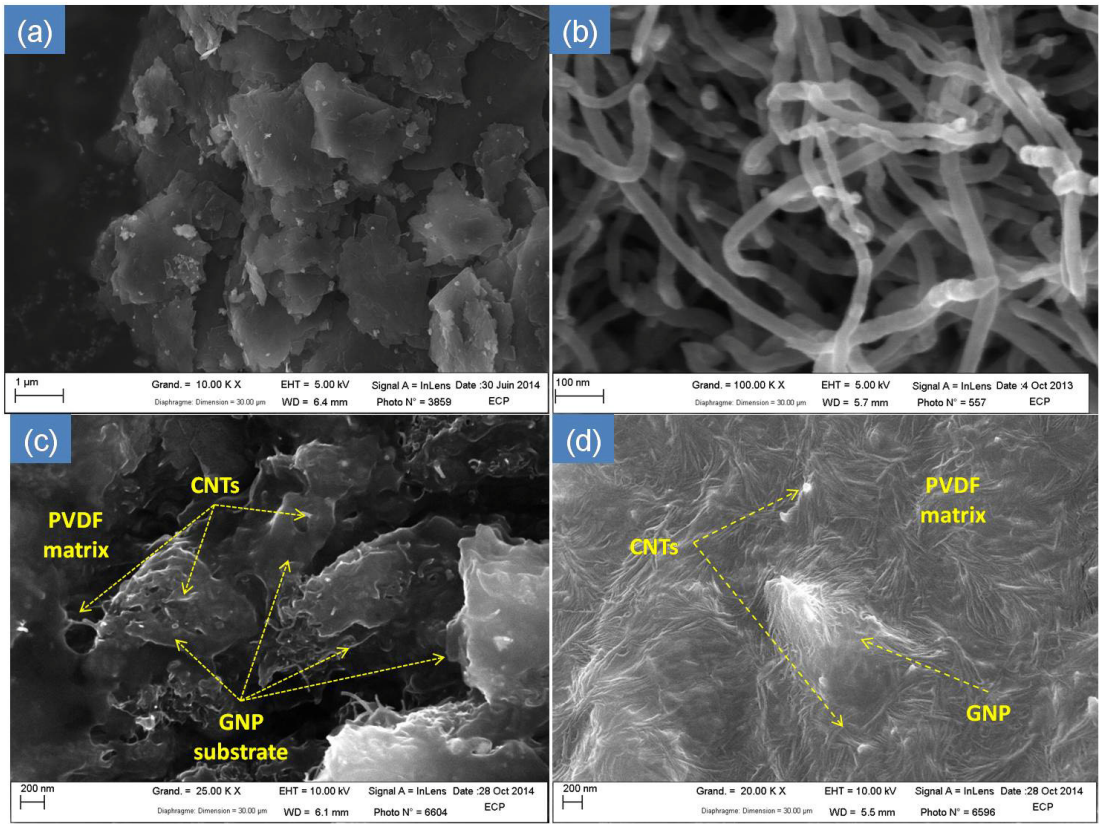

Fig.3-2 *SEM image of (a) as-received GNPs particles with stacked multi-layer constructions and (b) as-received frizzy CNTs structures. The SEM morphology of the fractured surface of (c) GCHs/PVDF binary composite and (f) GNPs/CNTs/PVDF ternary composite.*

From the viewpoint of composite, this hybrid construction can relive the CNTs aggregation, and enhance the interfacial area between GCHs and polymer matrix greatly. SEM image of fractured surface of the GCHs/PVDF composite is presented in Fig. 3-2c. Both GNP substrates and grown CNTs that aligning on the surface of GNP are well coated and embedded in the matrix phase, indicating the tight interfacial adhesion formed between hybrids filler and PVDF matrix. The largely increased interfacial area given by the GCHs coupling construction could be considered as a critical issue to be responsible for the excellent performance of GCHs/PVDF composite. This will be discussed in following paragraphs. Fig. 3-2d shows the typical SEM image of fracture surface of ternary composite. Be similar to its binary counterpart, the independent bi-filler are well embedded in the PVDF as well.

3.3.3 XRD spectra

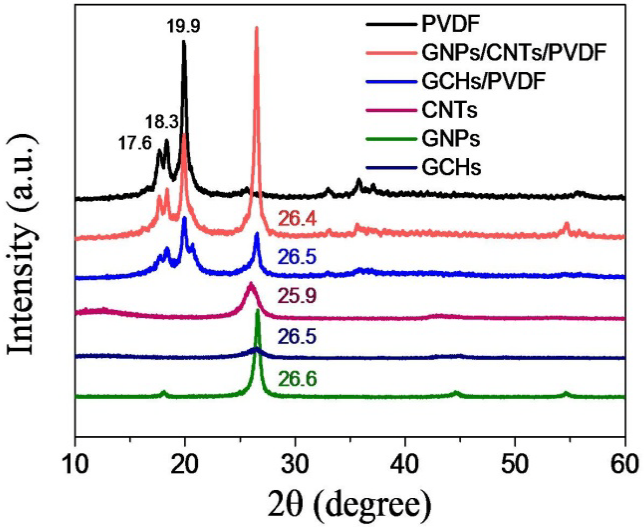

Fig.3-3 *X-ray diffraction patterns of CNTs, as-received GNPs, as-synthesized GCH particles, pure PVDF polymer, GCHs/PVDF binary composite and GNPs/CNTs/PVDF ternary composite.*

Three different conducting structures, pure PVDF polymer and its binary/ternary composites were characterized by X-ray diffraction (XRD) so as to better understand the compounding procedure (see Fig.3-3). It is observed from the XRD pattern of GCHs that the typical peak around 26.46° (corresponding to GNPs) shows a sharp reduction and a slight shift to left. This could be explained due to the processes of the thermal exfoliation of multi-layered GNPs substrates and the growth of CNTs during the CCVD reaction, which has been reported in the previous chapter. Then, the typical peak of ternary composite (26.4°) situates between peaks of GNPs (26.6°) and CNTs (25.9°), indicating these two conducting phases were effectively distributed in the PVDF composite.

Furthermore, the typical XRD peaks correspond to the a-crystalline phase: 17.6°, 18.3° and 19.9° can be observed clearly from the pure PVDF and its composites. It is

worthy to note that a significant XRD peak at 20.26° was detected from the curve of GCHs/PVDF binary composite, which just relative to the β-crystalline phase of PVDF. This unusual peak implies two issues: loading nano-particles could influence the crystalline structures of PVDF; There is a possibility of that the addition of GCHs could give rise to the formation of β- crystalline phase.

3.3.4 Frequency-dependent dielectric properties of binary and ternary composites

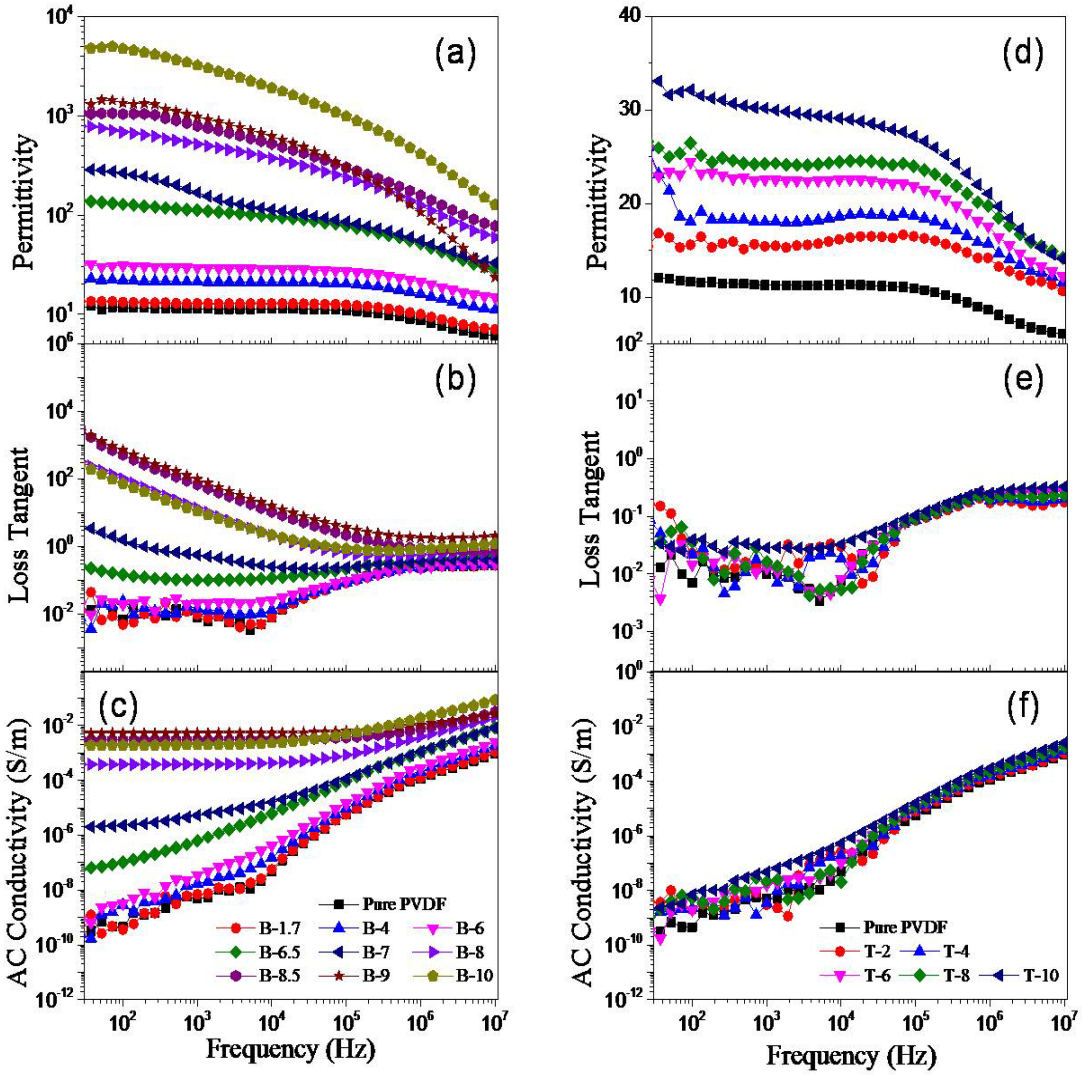

*Fig.**3-4** The frequency-dependence at room temperature of (a) and (d) the dielectric permittivity, (b) and (e) loss tangent, and (c) and (f) ac conductivity of GCHs/PVDF binary composites and GNPs/CNTs/PVDF ternary composites, respectively.*

Fig.3-4 compares the frequency-dependent dielectric performances between binary and ternary composites with equivalent mass ratio of GNPs and CNTs. In the low-frequency range (<10^4 Hz), when f_{GCHs} below 7 wt.%, the dielectric permittivity of binary composite is relatively independent on the frequency change. However, with the enhancing GCHs loading, significant reductions of dielectric permittivity can be achieved (see Fig.3-4a). As presented in Fig.3-4b, on one hand, when f_{GCHs} is low, the loss tangent maintains at relatively low values (~0.2) under testing frequency range, meanwhile, the similar dielectric relaxation with pure PVDF polymer were shown. On the other hand, composites with the high f_{GCHs} show a shapely augmented loss tangent, which is potential to be applied as electromagnetic wave materials.

According to Fig.3-4c, the AC conductivities of composites with low f_{GCHs} grow linearly with the increasing frequency. While, under higher f_{GCHs} range, the AC conductivity values not only increase by over several orders of magnitudes, but also display the typical frequency-independency within a low frequency range.

Compared to the binary composites, the ternary counterparts show the obviously different dielectric behaviors which are similar to the binary composites with filler loading under 6 wt.% (see Fig.3-4d-f). Notably, under the testing frequency range, the ternary composites remain electrically-insulating invariably, even the sample T-10 with the equivalent conducting phase loading as high as 10 wt.%.

3.3.5 Linear fitting the percolation threshold

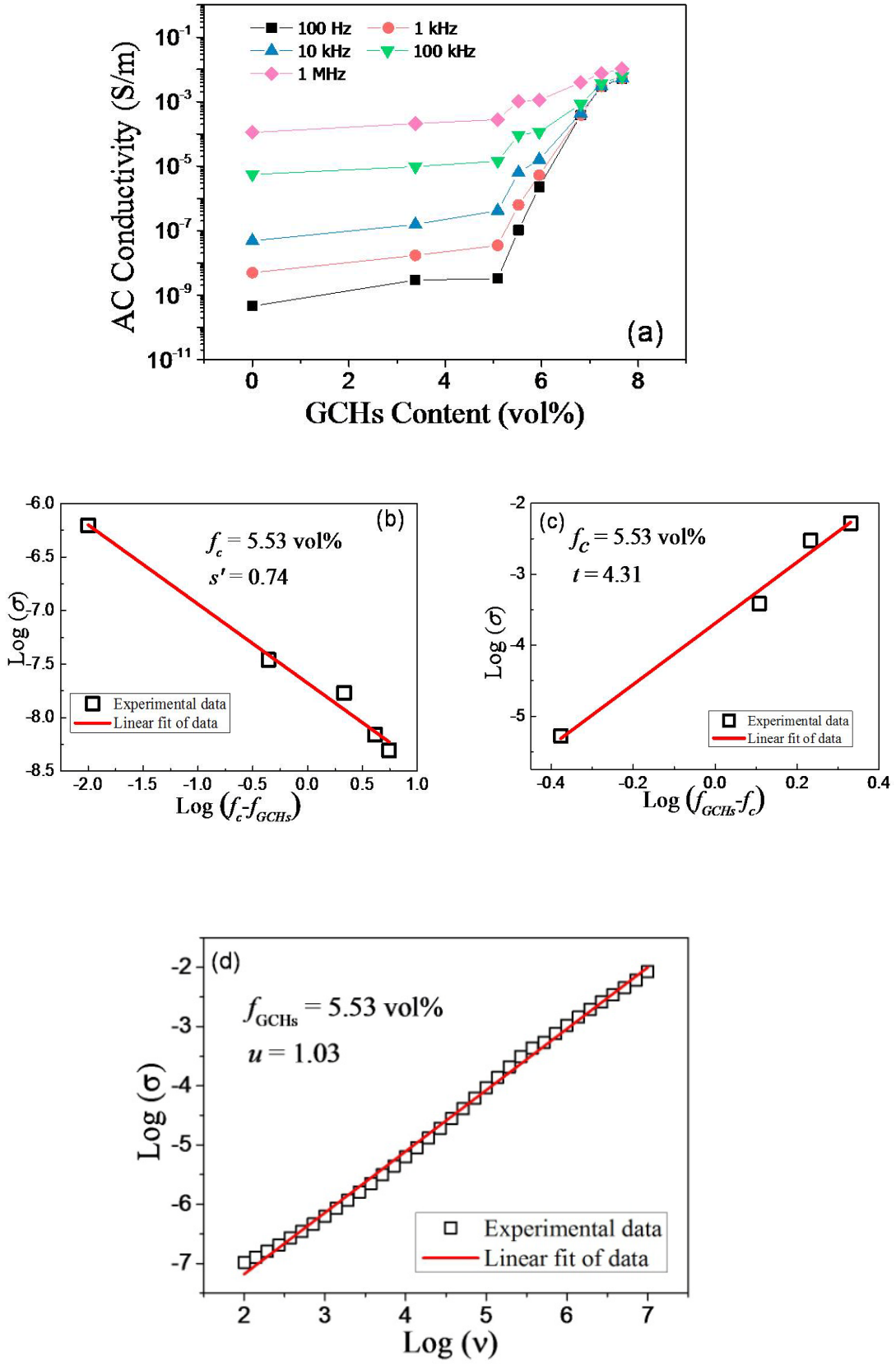

Fig.3-5 *(a) Dependence of the AC conductivity (measured at 1 kHz) of the*

GCHs/PVDF binary composites as a function of the GCHs volume fraction measured at room temperature. (b) and (c) show the best fits of the AC conductivity to Equation 3-1 and 3-2. (d) The linear fitting to experimental AC conductivity according to Equation 3-3.

Fig.3-5a exhibits AC conductivity σ_{AC} of GCHs/PVDF binary composites as a function of GCHs loading at room temperature. It can be clearly noticed that σ_{AC} of binary composites enhanced gradually with the increasing GCHs loading, while sudden enhancements occurred when GCHs loading approaches to a critical value, the percolation threshold. The significant change of electrical property illustrates the formation of internal conductive network. According to the percolation theory, σ_{AC} of composites that closed to the percolation threshold f_c can be assessed utilizing the power laws:

$$\sigma_{\mathrm{AC}}\left(f_{GCHs}\right) \propto \left(f_c - f_{GCHs}\right)^{-s'} \qquad \text{for } f_{GCHs} < f_c \qquad (3\text{-}1)$$

$$\sigma_{\mathrm{AC}}\left(f_{GCHs}\right) \propto \left(f_{GCHs} - f_c\right)^{t} \qquad \text{for } f_{GCHs} > f_c \qquad (3\text{-}2)$$

Where f_{GCHs} is the volume fraction of GCHs loading, *s'* and *t* are the critical exponent in insulating and conducting region, respectively. Notably, according to the power laws, the best linear fittings of experimental σ_{AC} both in insulating and conducing region provide a same f_c equals to 5.53 vol.%. (see Fig.3-5b and c) The critical exponent in insulating region s' equals to 0.74, which approaches the universal ones ($s' \approx 0.8$-1). The *t* in conducting region equals to 4.31, which is higher than universal values ($t \approx 1.6$-2). The achieved deviation of critical exponents might be attributed to the special construction of GCHs and the tunneling between only closest adjacent particles is taken into account, which could be responsible for the nonuniversality of critical exponents of percolation power laws.[233]

When the f_{GCHs} is very close to the f_c, the power law of percolation threshold gives:

$$\sigma \propto \omega^{u}, \quad \varepsilon \propto \omega^{u-1} \qquad \text{for } f_{GCHs} \to f_c \qquad (3\text{-}3)$$

Where $\omega = 2\pi\nu$, ν is the frequency, u is the corresponding critical exponent. The

experimental data of B-6.5 offers u = 1.03, which could be considered as corresponding to the theoretical value: $u = t/(s'+t) = 4.31/(0.74+4.31) = 0.85$. The fitting of experimental data can be seen in Fig.3-5d.

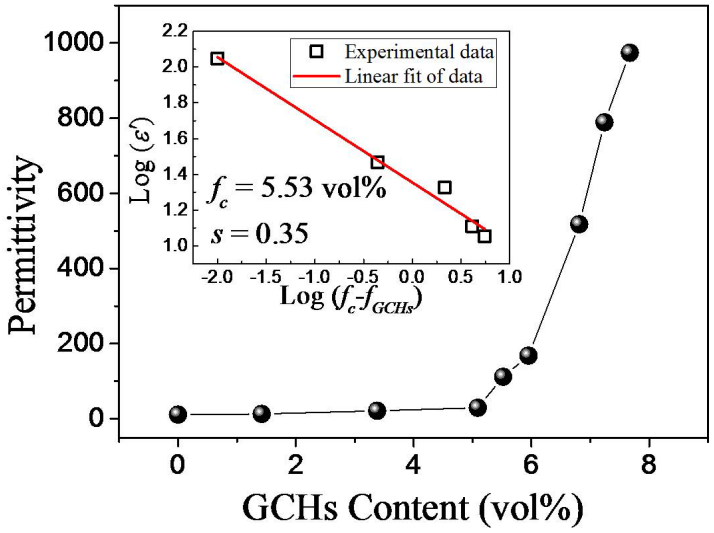

Fig.3-6 *Dependence of the dielectric permittivity (measured at 1 kHz) of the GCHs/PVDF binary composites as a function of the GCHs volume fraction measured at room temperature. The inset shows the best fit of the permittivity to Equation 3-4.*

Besides σ_{AC}, the permittivity of binary composite shows a giant increase as well, when the GCHs loading approaches to f_c. Fig. 3-6 depicts the permittivity as a function of f_{GCHs} at 1 kHz. At this critical region, the relationship between permittivity of composites and f_{GCHs} can be evaluated as follow:

$$\varepsilon'(f_{GCHs}) \propto (f_c - f_{GCHs})^{-s} \qquad \text{for } f_{GCHs} < f_c \qquad (3\text{-}4)$$

After fitting linearly the log-log slot, the f_c =5.53 vol.% and the critical exponent s = 0.35 can be achieved (see the inset of Fig.3-6).

3.3.6 Enhanced dielectric permittivity

The relative enhancement of permittivity $\varepsilon/\varepsilon_{PVDF}$ provides directly an influence

of the loaded fillers to the dielectric property of composites. For the traditional ceramic filled dielectric composites, when the relative enhancement of permittivity reaches to 10 at 1 kHz, their loading content would be as high as more than 40 vol.%. In this case, the flexible superiority of polymer matrix will be crucially destroyed. However, as shown in Fig. 3-7a, compared to the pure PVDF polymer, the GCHs/PVDF composite shows an enhancement of 400-fold at the volume fraction 8.5 vol.%. Furthermore, the CNTs/PVDF composite prepared by melt-mixing at the same filler volume fraction and testing frequency just showed a $\varepsilon/\varepsilon_{PVDF}$ less than 8.[134] The results further indicate advantages of GCHs fillers: (1) Problem of the entanglement and aggregation of CNTs has been improved; (2) The formation of conductive network can be simplified by these conductive "hub" structures.

In addition, with the consideration of practical applications, the loss tangent of dielectric composites should be lower than 0.1 at least. The dilemma between high permittivity and accompanying high loss tangent is a long-term challenge for percolative composites. In order to fix the applicable range of GCHs/PVDF composite, Fig.3-7b illustrates the relationship between integrating dielectric property and GCHs loading content. The horizontal red line corresponds to the loss tangent equals to 0.1, giving the applicable range for composites. While, the vertical red line indicates the obtained maximum permittivity and its corresponding GCHs loading content. Particularly, the maximum permittivity of ~105 can be achieved at the GCHs loading just below threshold. Such enhancement of permittivity at applicable range is competent to make GCHs as a promising candidate for energy storage applications.

It is worth to note that the percolation threshold f_c =5.53 vol.% achieved from GCHs/PVDF binary composite is much lower than that of GNPs/CNTs/PVDF ternary composite with the equivalent conducting phase fractions. Moreover, such low f_c is just a half of that of CNTs/PVDF composites (f_c = 10.4 vol.%) using the similar melting mixing procedure in our previous work.[134]

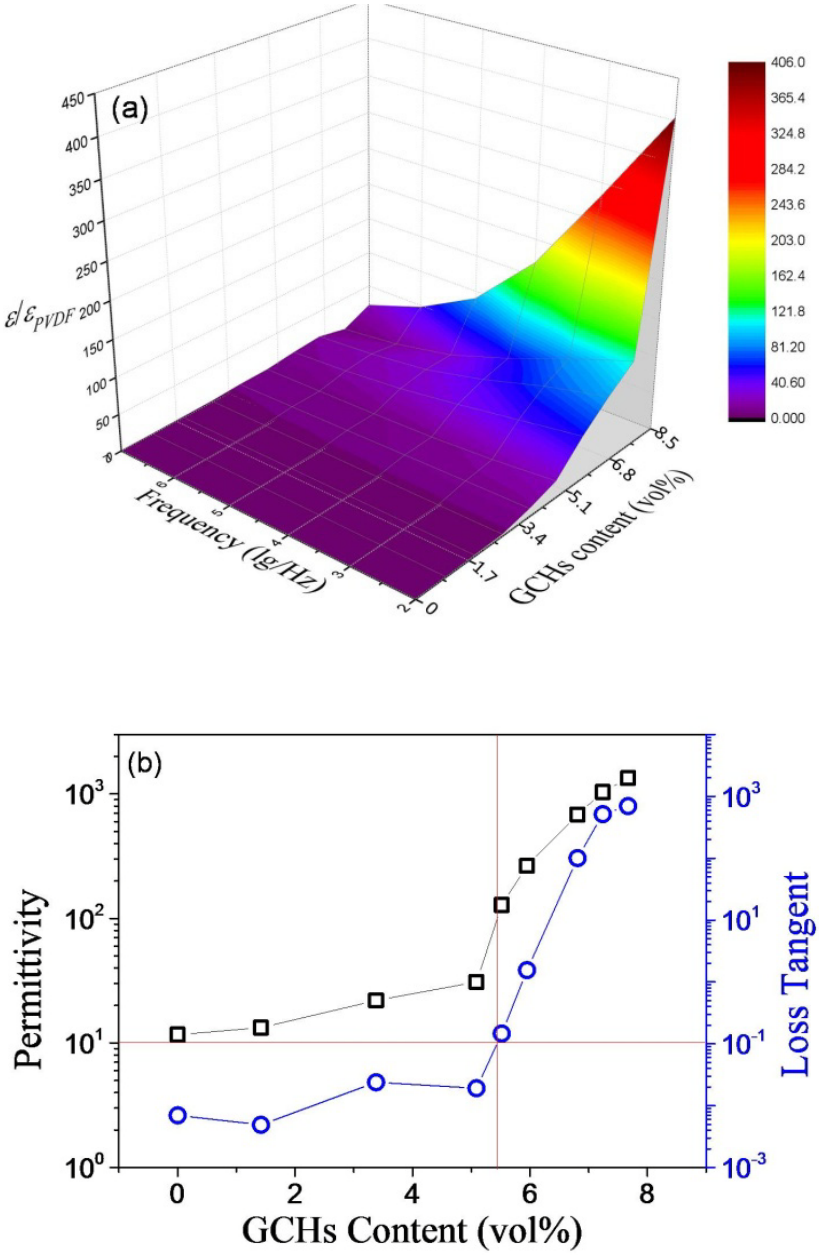

Fig.3-7 *(a)Dependence of the relative enhancement of the dielectric permittivity $\varepsilon/\varepsilon_{PVDF}$ on frequency and GCHs volume fractions;(b)Relative permittivity, loss tangent at 1kHz vs. GCHs volume fraction curves*

3.3.6.1 Typical microcapacitors construction

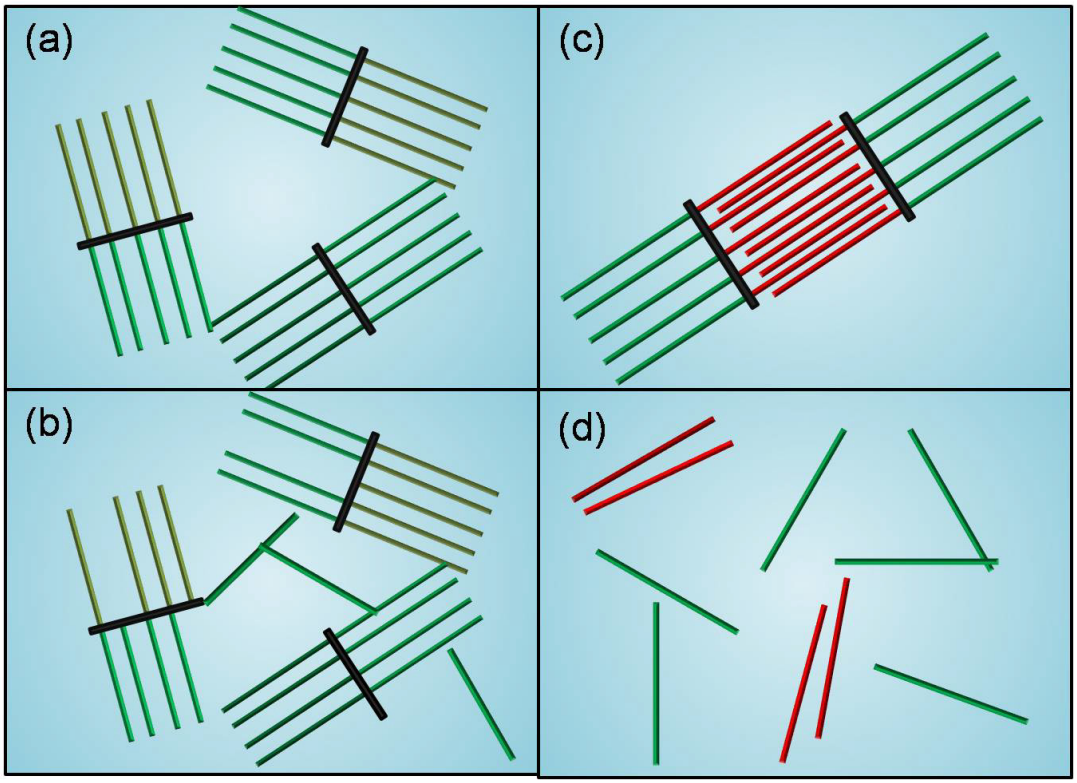

Fig.3-8 *Schematic diagrams of four different potential interaction approaches among the conducting phase of GCHs/PVDF binary composite: the electrical conducting among (a) GCHs-GCHs and (b) GCHs-CNTs, the microcapacitor construction formed by (c) GCHs-GCHs and (d) CNT-CNT. The synthesized CNTs, GNP substrate and microcapacitor construction are demonstrated as green sticks, black sticks and pairs of red sticks.*

Fig.3-8 schematically illustrates 4 different potential interactions among the conducting phase of GCHs/PVDF binary composite. As mentioned before, the totally conductive GCHs construction can be considered as a "wire concentrators", where each synthesized CNT served as a single conducting wire. These particular constructions possess large active space. Just a simple charge migration occurs between two CNTs of adjacent GCHs, respectively, could activate these two whole GCHs particles (both GNP substrate and every synthesized CNT connecting on the substrate) being conductive (see Fig.3-8a). Furthermore, honestly, it is unavoidable that certain CNTs were detached from the GNP substrate during melt-mixing process.

However, some of these detachments may serve as "bridges" in connecting neighboring GCHs electrically (see Fig.3-8b). Thus, the occurring possibility of electrical tunneling and ohmic conduction enhanced greatly, leading to such a low f_c of GCHs/PVDF binary composites obtained.

The achieved excellent dielectric performance could be attributed to several reasons. Firstly, the melt-blending process not only improves the filler dispersion, but also provides an intensive interaction at molecular level between π-electron clouds of GCHs and F groups of PVDF chains with strong electrophilicity. Although composites fabricated by melt-blending show higher f_c than ones by solution-blending in many reports, the melt-blending process that without solvent-pollution is the potential and practical way to achieve industrial mass production. Then, the reinforced Maxwell-Wagner-Sillars(MWS) effect contributes to the improved permittivity. The construction of vertically-aligned CNTs arrays benefits to ameliorate the CNTs aggregation and entanglement, expand interfacial area and promote the interfacial polarization effectively.

Moreover, be different from the average electrical field theory, the augmentation of permittivity when filler loading approaches to f_c could be explained by employing the microcapacitor model. Namely, conducting fillers distributed in the insulating matrix can form a series of filler-matrix-filler (electrode-dielectric-electrode) constructions. Thus, a large capacitance and then an improved permittivity can be contributed by the integrating effect of these microcapacitors. On one hand, due to the electrically conductive feature of GNP substrate, a typical microcapacitor structure could be achieved among GCHs particles. It is possible that CNTs arrays of neighboring hybrids insert to each other spatially to form the special microcapacitor construction, rather than the traditional microcapacitor structure formed by CNTs on the same substrate of other hybrids (see Fig.3-8c). On the other hand, a part of local microcapacitor structure can be formed by the randomly distributing detached CNTs as well (see Fig.3-8d). These two different microcapacitor modes make an indispensable contribution to the improvement of dielectric permittivity of

GCHs/PVDF binary composites.

3.3.6.2 Formation of β crystalline phase

Besides the contribution made by improved interfacial polarization and typical microcapacitor model, the crystalline phase composition of PVDF also plays an important role in determining the dielectric performance of PVDF-based composite. In fact, hemicrystalline PVDF displays two main crystalline forms: α- and β-phase. The former is a nonpolar crystal structure with a *TGTG'* (*T*-trans, *G*-gauche+, *G'*-gauche-) dihedral conformation arrangement in a centrosymmetric unit cell. However, the latter shows total *TTTT* conformation, leading to a polar non-centrosymmetric crystal. The particular structure endows the *β*-phase with the highest dipolar movement and superior dielectric performance, compared to other crystalline phases of PVDF.[275-278]

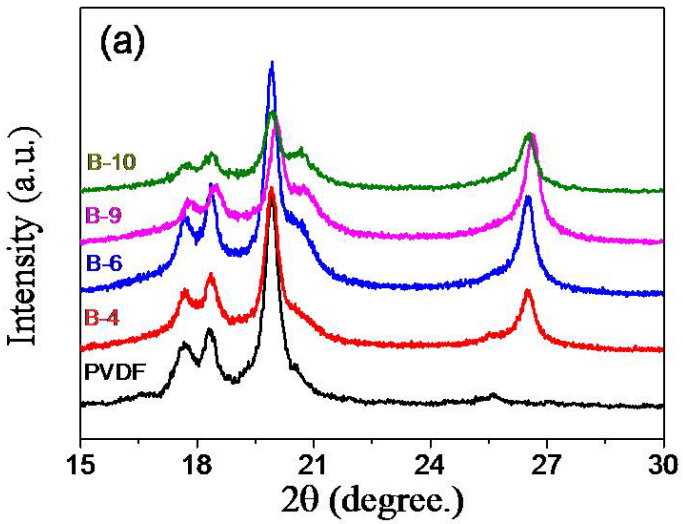

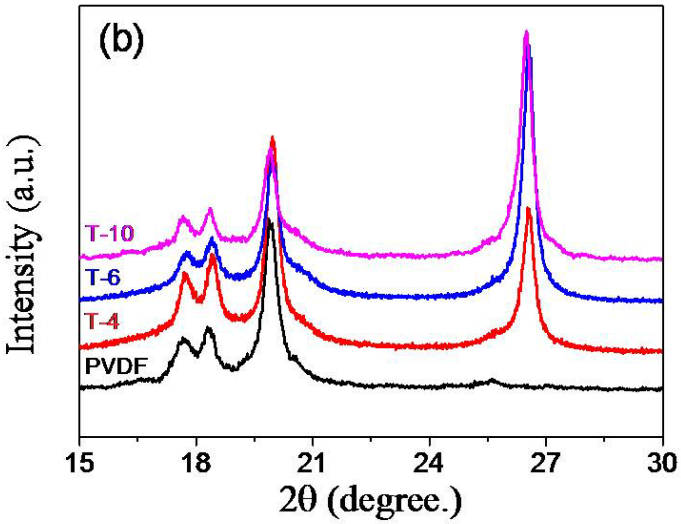

Fig.3-9 *X-ray diffraction patterns of pure PVDF polymer and (a) GCHs/PVDF binary composite: B-4, B-6, B-9 and B-10 and (b) GNPs/CNTs/PVDF ternary composite:T-4, T-6 and T-10.*

As mentioned before, the typical XRD peak at 20.26° corresponds to the β-phase PVDF. Notably, this typical peak can be detected from all the binary composites with different f_{GCHs}, but absent from any ternary composites. The relative comparison of XRD patterns between binary and ternary composites is presented in Fig.3-9.

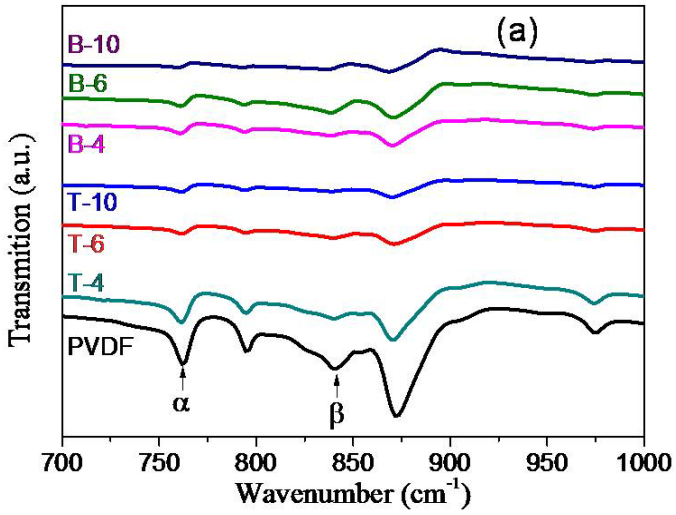

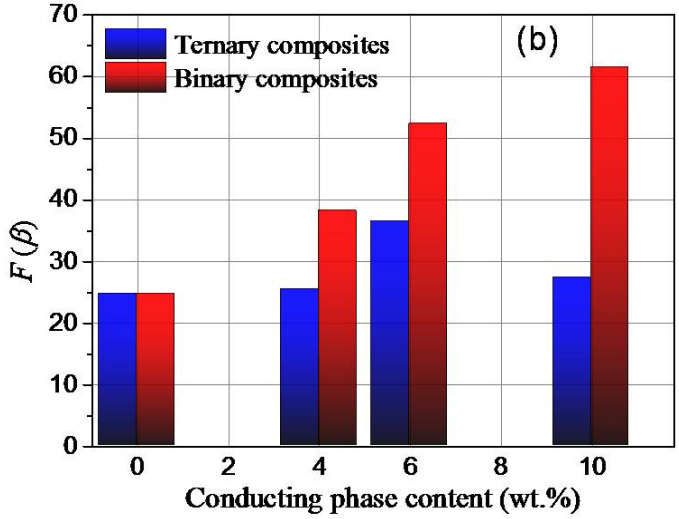

Fig.3-10 *Comparison of (a) FTIR spectroscopy and (b) fraction of □-phase of pure PVDF polymer, GCHs/PVDF binary composites and GNPs/CNTs/PVDF ternary composites with equivalent conducting phases of 4 wt.%, 6 wt.% and 10 wt.%, respectively.*

FTIR spectroscopy was performed to identify crystalline forms and phase composition of pure PVDF and the PVDF-based binary and ternary composites. Presented in Fig.3-10a is the achieved infrared spectroscopy where the marked transmittance bands 766 cm^{-1} and 840 cm^{-1} corresponding to α- and β-phase, respectively. The relative fraction of the β-phase ($F(\beta)$) can be evaluated by:[277]

$$F(\beta)=\frac{A_\beta}{(K_\beta/K_\alpha)A_\alpha+A_\beta} \tag{3-5}$$

where A_α and A_β are the area of the absorbance peaks at 766 cm^{-1} and 840 cm^{-1}, respectively; K_α and K_β the absorption coefficients at the respective wavenumber, which values are $6.1*10^4$ and $7.7*10^4$ cm^2 mol^{-1}, respectively.

The relevant $F(\beta)$ of samples pure PVDF, composites B-4, B-6, B-10, T-4, T-6 and T-10 were calculated and displayed in Fig.3-10b. It is observed that the $F(\beta)$ of binary composites is higher than that of ternary ones with same conducting phase loading. Notably, in contrast with pure PVDF polymer, the $F(\beta)$ of B-10 increased by surprising 150%. This unexpected result could be explained as that: usually, the β-

phase of PVDF can be transformed from α-phase via stretching process which gives rise to an alignment of polymer chain into crystals. The molten injection molding is able to provide a torque to GCHs, leading to an orientation along the injecting direction to a certain extent. Compared to the entangled CNTs and stacked GNPs of ternary composites, oriented GCHs and their vertically-aligned CNTs arrays benefit the alignment of PVDF chain into crystals along the CNT arrays and the formation of β-phase. Thus, the dielectric performance of binary composite achieved further improvement.

3.3.7 Temperature dependence of dielectric properties

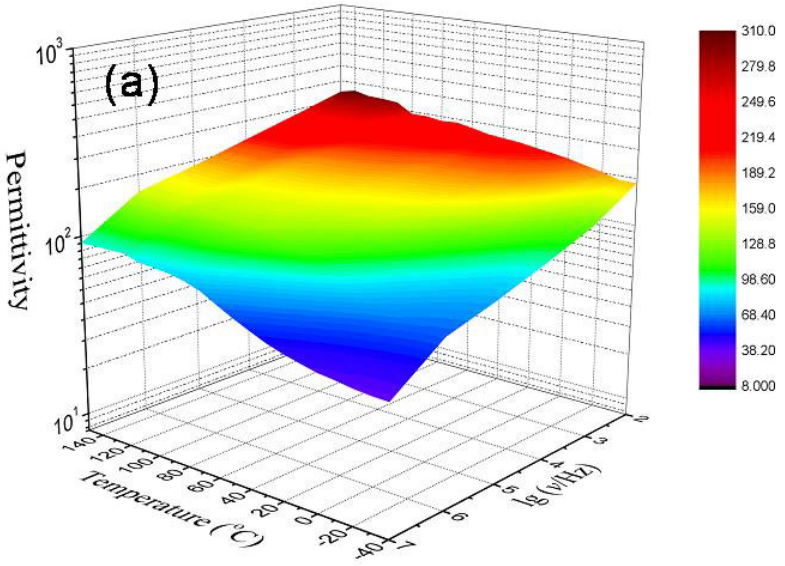

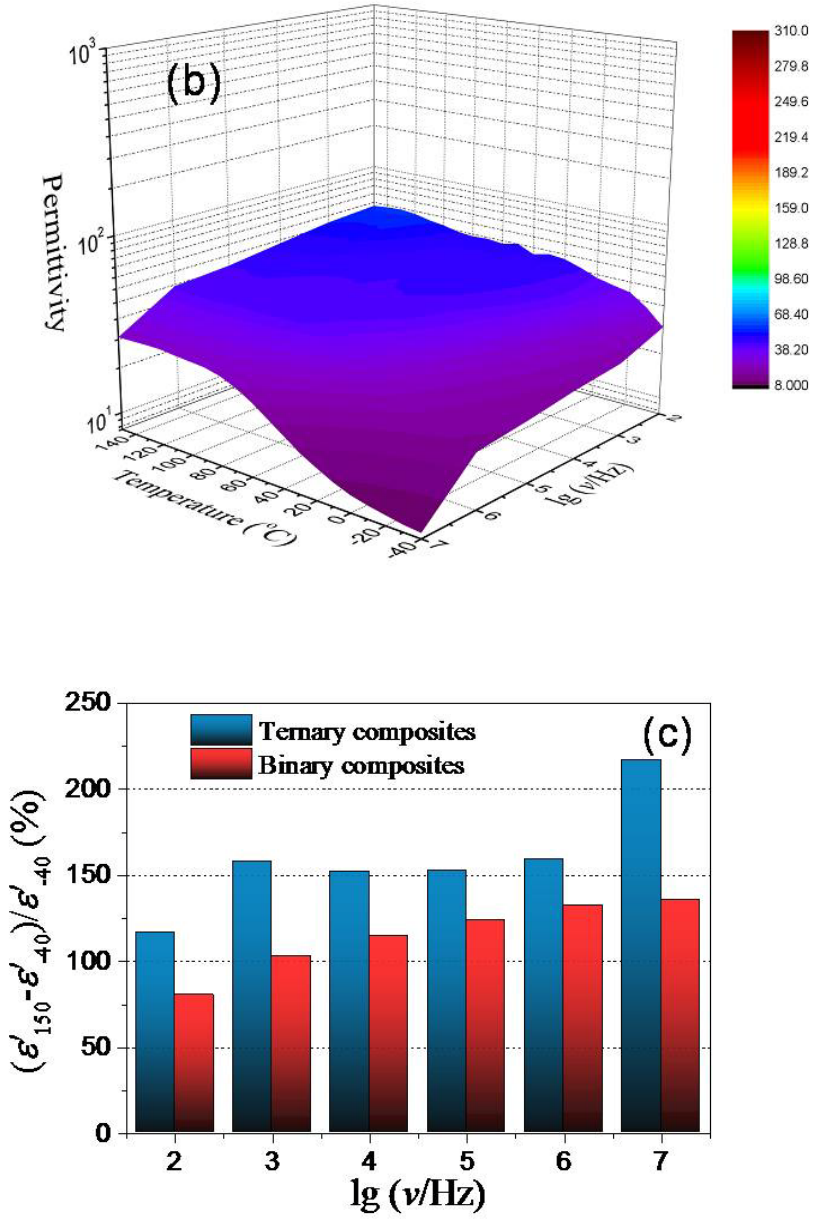

Fig.3-11 *Dependence of relative permittivity on frequency and temperature for (a) GCHs/PVDF binary composite B-6.5, and (b) GNPs/CNTs/PVDF ternary composite T-6.5. (c) The dependence of variation percentages of permittivity on frequency at two testing boundary temperatures: -40 °C and 150 °C.*

In order to investigate the influence of temperature on dielectric properties and compare the thermal stability of binary and ternary composites, Fig.3-11a and b illustrate the permittivity of samples B-6.5 and T-6.5 at wide temperature range of -40 °C to 150 °C. Under the same color map scales, the binary composite shows a

significantly high permittivity values than ternary ones. Be similar to the dielectric response at room temperature, the permittivity of both binary and ternary composites reduces with the increasing frequency under wide temperature range.

In addition, a distinct positive temperature-dependent dielectric permittivity are noticed, which can be ascribed to that: PVDF is semi-crystalline polymer with T_g~-20 ^oC and T_m~160 ^oC. At the room temperature and below, the movements of PVDF crystalline chains are limited, which is hard to respond to the external electrical fields. However, with the enhancing temperature, the mobility of PVDF chains, especially the chains in the crystalline region, is able to liberate significantly.[222, 279-280] Thus, the enhanced polarization gives rise to the improvement of permittivity.

The comparison of thermal stability of binary and ternary composites is demonstrated in Fig.3-11c. For evaluating quantitively the thermal stability of permittivity, the variation percentages of permittivity at testing boundry temperatures $((\varepsilon'_{150}-\varepsilon'_{-40})/\varepsilon'_{-40})$ were calculated, where the ε'_{150} and ε'_{-40} are the permittivity measured at the temperature -40 and 150 ^oC, respectively. It is noticed that under the full testing frequency range, the binary composites show smaller change of permittivity than ternary counterpart. The reinforced MWS effect resulted from greatly increased interfaces between GCHs coupling constructions and PVDF matrix could be responsible for the higher thermal stability of GCHs/PVDF binary nanocomposites.[127, 134]

3.4 Conclusions

In conclusion, we have demonstrated that GCHs/PVDF nano-dielectric composites with improved dielectric performance were prepared. The typical totally-conductive and lightweight GCH constructions were achieved by using CCVD method, where vertically-aligned CNTs arrays can be well synthesized on the surface of a number of exfoliated GNP substrates. The mechanical melt-mixing process can not only offer the good filler dispersion, but also provides an intensive interaction at

molecular level. More importantly, the way of restricting the utilization of chemical solvent is potential to drive the mass-production of the composites into industrial scale. Compared to the ternary counterpart with equivalent conducting phase contents, the GCHs/PVDF binary composites showed a significant transition from semi-conducting to conducting state when the GCHs loading increased to 10 wt.%. Due to the conducting coupling construction of GCHs, a greatly reduced percolation threshold of binary composites was obtained (5.53 vol.%) according to the classic threshold theory. The parallelly-arranged CNT arrays are able to promote the formation of microcapacitor networks and induce the variation of crystalline phases composition of PVDF matrix, which should be responsible for the improved dielectric properties of binary composites. In addition, the results of temperature-dependent permittivity showed that compared to the mixture of GNPs/CNTs served as filler, loading GCHs is capable of endowing PVDF-based composite with a higher thermal stability. The approach of redesigning the CNTs construction can effectively ameliorate the CNTs dispersion and reduce the percolation threshold, providing a promising strategy for energy storage applications in future.

Chapter IV

Flexible GNP-CNTs hybrids/PDMS functional elastomers

4.1 Introduction

Piezo-resistive (PR) materials with merits of flexible, sensitive and easy-production, allowing applied pressure to be quantified through corresponding electrical resistance changes,[256, 281-283] have drawn great interests for their applications in many fields, such as finger sensing, artificial-skin and wearable electronic devices.[94, 284-287] In order to combine the intrinsic advantage of each component and effectively widen their applications, recently, composing conductive fillers with flexible polymer matrix as composites becomes an efficient approach. According to the percolation theory, the typical PR behavior is generally observed at the filler concentration beyond the percolation threshold (f_c), where the formed internal conductive network reconstructs itself synchronizedly with external applied pressure, showing a measurable electric resistance deviation.

High sensitivity is the key issue of evaluating the PR behavior of composites, which can excite more pronounced resistance change response under a slight stimulus. To maintain the flexibility of polymer matrix and design the conductive network reasonably have been considered as effective approaches in improving the PR sensitivity. To retain the intrinsic flexibility, a number of studies have focused on decreasing the f_c of composites.[230] In fact, the conductive network structure is strongly dependent on the shape and aspect ratio of fillers. The composites with carbon black and metallic particles as 0-dimensional (0D) conductive fillers showed

remarkable PR response, owing to their high intrinsic electrical conductivity.[284, 288] However, to form conductive network, the high filler loading could inevitably destroy the flexibility of composites. In very recent years, a blooming development made graphene as one of the most popular and competitive nano-fillers, due to its extraordinary overall performance.[289-290] Their 2-dimensional (2D) structure can substantially increase interfacial adhesion with matrix, and endow composite with optimized performance. Nevertheless, the difficulty, time and cost of the composite processing procedure have to be raised by the enormous surface energy of graphene. In our previous report that the alkyl was grafted onto graphene as conductive loading, PDMS based composites showed high sensitivity and low f_c.[253] Whereas, much solvent was utilized which limited the possibility of industrial-scale production in short term. Graphite nanoplatelets (GNPs) served as another type of 2D filler, composing of tens of natural flake graphite sheets, have endowed the composites with excellent performances in recent researches.[232, 291-292] However, it is believed that their functionality could be further improved by exfoliating GNPs into individual GNP layers. Among these conductive fillers, carbon nanotubes (CNTs) have been most intensively studied because their typical 1-dimensional (1D) structure with high aspect ratio and outstanding intrinsic properties. But how to solve the problem that CNTs are easily frizzy and entangled in the polymer matrix is a long term challenge. It is worthy to mention that the high aspect ratio structure of CNTs could lead to opposite influences on reducing the f_c and enhancing the PR sensitivity, respectively. On one hand, it has been proved that the percolation threshold is inversely proportional to the aspect ratio. On the other hand, in contrast to the CNTs with high aspect ratio, those with low aspect ratio prefer to orientate with the deformation, hence their composites would show higher sensitivity to external stimulus.

To overcome these problems, a special coupling micro-architecture of GNP-CNTs hybrids (GCHs) was synthesized through the approach of CCVD. Different from other CNTs-substrate hybrid structures, GCHs served as the distinctive conductive filler with features of all-carbon composition, particular coupling structure

and low intrinsic density. Especially, GNP substrates are capable of working as the "wire concentrators" or "transport hubs", connecting with all the conductive single CNTs as "sideways" directly. These electrical conductive "hub" structures could effectively promote the interconnection among hybrids and facilitate the formation of conductive network. In addition, the PR behavior of composite based on micro-nano hybrids have rarely been reported, particularly for the all-carbon GCHs loaded composite.

Polydimethylsilicone (PDMS) that utilized as the flexible matrix of PR composite has received a wide attention and great approval, due to its excellent thermal stability, fast response speed, high elasticity, easy-production and low-cost.[293] Notably, the particular biocompatibility of PDMS could benefit the potential application as artificial skin.

In this chapter, we present the advanced GCHs/PDMS composites with high PR performance, prepared through mechanical blending GCHs with PDMS matrix using the three-roll mill at room temperature. The GCHs particles with 1D-2D coupling structure were precisely synthesized by CCVD approach. The mechanical blending process without chemical solvent can not only keep the hybrid structure from breaking but provide an excellent interfacial adhesion with matrix. In comparation with PDMS-based composites loading equivalent CNTs, GNPs, mixture of GNPs/CNTs, an ultra-low percolation threshold and the significant positive PR behavior with high sensitivity and stability of GCHs/PDMS composite were achieved. The temperature-dependent PR behavior indicates that the composite can be successfully served as temperature sensor. In addition, the result of the typical finger-sensing experiment indicates that the route of designing conductive network to improve the PR performance of flexible composite is reasonable. The GCHs/PDMS composite could be potentially applied as artificial skin with high PR performances.

4.2 Experimental

4.2.1 Materials and sample preparation

Graphite nanoplatelets with hundreds nm in thickness and 4-5 μm in diameter, provided by Xiamen K-Nano Graphene Technology Co.(China) The commercial MWCNTs provided by Shenzhen Nanotech Port Co. (China). Their length and diameter were about 5-15 um and 20-40 nm. The hydroxyl-terminated PDMS (50 000 mPa·s, from Sigma-Aldrich) was chosen as the flexible insulating elastomer matrix in our experiment.

The GCHs particles were synthesized through the floating-catalyst CVD method without any pre-treatment, according to the procedures in chapter 2. The mixing process of GCHs/PDMS nanocomposite was done using a three-roll mill (EXAKT 80, Germany) at room temperature, with the hybrid volume fraction ranging from 0 to 1.5 vol.%. A long mixing time (45 min) and a low mixing shearing rate (50 rpm) were used for not only obtaining an excellent dispersion but also keeping the hybrid architecture from being damaged caused by an over-strong mechanical shear as much as possible. Then, the curing agent tetraethyl orthosilicate and an accelerant dibutyltindilaurate (both from Sigma-Aldrich) were added into the mixture. The resulting composite was poured out into a metal mould and cured under a nominal compression of 100 bar, at room temperature. The final disk-shape samples with diameter of 10 mm and thickness of 3 mm were prepared for uniaxial compression. The rectangle film samples with area of 10×80 mm^2 and thickness of 150 μm were prepared for finger sensing(see the Fig.4-1).

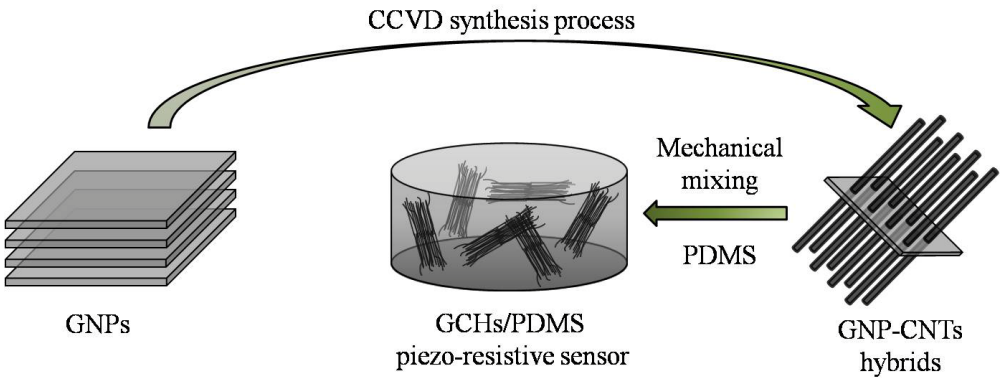

Fig.4-1 *Schematic illustration of the preparation of GCHs particles and GCHs/PDMS composites.*

4.2.2 Sample characterization

General Characterization. Scanning electron microscope (ZEISS LEO 1530 Gemini) was used to observe the morphology of the fillers and the fractured surfaces of GCHs/PDMS composite. The dielectric performances were evaluated in the frequency range of 10^3-10^6 Hz using an impedance analyzer (Solartron 1260). X-ray diffraction (XRD) patterns of the GCHs/PDMS composites were measured on XRD detector (BRUKER D2 PHASER with X Flash 430).

Real-time piezoresistivity testing. The real-time piezoresistivity tests were carried out on a combination of a universal testing machine (Instron 5544) and an electrometer (Keithley 2400). Loading-unloading compression cyclic operation with a constant crosshead rate of 1 mm·min^{-1} and the measurement of volume electrical resistance by the two-probe method well performed, respectively. To reduce the contact resistance, Pt electrodes were coated onto both sides of the samples through the plasma sputtering approach prior to the measurement. The electrical performance data were recorded through a LabVIEW program. The temperature-dependent PR performance was characterized as a function of temperature using supporting temperature chamber.

4.3 Results and discussion

4.3.1 Morphological characterization

Both the fillers distribution and the interfacial condition between fillers and matrix play crucial roles in evaluating the stability of composites. Fig. 4-2(a) shows the SEM morphology of the fractured surface of the GCHs/PDMS composite, where GCHs are well distributed in the soft PDMS matrix without aggregation. The 1D-2D coupling structure displays the maximum effective surface, leading to a largely augmented interfacial adhesion. Furthermore, the individual CNTs are bonded on the GNP substrate and separated to each other by the insulating PDMS matrix, forming the conductive "hub" structure. The "hub" structure can be embedded tightly in PDMS matrix without obvious break (see Fig. 4-2b), which makes GCHs/PDMS composite scalable from laboratory to industrial scale.

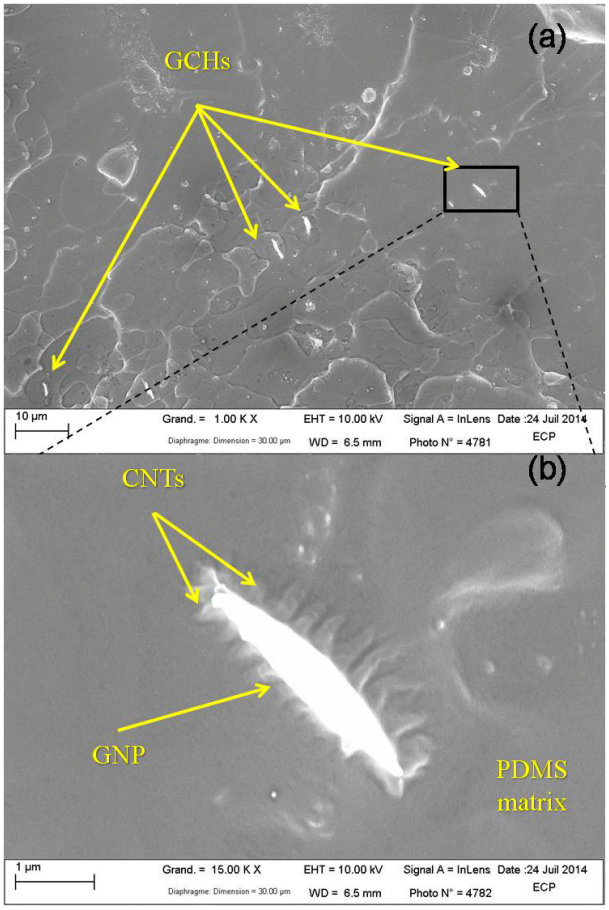

Fig.4-2 *(a) SEM image of the fracture surface of the GCHs/PDMS composite. (b) High-magnification image of GCH particle well embedded in the matrix.*

4.3.2 Electrical performance

4.3.2.1 Enhanced dielectric permittivity

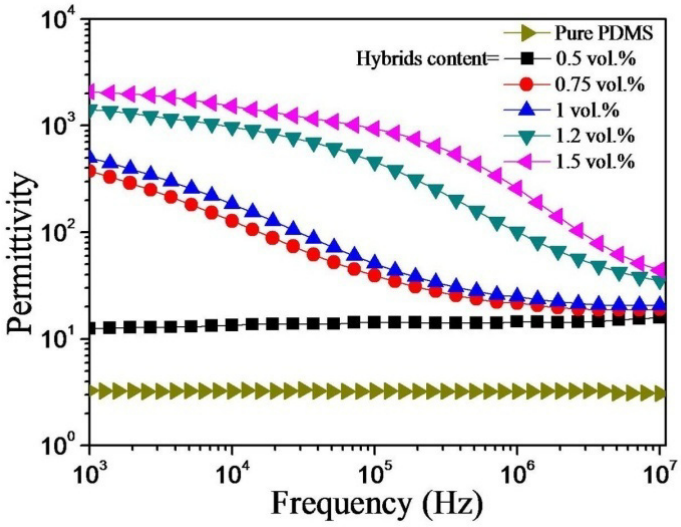

Fig.4-3 *Dependence of dielectric permittivity on frequency of the GCHs/PDMS composites with different GCHs loading at room temperature.*

In order to ascertain the percolation threshold, the important signal of forming the conductive network, the dielectric performance of GCHs/PDMS composite in the frequency range of 10^3-10^7 Hz was characterized. As demonstrated in Fig.4-3, the dielectric permittivity of composite enhanced significantly with the increasing GCHs loading. Particularly, only 1.5 vol.% GCHs can augment the dielectric permittivity of composite 700 times higher than the PDMS matrix ($\varepsilon_r \sim 3.3$) at 10^3 Hz. When over the f_c, the permittivity exhibits an obvious frequency dependence, which is mainly because that newly formed conductive networks are prone to be influenced by the alternating electric field, and the polarization rate of composite cannot keep up with

the changing electric field immediately

4.3.2.2 Low percolation threshold

The dielectric percolation effect is one of the most important signals of forming the conductive network, hence the electrical performance of GCHs/PDMS composite was characterized. Fig. 4-4 demonstrates the dependence of AC conductivity (σ_{AC}) of GCHs/PDMS composite on filler concentrations at the frequency range of 1 kHz - 1 MHz, from which an obvious percolation transition from insulating (σ_{AC}~10^{-9} S m^{-1}) to conducting (σ_{AC} ~10^{-2} S m^{-1}) with the increasing GCHs loading can be noticed. Notably, more than 4 orders of magnitudes rise of σ_{AC} can be achieved under the range of GCHs loading from 0.5 to 0.9 vol.%, illustrating the constructing process of inner conductive network. The conductivity of composite that approaches to the percolation threshold can be evaluated using the following power law:

$$\sigma \propto \left(f_{\mathrm{GCHs}} - f_c\right)^t \qquad \text{for } f_{GCHs} > f_c \qquad 4\text{-}1$$

where f_{GCHs} and f_c are the volume fraction of conductive GCHs particles and the percolation threshold of the composite, respectively, and t is the critical exponent in the conducting region. The best fits of the experimental conductivity values to the log-log plots of the power laws provides f_c = 0.64 vol.% (see the inset in Fig 4-4). The critical exponent in the conducting region, t = 1.76, is in accord with the universal values ($t \approx$ 1.6-2) for the composite loading three-dimensional conductive fillers from the percolation theory. It is worthy to note that such low percolation value was rarely reported in most PDMS-based composite using the carbon series materials as conductive filler. It mainly ascribed to these fully conductive multiple-branching “hub” structures, which can not only enhance the interfacial area and polarization, but extend their effective contact space. Thus, the construction of internal conductive network was facilitated effectively.

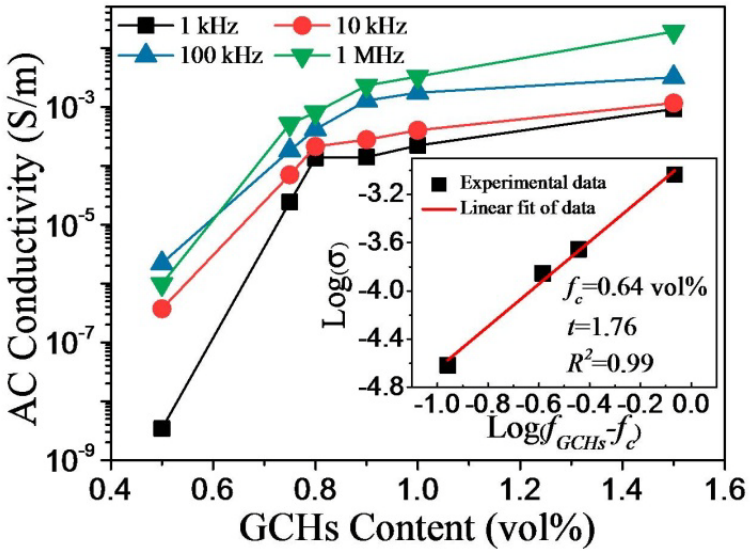

Fig.4-4 *AC conductivity of the GCHs/PDMS composites with different GCHs loading at room temperature. The inset shows the best fit of log(σ) vs. log(f_{GCHs}-f_c)*

4.3.3 Application as highly-sensitive piezo-resistive pressure sensors

4.3.3.1 Loading concentration-dependent piezo-resistive behavior

To study the relationship between PR behavior and the GCHs loading under relevantly low stimulus, the maximum applied pressure was restricted to 0.32 MPa. The resistance change (R/R_0)-pressure curves averaged from more than 3 independent tests are depicted in Fig.4-5. A step-wise compression (1 mm min^{-1}) was applied to the disk-shape samples until the maximum force. A series of positive pressure dependence of resistance can be observed for all tested GCHs loading. Noteworthily, the composites with filler concentrations in the vicinity of the percolation threshold show larger resistance changes under same pressures than those with much higher filler concentration. Due to the particular conductive structure of the GCHs, the sensitive conductive network can be formed at such low concentration via the tunneling effect. However, with increasing filler content, the connection mode of conductive network transfers from the tunneling state to the filler overlapping state, in which there are

enough quantity of GCHs to overlap each other. Thus, the inner conductive network becomes relatively stable, and insensitive to external stimulus.

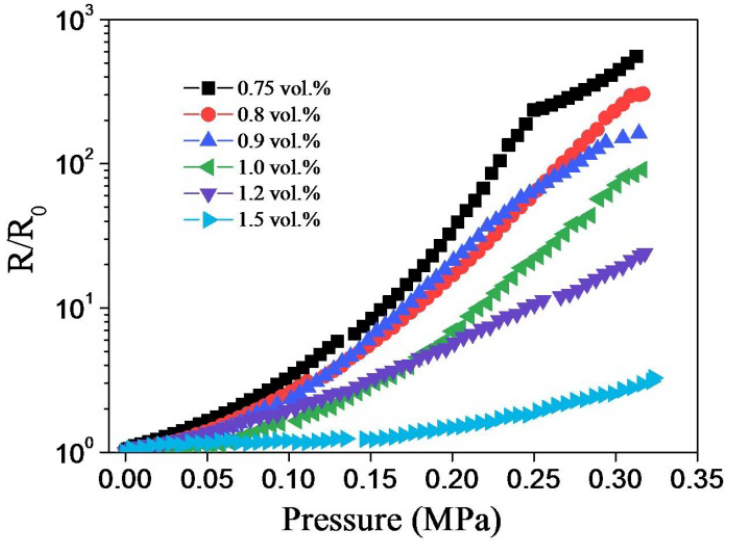

Fig.4-5 *Typical PR behaviors variation of GCHs/PDMS composites with various GCHs loading under uniaxial compression.*

4.3.3.2 Piezo-resistive sensitivity

Sensitivity is one of the most important parameters to evaluate the functional property of PR materials. It is better for composites to possess the large response under slight stimuli. Fig.4-6 presents the relative resistance change of composite with GCHs 0.8 vol.% under very low compression loads: 1N, 2N, 3N and 4N. Due to the area of sample is 7.85×10^{-5} m^2, their pressure sensitivities can reach to 0.16 kPa^{-1}, 0.26 kPa^{-1}, 0.27 kPa^{-1} and 0.34 kPa^{-1}, respectively. Such high sensitivities obtained under ultralow compression loads make GCHs/PDMS composites competent for highly sensitive sensing application. In addition, even under compression load as low as 1N, the outputting resistance signal can well express the whole loading-unloading process.

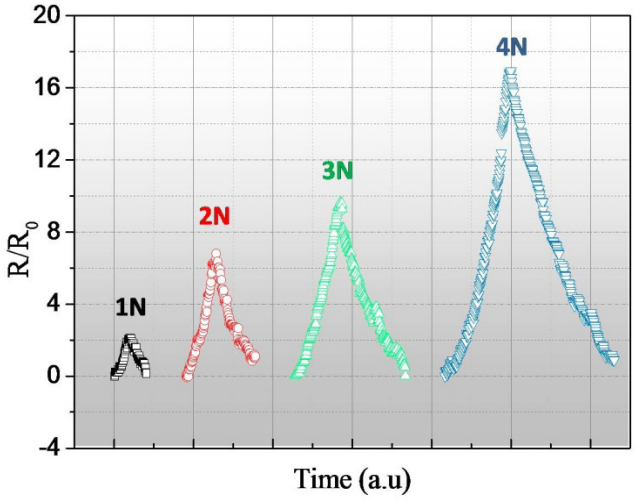

Fig.4-6 *The relative resistance change of composite with GCHs 0.8 vol.% under a very low charge, showing an excellent piezo-resistive sensitivity.*

Generally, the sensitivity of strain sensors and pressure sensors can be evaluated by the gauge factor (GF) and pressure sensitivity (PS), respectively.[291]

$$\mathrm{GF} = \frac{\Delta R / R_0}{\Delta l / l_0} = \frac{\Delta R / R_0}{\varepsilon} \tag{4-2}$$

$$\mathrm{PS} = \frac{\Delta R / R_0}{p} \tag{4-3}$$

where R_0 is the nominal resistance in the unloaded state (pressure and strain are equal to 0), ΔR is the resistance change, l_0 and Δl are the original thickness of sensor sample in the unloaded state and the thickness change, respectively, p is applied pressure. The dependence of GF and PS values, calculated by the average during the cyclic tests without the first cycle, on filler concentrations was illustrated in the Fig.4-7.

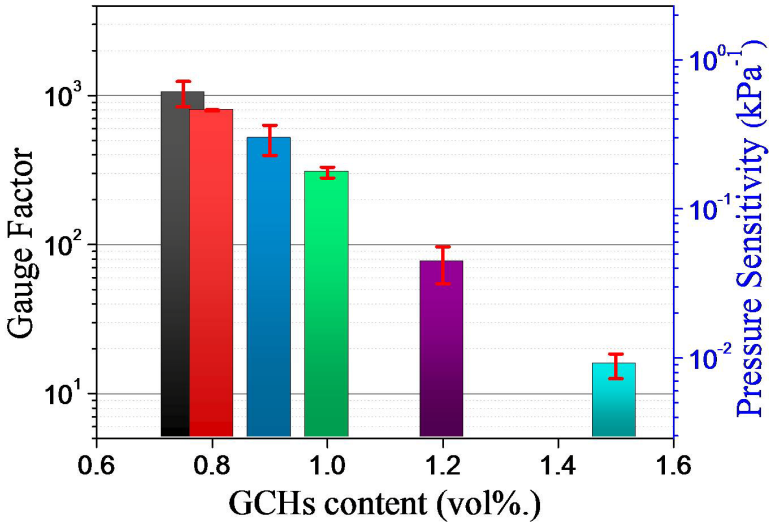

Fig.4-7 *Piezo-resistive sensitivities of GCHs/PDMS composites with various GCHs loading under uniaxial compression.*

Similar to the AC conductivity, both GF and PS values decrease with the increasing filler content. Especially, an outstanding sensitivity (GF~10^3, PS~0.6 kPa^{-1}) can be achieved from the sample with the GCHs content of 0.75 vol.% under the pressure of 0.32 MPa. This result is quitely competitive among reported carbon filler/ PDMS composites (see Table.4-1).

Table 4-1*. Comparison of the piezo-resistive sensitivity of carbon-fillers/PDMS composites under the small applied pressure.*

Type (specific)	f_c *(vol.%)*	PS*(kPa^{-1})	GF	Conditions	Ref
GNP-PDMS	0.9	0.067		0.3 MPa	[94]
CB-PDMS	-	-0.001		0.3 MPa	[294]
CB-PDMS		<0.001		0.3 MPa	[295]
CNT-PDMS	-		1.25	Strain~0.4	[296]
CNT film-PDMS	-	~0.33		3 kPa	[15]
Carboxyl-MWCNT-PDMS	-	0.013		3 MPa	[297]
CNT-PDMS	-		~2-3	Strain~100%	[298]
P3HT-CNT-PDMS	-	0.0017		0.12 MPa	[299]
CNT-CB-PDMS	-				[300]

(AR of CNT=117)		0.01		0.3 MPa	
(AR of CNT=437)		0.01		0.3 MPa	
Alkyl-Graphene-PDMS	0.63	<0.1		1 MPa	[253]
GCHs-PDMS	0.56	0.6	~1000	0.32 MPa	

*The pressure or strain sensitivities were calculated and estimated from the curves in relevant references.

Thanks to the "hub" structure, on one hand, one GCH particle can be totally activated by and conducted to another through even just an one-point contact or weak tunneling effect taking place on any single CNT of GCHs(see Fig.4-8). On the other hand, the relatively low percolation threshold could well retain the flexibility of PDMS matrix for composite, allowing a large deformation under small pressure. Therefore, the composite is greatly sensitive to the applied pressure.

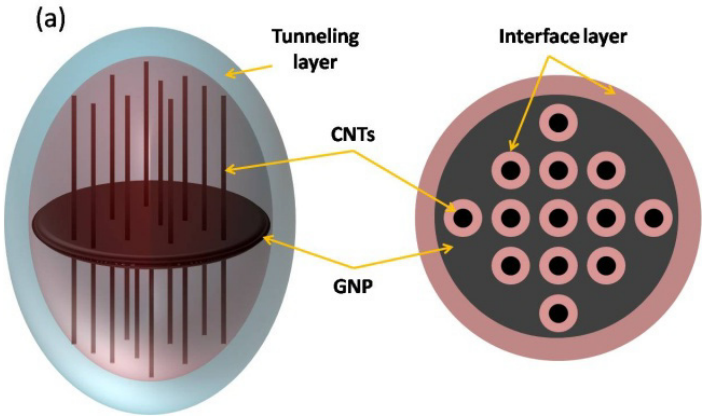

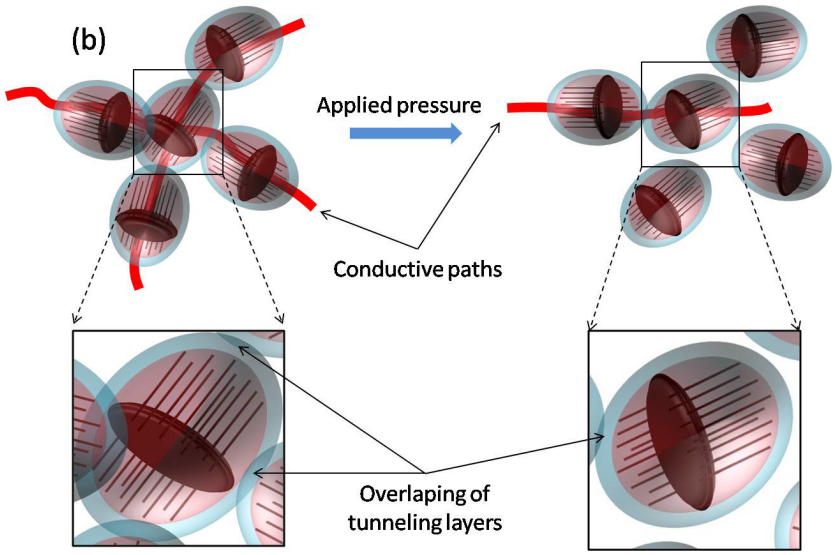

Fig.4-8 *Schematic of (a) the construction of GCHs with improved interfacial area and effectively conductive space. (b) the "hub" structure of GCHs is capable of multi-point communicating with neighboring particles via direct contact or tunneling effect. While, the multi-point communicating is easily influenced by applied pressure, transforming the conductive "traffic hub" to the "isolated island"*

4.3.3.3 Theoretical explanation

By reason of its stable performance, the sample with 0.8 vol.% GCHs was chosen to study the piezo-resistive behavior of the GCHs / PDMS composite in detail (see Fig.4-9a). Based on the influences on conductive network that induced by the increasing external pressure, the piezo-resistance correlation can be devided into three parts. A sequence of exponential fitting were made for each part, according to the modified formulas that derived from the tunneling effect (see insets in Fig 4-9a). Fig.4-9b illustrates schematically the inner conductive network constructions for three parts, respectively.

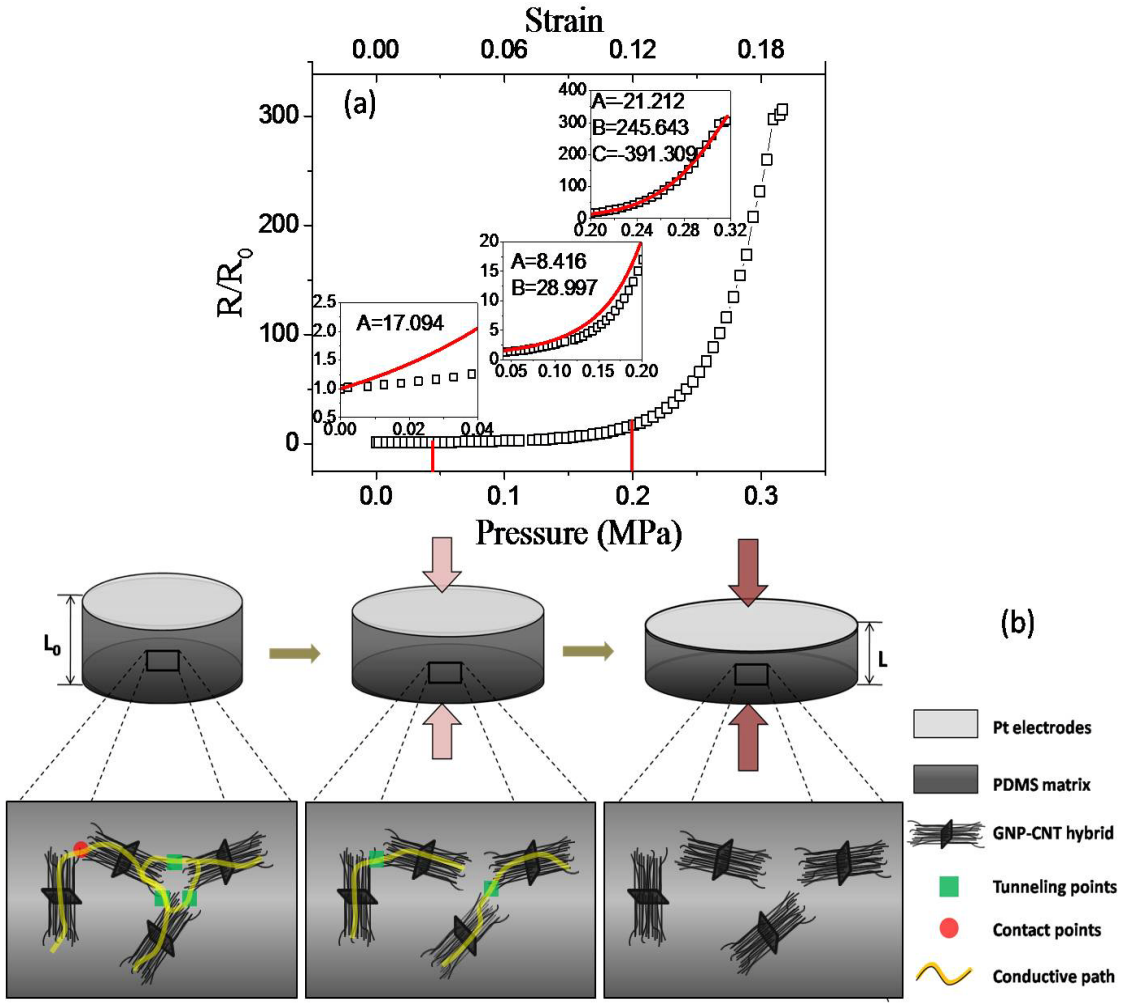

Fig.4-9 *(a)The resistance change on the applied pressure and strain of GCHs/PDMS composite with 0.8 vol.%. GCHs. The inset images show the 3-step theoretical fit of experimental data. (b) Schematic diagram of the dependence between the internal conductive network structure and the external applied pressure of 3 steps.*

The fitting models were derived from the previous electrical resistance model, which are as follows:[94]

$$\frac{\mathrm{R}}{R_0}=\left(\frac{Ns}{N_0 s_0}\right)\exp\left[\frac{4\pi}{h}\sqrt{2m\varphi}\left(s-s_0\right)\right] \tag{4-4}$$

$$s=s_0\left[1+\left(\frac{|l-l_0|}{l_0}\right)\right] \tag{4-5}$$

$$p=E\left(\frac{|l-l_0|}{l_0}\right) \tag{4-6}$$

Where R, R_0, N, N_0, s, s_0 are the total resistance of composite, the number of conductive paths and the minimum distance between conductive fillers of loading state and initial unloading state, respectively. l is the thickness of disk-shaped composite under applied compression, l_0 is the initial thickness. h the Plank constant and m the electron mass. φ is the potential barrier height between the neighboring fillers. p and E are the applied compression pressure and elastic modulus of composite, respectively.

Firstly, the fully conductive network that is mainly made up via the tunneling effect among fillers. A tiny resistance change can be observed under the applied pressure from 0 to 0.04MPa. Hence, we call the first part as "tunneling state". Due to the influence of applied pressure to the re-orientation of fillers is slight, the correlation of piezo-resistive behavior of this part is as follow:

$$N = \frac{N_0}{\exp\left[A_1\left(\left|l - l_0\right|/l_0\right)\right]} \tag{4-7}$$

$$\mathrm{R}/R_0 = \left(1 + p\right)\exp(A \times p) \tag{4-8}$$

Where A_1 is a constant, A=[$\frac{4\pi}{h}\sqrt{2m\varphi}$ s+A_1]/E.

When the applied pressure increases to 0.04-0.2 MPa, this range is defined as "transitional state". In this state, GCHs particles begin to move and re-orientate with the deformation of PDMS matrix. Some initial contacting joints loosen and others are separated. The former ones continue connecting the circuit to keep the functionality of the conductive network through the tunneling effect. However, the latter ones are responsible for the partial break of the conductive paths. Therefore, the resistance of composite exhibits a measurable enhancement. The relationship between R/R_0 and the pressure can be fitted as follow:[94]

$$N = \frac{N_0}{\exp\left[A_2\left(\left|l - l_0\right|/l_0\right) + B\left(\left|l - l_0\right|/l_0\right)^2\right]} \tag{4-9}$$

$$\mathrm{R}/R_0 = \left(1 + p\right)\exp(A \times p + B \times p^2) \tag{4-10}$$

Where A_2 and B are constants, A=[$\frac{4\pi}{h}\sqrt{2m\varphi}$ s+A_2]/E.

With the further increasing pressure, more intense re-orientation takes place. The distance between two GCHs becomes beyond the tunnel distance. Plenty of GCHs are separated by the continuous and insulating PDMS matrix, resulting in the "discontinuous state". Due to the special network construction, a small re-orientation of GCHs might result in a huge role transformation from the "transport hubs" to the "isolated islet", subsequently damaging the conductive network. Hence, the composite with GCHs as conductive units is more sensitive to the applied pressure. The modified function used to fitting PR behavior is:

$$N = \frac{N_0}{\exp\left[A_3\left(|l-l_0|/l_0\right)+B\left(|l-l_0|/l_0\right)^2+C\left(|l-l_0|/l_0\right)^3\right]} \quad (4\text{-}11)$$

$$\mathrm{R}/R_0 = (1+p)\exp(A\times p + B\times p^2 + C\times p^3) \quad (4\text{-}12)$$

Where A_3, B and C are constants, $A=[\frac{4\pi}{h}\sqrt{2m\varphi}\,\mathrm{s}+A_3]/E$.

According to the Equ.4-8, 4-10 and 4-12, the resistance change of mentioned three states can be fitted exponentially, where the parameters of fittings are summerized in Table.4-2

Table 4-2. *Fitting coefficients and R^2 of three states.*

	Initial state	Transitional state	Discontinuous state
A	17.094	8.416	-21.212
B	-	28.997	245.643
C	-	-	-391.309
R^2	0.966	0.99	0.998

4.3.3.4 Synchronicity and repeatability

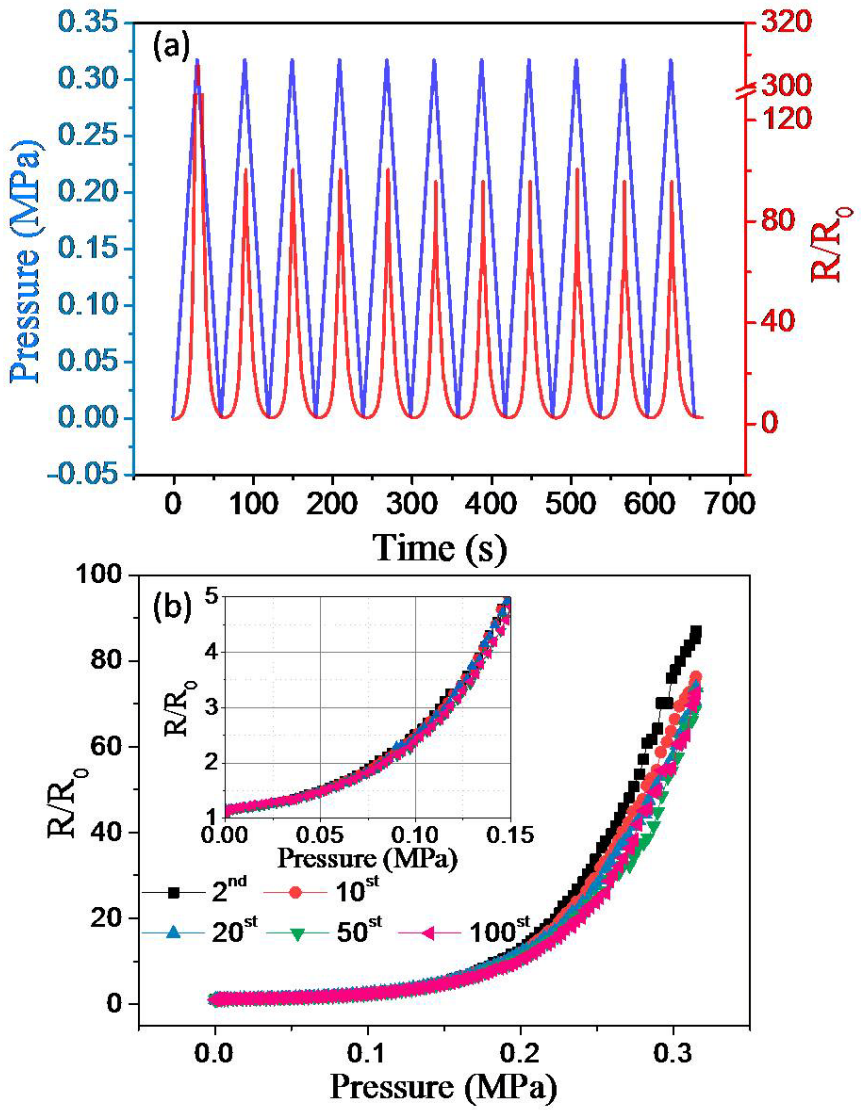

Fig.4-10 *(a) The relative resistance (R/R_0) and applied pressure vs. time under periodic loading-unloading tests; (b) (R/R_0) under 100 loading-unloading cycles with the pressure ranging from 0-0.31MPa. The inset shows the consistent PR response under 100 loading-unloading cycles with the small applied pressure ranging from 0-0.15MPa.*

Besides high sensitivity, rapid electrical resistance response and excellent repeatability are also considered as critical properties of ideal piezo-resistive materials. To detect the dynamic synchrony between the cyclic pressure and corresponding

resistance change, the multi-cycle piezo-resistive tests were done on the sample with GCHs 0.8 vol.%. An excellent real-time response with little hysteresis and shoulder peak was noticed in the Fig.4-10a. Although a distinct piezo-resistive response at the first cycle was observed resulted from the Mullins effect,[301] the stable and excellent resistance changes (R/R_0 >90) can be achieved in the following 10 cycles. An excellent repeatability is a decisive property for practical application. Fig.4-10b shows that the long-term PR behavior of the composite with 0.8 vol.% GCHs during 100 loading-unloading cycles under the pressure range (0-0.32 MPa). Although the value of R/R_0 can be stably maintained over 70, there were a small decline of maximun resistance change and a slight augmentation of minimum resistance change after a high number of cycles. This could be interpreted by that the structure of the conductive networks was permanently modified by long term periodic loading-unloading process. Particularly, in our experiment, this permanent modification could be dependent on three aspects. Firstly, the continuous breakdown-reconstruction process of GCHs conductive network. Secondly, there is an irreversible modification of the interfacial interaction between GCHs and PDMS matrix. Thirdly, the inherent structure of GCHs fillers might be broken under the fast and long term alternating charge. In addition, the minimum R/R_0 value augments slightly with the increasing cycle numbers, which further indicates that the structure of the conductive networks was permanently modified indeed. Besides, in the range of ultra-low stimulus (lower than 0.1 MPa) the piezo-resistive response tends to provide an excellent consistency (see the inset of Fig.4-10b).

4.3.3.5 Temperature dependence of the piezo-resistive properties

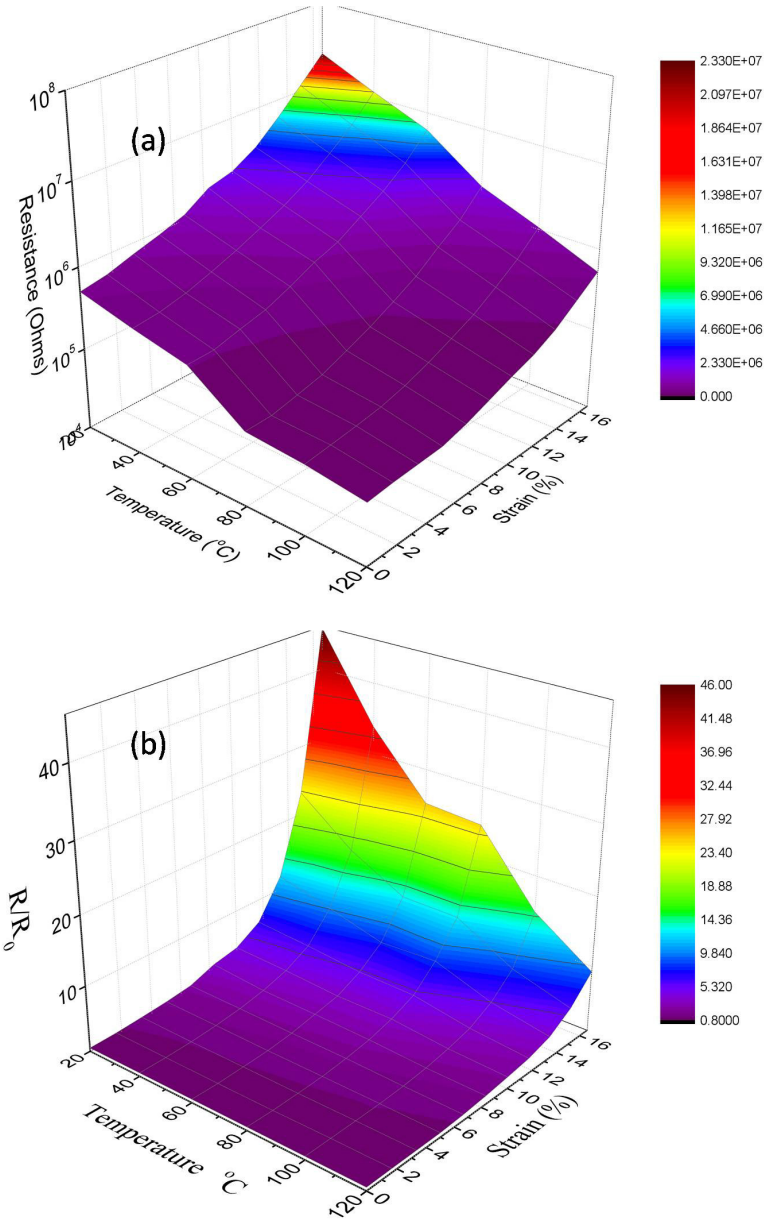

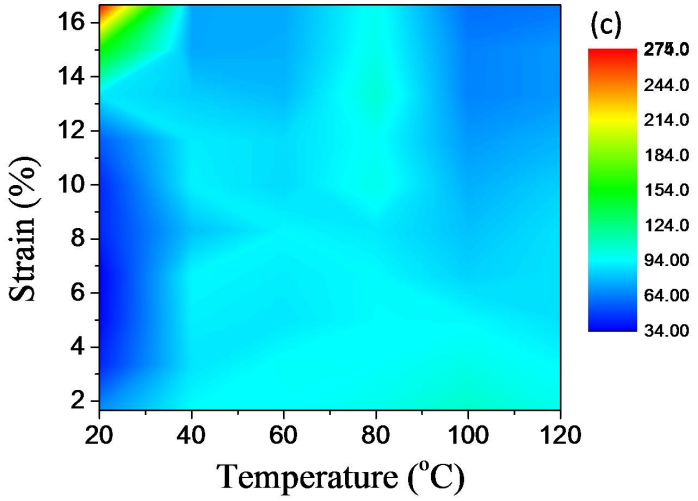

Fig.4-11. *Temperature-dependent PR property of GCHs/PDMS composites. (a) Resistance change (b) relative resistance enhancement at the function of temperature and applied strain. (c) The distribution of gauge factor in the temperature-strain matrix.*

Sensing temperature is another key functionality of human skin that is able to keep people from injury and offers information about the surrounding environment.[256] In fact, majority of tactile sensors are inherently sensitive to temperature. As previously mentioned in Chapter-1, polymer-based composites loaded with conducting fillers exhibit large changes in resistivity with temperature, such as the PTC and NTC effect. The resistance change originates from the thermal expansion of the polymer matrix, giving rise to a modification of conductive network and a change to electrical resistance. However, due to the crosslinked molecule structure, PDMS has intrinsic relatively high thermal stability. Fig.4-11 shows the temperature-dependent PR properties of GCHs/PDMS composite with GCHs loading content about 0.8 vol.% under testing temperature range from 20 °C to 120 °C and the increasing compression strain until 17%. During the measurement, temperature of chamber and deformation of sample can be well controlled, the outputting electrical information can be recorded using the electrometer (Keithley 2400).

Fig.4-11a is the temperature-dependent resistance change under uniaxial

compression. It is observed that the electrical resistance of composite augments with increasing strain, namely, the typical positive piezo-resistive behavior, under the whole testing temperature range, which is in accordance with the results at room temperature. Besides, the electrical resistance shows a significant reduction when composite samples is heated. It could be explained as that the thermal agitation effect drives charges to move more easily. While, the expansion of free volume of PDMS molecular chains also provides a better surrounding to the movement of charges, which promotes the formation of conductive network.[280]

The temperature-dependent relative resistance variation (R/R_0) under increasing strain is exhibited in Fig.4-11b. It is worth to note that under the same strain, the R/R_0 at high temperature range is significantly higher than that at low temperature range. For example, under the maximum strain, the R/R_0 of composites equals to 45 at 20 ^oC and reduces to around 10 when is heated to 120 ^oC. In fact, according to the result of Fig.4-11a, the electrical resistance decreases sharply at high temperature, where the internal conducting network has been constructed stably and is not as sensitive as the initial conducting network at room temperature. Thus, such large drop of R/R_0 could occur.

The strain-sensitivity, namely, gauge factor indicates the varying rate of relative resistance change, which is a complex parameter influenced by a number of factors, such as internal conducting network, electrical conductivity and aspect ratio of filler, especially, the features of elastic crosslinking network. The distribution of gauge factor of GCHs/PDMS composite in the temperature-strain matrix is shown in Fig.4-11c. It is observed that at room temperature range, the GF values augment from around 40 to 270 at the maximum strain. This tendency can be explained by the previously mentioned model in section of Theoretical Explanation. However, at high temperature range, the GF value showed a slight decrease with increasing strain, which may be ascribed to the integrating effect of the expansion and strain-driving orientation of PDMS molecular network to the elasticity of composite.

4.3.3.6 Wearable finger film-sensor

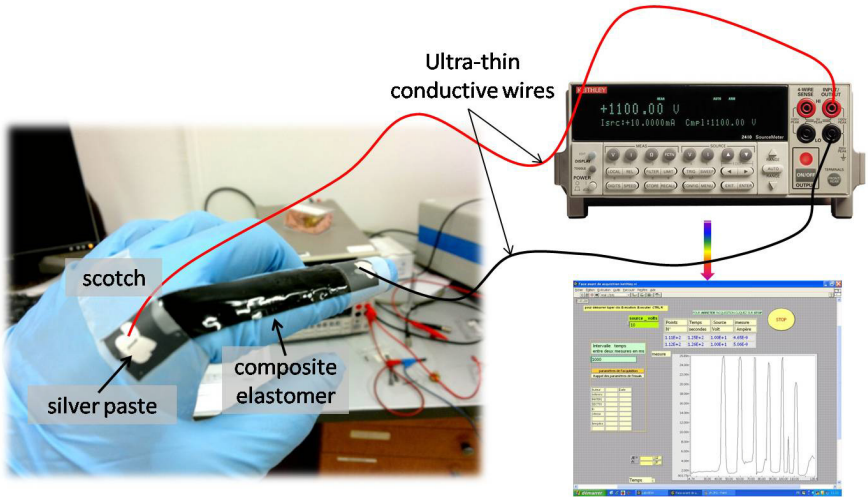

Fig.4-12 *Setup of the finger sensor testing system using the the typical GCHs / PDMS composite film as sensor.*

To achieve the promising functionalities of artificial skin such as human-machine interaction and motion recognition, the typical GCHs / PDMS composite film finger sensor was fabricated using the similar preparation process. The film finger sensor was fixed onto the surface of a stretchable nitrile glove. Silver paste was coated between the film finger sensor and the ultra-thin conductive wire (used for reducing the contact disturbance induced by movement) to reduce the contact resistance (see Fig.4-12).

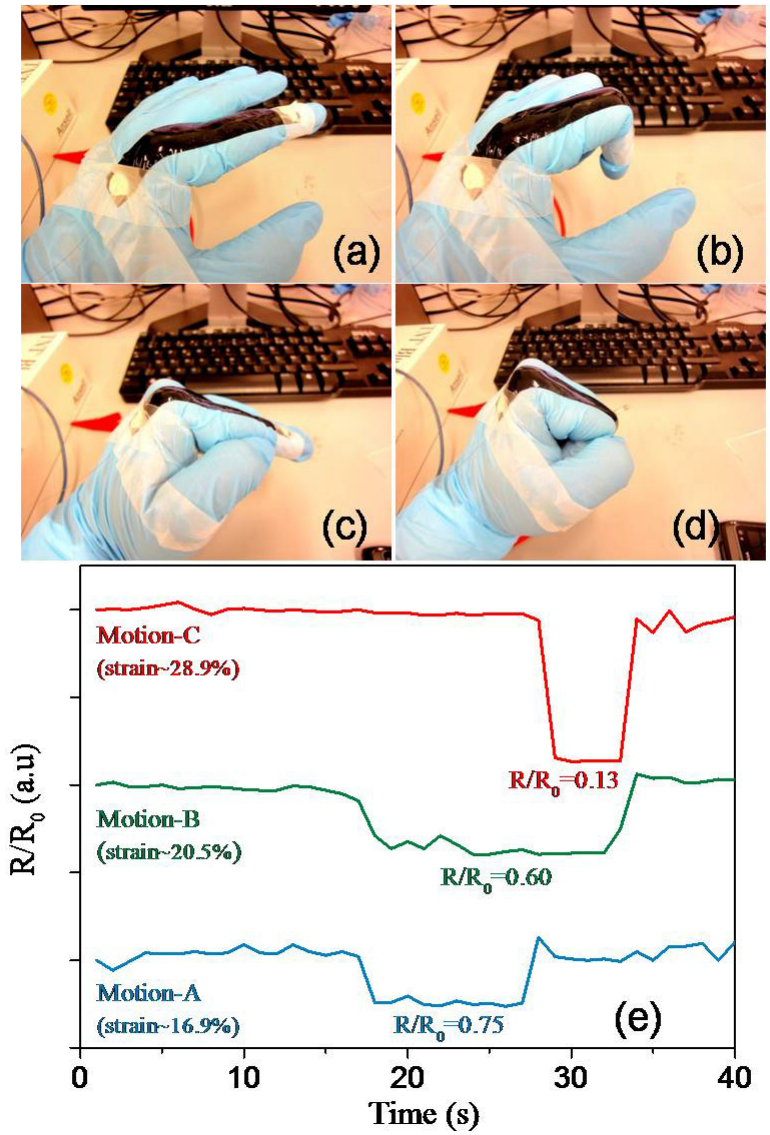

Fig.4-13 *The GCHs/PDMS composite film served as finger movements detections. (a) Photograph of the relaxing state of finger. (b-d) Photographs of three distinct motions (A, B and C) that bending the second joint, the third joint of index finger and clenching, respectively. (e) Relative resistance changes for each independent movement.*

As illustrated in Fig.4-13a, we considered the relaxing straight index finger as the initial state, the collected electrical signals were the base line. In Fig.4-13b-d, three simple motions were chosen to evaluate the response performance of film finger sensor: A, B and C are the motions of bending the second joint, third joint of index finger and clenching, respectively. Moreover, the tension deformation amplitudes of

these motions were calculated as 16.9%, 20.5% and 28.9%, respectively. Fig.4-13e shows the distinctive real-time resistance changes (R/R_0 of motions A, B and C are 0.75, 0.6, 0.13, respectively) and their unique duration times, which are perfectly in accordance with the different amplitudes of motions and corresponding action times. A particularly negative piezo-resistance response under tension deformations was revealed, because it is difficult for GCHs to orientate along the thickness direction during the pressure-casting process, especially for film samples. With the enhanced tension strain, GCHs prefer re-orientating near to the tension direction. The anisotropic degree increases correspondingly and the tunneling effect may take place more easily. Therefore, the composite film finger sensor that using GCHs as conductive filler can not only response to subtle actions but also distinguish them accurately, which makes the composite good candidate for artificial skin and wearable pressure sensor applications.

4.4 Comparison with PDMS-based elastomers using CNTs, GNPs and CNTs/GNPs mixture as conducting phase

4.4.1 CNTs or GNPs as the single conducting filler

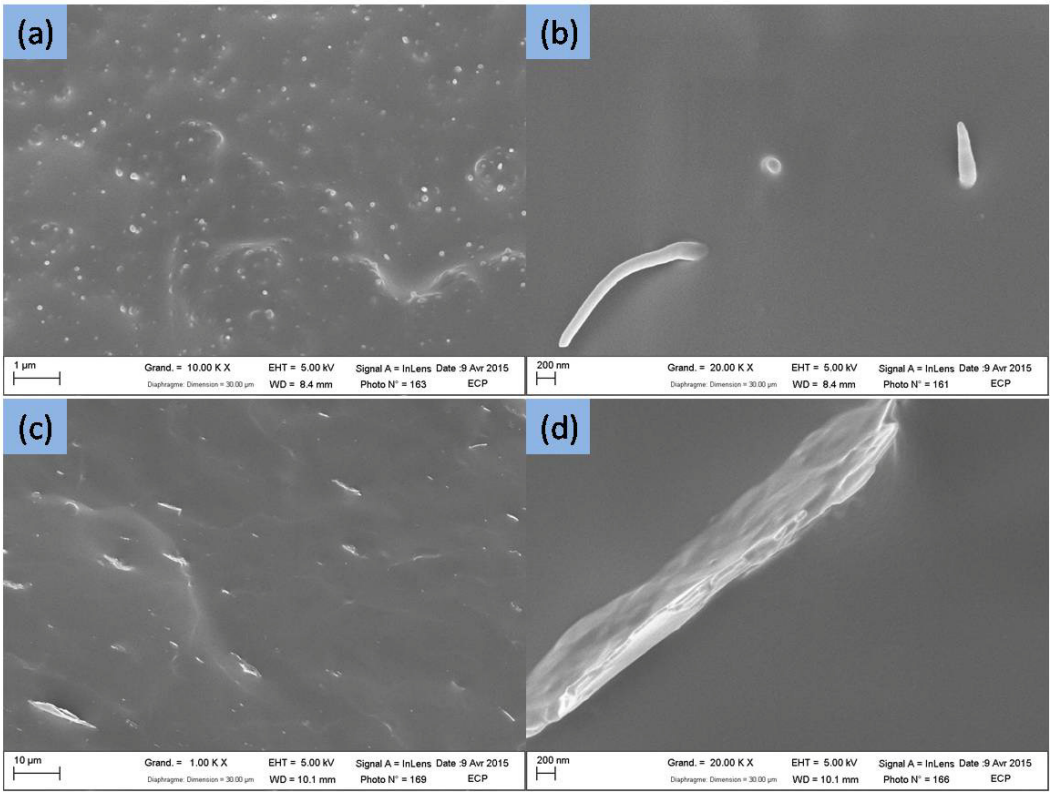

Fig.4-14 *Typical SEM images of fractured surface of (a) CNTs/PDMS composite and (c) GNPs/PDMS composite.(b) and (d) are the high-magnification images of (a) and (c), respectively.*

In order to make a comparison with GCHs/PDMS composite, the GNPs/PDMS and CNTs/PDMS composites were prepared with the similar processing procedure. Fig.4-14 shows that both CNTs and GNPs can be well distributed into the PDMS matrix using the mechanical blending approach, respectively. Similarly, the tight cohesion between conducting fillers and PDMS matrix can be clearly observed from the high-magnification images.

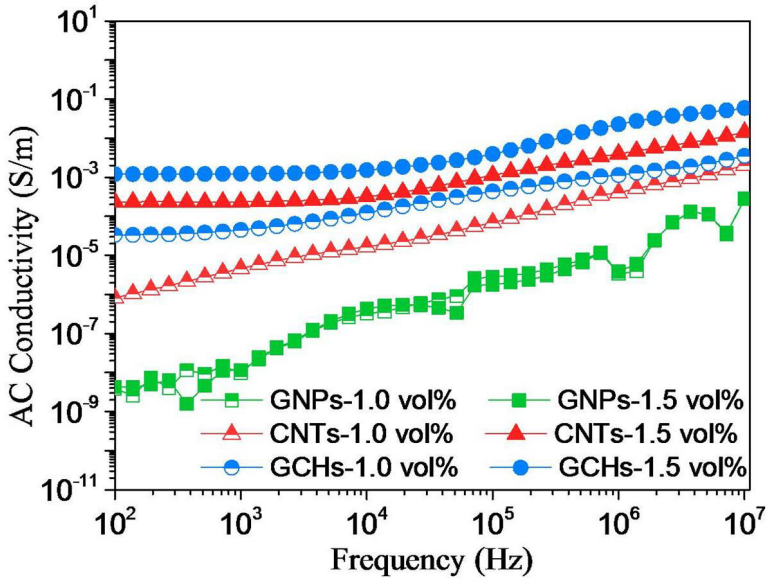

Fig.4-15 *The AC conductivity of PDMS-based composites loading GNPs, CNTs and GCHs with volume fraction of 1.0 vol.% and 1.5 vol.%, respectively.*

The electrical performance of CNTs/PDMS, GNPs/PDMS and GCHs/PDMS composites with two different volume fractions can be seen in Fig.4-15. Typically, the general percolation threshold (f_c) ranges of these 3 kinds of composites could be estimated from the testing results of AC conductivities. The f_c of both GNPs/PDMS (>1.5 vol.%) and CNTs/PDMS composites (~1.0 vol.%) is higher than that of GCHs/PDMS composites (~0.64 vol.%). Such low f_c could be ascribed to the effective interconnection among GCHs fillers. Due to the conductive network of samples cannot be formed when filler content lower than f_c, the sample with CNTs content of 1.2 vol.% was chosen to compare the piezo-resistive behavior with the composite with 0.8 vol.% GCHs (see Fig.4-16). Although the filler contents of two samples are close to their own f_c, the resistance change under 0.32 MPa of CNTs/PDMS composite is around 75, which is lower than that of GCHs sample (~95). Therefore, compared with CNTs/PDMS and GNPs/PDMS composite using the same processing procedure, the lowest percolation threshold can be achieved with GCHs/PDMS composites.

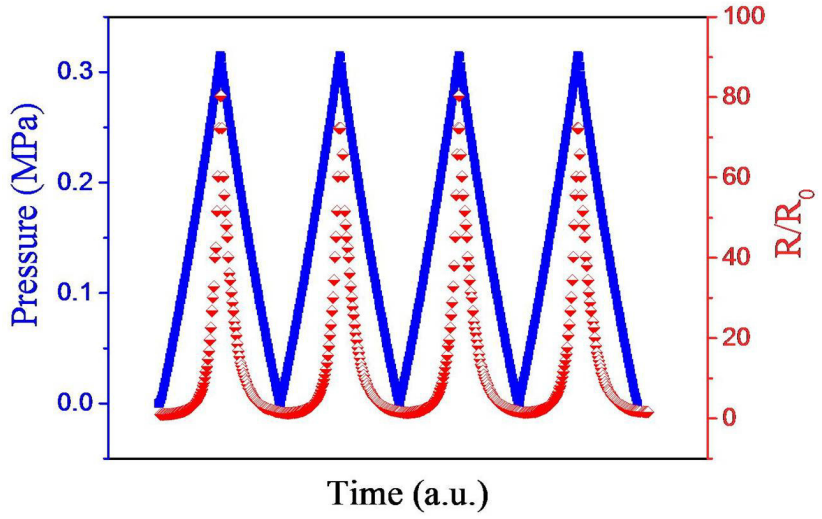

Fig.4-16 *The piezo-resistive behavior of CNTs/PDMS composite with CNTs content of 1.2 vol.%.*

4.4.2 CNTs and GNPs as the double conducting fillers

Recently, several groups reported that the hybrid nanofiller system with two or three different aspect ratios leads to better electrical property of composites, producing a typical synergetic effect. In order to further illustrate the distinctive role of GCHs particles in constructing conductive network, the equivalent double-formed filler of GNPs and CNTs filled PDMS-based composite were prepared. The weight ratio between individual GNPs and CNTs are carefully controlled as 1, which is in accordance with that of GCH particles. The concentrations for GCHs single filler and GNPs/CNTs double filler in composites are shown in detail in Table 4-3.

Table 4-3 *Different composition of 4 PDMS-based composite samples.*

Sample[1]	GCHs content (wt.%)	CNTs content[2] (wt.%)	GNPs content[2] (wt.%)
1	1.52	-	-
2	2.28	-	-

3	-	0.76	0.76
4	-	1.14	1.14

[1]Sample 3 and 4 are samples that GNPs/CNTs/PDMS three-phase composite with equivalent contents of GNPs and CNTs to GCHs/PDMS composites, sample 1 and 2, respectively.

[2]The mass ratio between CNTs and GNPs substrate of GCHs particles is approximately equal to 1.

The SEM images of the fractured surfaces of the GNP/CNT/PDMS composite are shown in Fig.4-17. After the mechanical mixing by the three-roll mill, GNPs and CNTs are well dispersed in the PDMS matrix. As shown in Fig.4-17b both nanoparticles are closely embedded in the PDMS matrix, indicating an excellent interfacial cohesion.

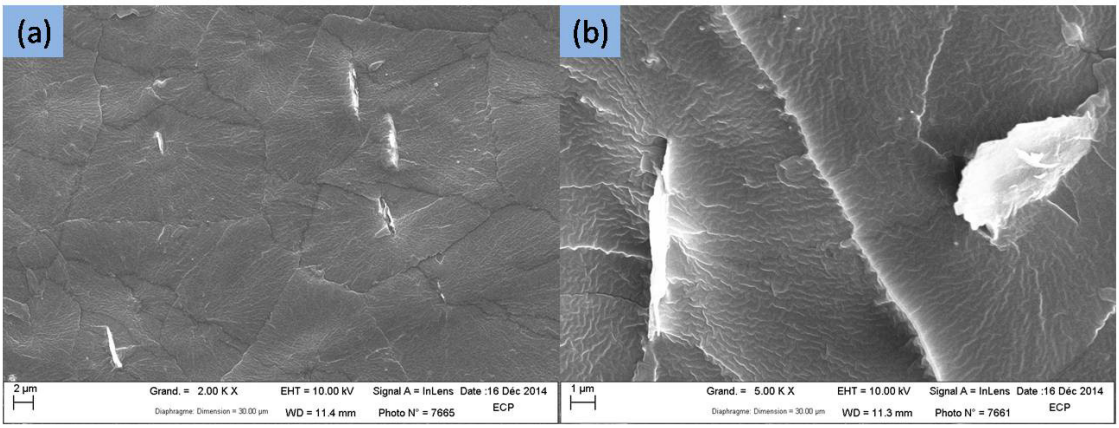

Fig.4-17 *(a) Typical SEM images of fractured surface of GNP/CNT/PDMS three-phase composite. (b) the high-magnification images*

Fig.4-18 shows the frequency-dependent dielectric properties of 4 samples. Compared to the pure PDMS polymer with the intrinsic permittivity of 3, both GCHs and mixture of GNPs/CNTs can effectively enhance the permittivity of composite under small loading contents. However, in comparison with the 3-fold increase obtained by GNPs/CNTs/PDMS composite, the equivalent addition of GCHs endows PDMS matrix with the surprising enhancement of permittivity near three orders of magnitudes at low frequency range (see Fig.4-18a).

In addition, as shown in Fig.4-18b, the values of AC conductivity of GCHs filled composites are higher than that of the mixture loaded counterpart more than 5 orders

of magnitudes.. Such distinction between conductor and insulator can be also proved by the large difference of loss tangent results (see Fig.4-18c).

The dramatic difference of dielectric properties between GCHs and mixture filled composites further indicates that GCH particles with their particular “hub” construction effectively improve the synergetic effect, leading to a more efficient conducting network and much lower percolation threshold.

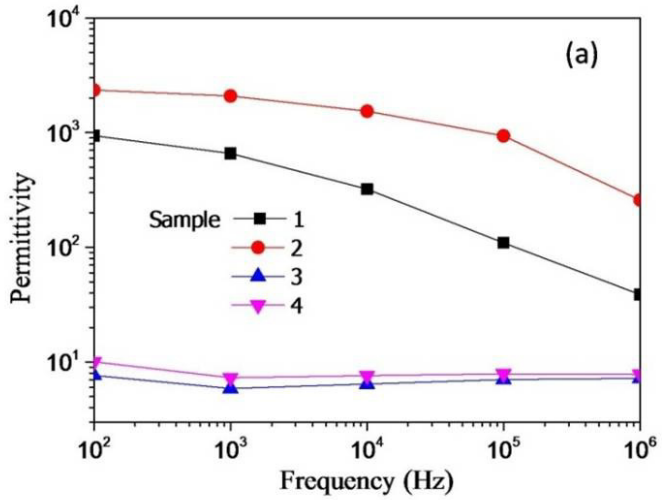

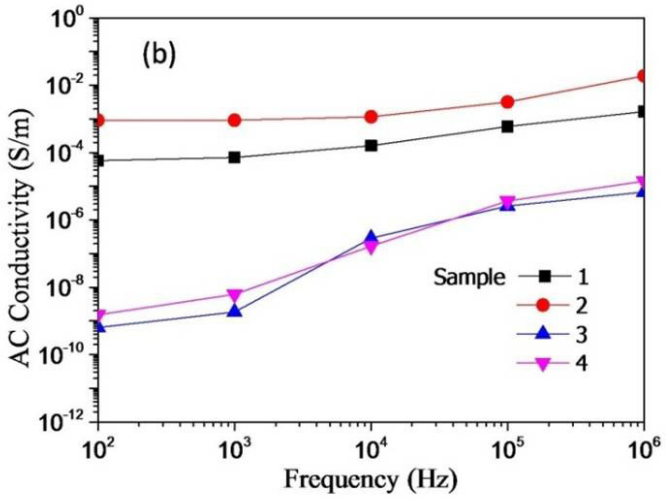

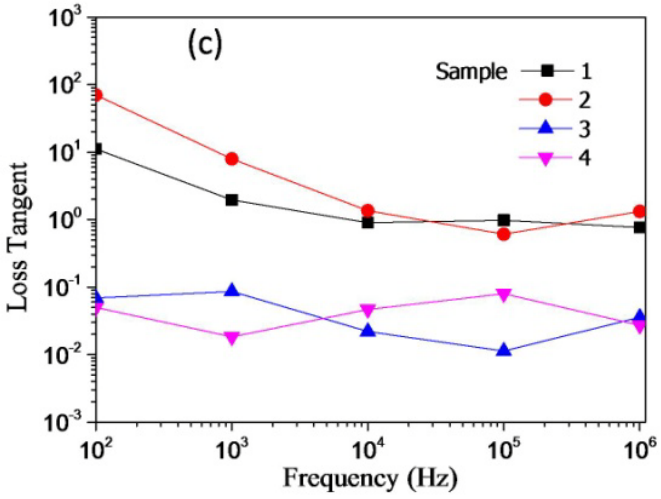

Fig.4-18 *Frequency-dependent (a) dielectric permittivity, (b) AC conductivity and (c) loss tangent of GCHs/PDMS composite and GNPs/CNTs/PDMS three-phase composite, respectively.*

4.5 Conclusions

In conclusion, the advanced GCHs/PDMS flexible composites with excellent PR behavior are prepared. The typical 1D-2D coupling GCHs structure is synthesized through the CCVD approach, in which GNPs aggregates can be effectively exfoliated to offer substrates for growing the vertically-aligned CNTs. Good dispersion and excellent interfacial adhesion can be achieved by the mechanical mixing process. According to the percolation theory, the composite shows a significant increase of AC conductivity with filler loading. An ultra-low percolation threshold (0.64 vol.%.) is achieved due to the "hub" structure of conductive units. Moreover, the modified 3-step theoretical exponential fit can well account for the more sensitive positive PR behavior of composite under uniaxial compression. Beyond the threshold, the PR sensitivity is inversely proportional to the GCHs content. Especially, the composite with 0.75 vol.% GCHs displays extraordinary sensitivity that the GF and PS value are as high as 10^3 and 0.6 kPa^{-1}, respectively. During the cyclic compression loading, the PR behavior of composites manifests a superior dynamic correspondency with applied

pressure. Meantime, the resistance response can retain at a relatively high level after 100 loading-unloading cycles. The temperature-dependent PR behavior indicates that the composite can make response to not only the deformation or applied pressure change, but also the operating temperature range. Notably, the typical finger-sensing experiment indicates that the GCHs/PDMS composites are competent to detect and even distinguish the slight finger motions. Compared to the PDMS-based composites filled with equvalent CNT, GNP or mixture of CNTs/GNPs, the GCHs/PDMS composites shows higher dielectric permittivity and electrical conductivity, an obviously lower percolation threshold and a higher PR performance. In summary, the strategy of conductive network design will contribute to the development of PR composites with higher performances and further drive the fabrication process to industrial scale.

General conclusions

This thesis is concentrated on designing, controlling and developing the GNP-CNTs hybrid micro-nano micro-architecture to ameliorate the dispersing problem of pristine CNTs in polymer matrix. The synthesized CNTs array construction endows both thermoplastics and thermosetting polymers with surprising functional properties. The main results could be concluded as follows:

I. Synthesis of GNP-CNTs hybrid construction.

Well-organized GNP-CNTs hybrid (GCH) constructions with distinct features of all-carbon composition, largely-improved specific surface area, totally-conductive structure and low intrinsic density were synthesized via floating CCVD process, where the grown CNT arrays vertically aligned on the surface of two-dimensional GNP substrates. The organizations of CNT arrays are greatly dependent on the various CVD parameters such as temperature, hydrogen ratios and synthesis time. A moderate synthesizing temperature around 650 ^{o}C benefits to exfoliate the pristine multi-layered GNPs into a number of individual-layered ones, promoting the deposition of carbon atomes and the growth of CNT arrays on these largely released platforms. At lower or higher temperature range, the growth of CNT arrays is inhibited by the inadequate decomposition of carbon source or the formation of amorphous carbon, respectively. With the increasing hydrogen ratio, the diameters of CNTs maintain in a stable range, while their length and corresponding aspect ratio showed a gradual reduction. Moreover, the mean length of synthesized CNT arrays quasi-linearly enhances with the reaction time, particularly, their corresponding slope was linearly fitted as 0.22.

The GCH construction with the mass ratio of CNTs and GNP substrate approximated at 1 can be achieved through precisely controlling temperature, hydrogen ratio and reaction time of 650 ^{o}C, 30%, and 10 min, respectively. Due to the

very slight quantity and the particular exiting form, the catalyst byproduct during CVD process makes little effect to electrical property of composite. It can well replace the pristine CNTs as a promising functional filler applied in composites.

II. The GNP-CNTs hybrid particles filled PVDF-based dielectric composites

The composite prepared through blending as-synthesized GCHs within the semi-crystalline thermoplastic polymer PVDF in molten state can achieve a significantly improved dielectric permittivity. The mechanical melt-mixing process can not only offer the good filler dispersion, but also provides an intensive interaction at molecular level. More importantly, the way of restricting the utilization of chemical solvent is potential to drive the mass-production of the composites into industrial scale. Compared to the GNPs/CNTs/PVDF ternary counterpart with equivalent conducting phase contents, the GCHs/PVDF binary composites showed a significant transition from semi-conducting to conducting state when the conducting phase loading increased to 10 wt.%. Due to the conducting coupling construction of GCHs, a greatly reduced percolation threshold of binary composites was obtained (5.53 vol.%) according to the classic threshold theory. The parallelly-arranged CNTs arrays are able to promote the formation of typical microcapacitor networks and β-crystalline phase of PVDF matrix, which should be responsible for the improved dielectric properties of binary composites. In addition, the results of temperature-dependent permittivity showed that compared to the mixture of GNPs/CNTs served as filler, loading GCHs is capable of endowing PVDF-based composite with a higher thermal stability. The approach of redesigning the CNTs construction can effectively ameliorate the CNTs aggregation and reduce the percolation threshold, providing a promising strategy for the future energy storage applications.

III. Flexible GNP-CNTs hybrids/PDMS piezo-resistive elastomers

The typical 1D-2D coupling GCH particles with their distinct completely-conducting structure facilitate the establishment of internal conducting network. This special feature is sufficient to make GCHs potential in piezo-resistive applications. The advanced GCHs/PDMS flexible composites with excellent PR behavior are prepared by the mechanical mixing process. The significant enhancements of both dielectric permittivity and AC conductivity were showed in composites with incresing filler loading. An ultra-low percolation threshold (0.64 vol.%.) is achieved due to the "hub" structure of conductive units. Moreover, the modified 3-step theoretical models that based on tunneling effect can well account for the exponential relationship between the sensitive positive PR behavior of composite and the uniaxial compression. Beyond the threshold, the PR sensitivity is inversely proportional to the GCHs content. Especially, the composite with 0.75.vol.% GCHs displays extraordinary sensitivity that the GF and PS value are as high as 10^3 and 0.6 kPa^{-1}, respectively, which is strongly competent in comparison with other carbon fillers. A significant PR response obtained even under compression load as low as 1N. During the cyclic compression loading, the PR behavior of composites manifests a superior dynamic correspondency with applied pressure. Meantime, the resistance response can retain at a relatively high level after 100 loading-unloading cycles. The temperature-dependent PR behavior indicates that the composite can respond not only the deformation or applied pressure change, but also the operating temperature range. Both electrical resistance and relative piezo-resistance change exhibit a significant reduction when composite samples is heated Notably, the typical finger-sensing experiment indicates that the GCHs/PDMS composites are competent to detect and even distinguish the slight finger motions. Compared to the PDMS-based composites filled with equvalent CNT, GNP or mixture of CNTs/GNPs, the GCHs/PDMS composites shows higher dielectric permittivity and electrical conductivity, an obviously lower percolation threshold and a better PR performance. In summary, the strategy of conductive network design will contribute to the development of PR composites with higher performances and further drive the fabrication process to industrial scale.

Perspectives

1. For the synthesis of GNP-CNTs hybrids constructions, the intrinsic features of GNP substrates could play an important role in influencing the organization of grown CNTs. To pre-treat GNPs substrates and make them thinner, higher aspect ratio and more uniform size distribution could be an effective strategy to achieve GCHs constructions with relatively uniform organization of CNTs.

2. Efforts are needed to investigate the interfacial connection between the grown single CNT and the GNP substrate. This investigation helps to explore the mechanism of CNT growth. Moreover, the quantification of interfacial interaction makes a crucial contribution to keep GCHs construction from breaking or detaching during the subsequent procedures such as reasonable surface functionalization and mixing process.

3. The electrical conductivities of micro SiC and graphite platelets are different. In comparison with GCH, the SiC-CNTs hybrid is not conducting completely, which gives rise to the difference of internal conducting network between two hybrids. More investigations are proposed to study the influence of the inherent characteristics of substrates to intrinsic electrical property of hybrids constructions, which may contribute to further lower the threshold of percolative composites.

4. Due to the energy density of dielectric material is proportional to the square of applied electric field, how to improve both the dielectric strength and dielectric permittivity of percolative composites is still a long-term challenge.

5. Apart from the uniaxial compression, it is promising to measure the piezo-resistive behavior of composites by various deformation forms such as tension, bending and

torsion, in order to evaluate the PR performance of a composite systematically and comprehensively. In addition, the reasonable design of PR devices is another important issue to expand their applicable potential.

References

[1] Iijima, S., Helical microtubules of graphitic carbon. *nature* **1991,** *354* (6348), 56-58.
[2] Iijima, S.; Ichihashi, T., Single-shell carbon nanotubes of 1-nm diameter. **1993**.
[3] Ruoff, R. S.; Lorents, D. C., Mechanical and Thermal-Properties of Carbon Nanotubes. *Carbon* **1995,** *33* (7), 925-930.
[4] Ajayan, P. M.; Zhou, O. Z., Applications of carbon nanotubes. *Top Appl Phys* **2001,** *80*, 391-425.
[5] Hassanien, A.; Tokumoto, M.; Ohshima, S.; Kuriki, Y.; Ikazaki, F.; Uchida, K.; Yumura, M., Geometrical structure and electronic properties of atomically resolved multiwall carbon nanotubes. *Appl Phys Lett* **1999,** *75* (18), 2755-2757.
[6] Wildoer, J. W. G.; Venema, L. C.; Rinzler, A. G.; Smalley, R. E.; Dekker, C., Electronic structure of atomically resolved carbon nanotubes. *Nature* **1998,** *391* (6662), 59-62.
[7] Thostenson, E. T.; Ren, Z. F.; Chou, T. W., Advances in the science and technology of carbon nanotubes and their composites: a review. *Composites Science and Technology* **2001,** *61* (13), 1899-1912.
[8] Elliott, J. A.; Sandler, J. K. W.; Windle, A. H.; Young, R. J.; Shaffer, M. S. P., Collapse of single-wall carbon nanotubes is diameter dependent. *Phys Rev Lett* **2004,** *92* (9).
[9] Baughman, R. H.; Zakhidov, A. A.; de Heer, W. A., Carbon nanotubes--the route toward applications. *Science* **2002,** *297* (5582), 787-92.
[10] Journet, C.; Bernier, P., Production of carbon nanotubes. *Appl Phys a-Mater* **1998,** *67* (1), 1-9.
[11] Saito, Y.; Nishikubo, K.; Kawabata, K.; Matsumoto, T., Carbon nanocapsules and single-layered nanotubes produced with platinum-group metals (Ru, Rh, Pd, Os, Ir, Pt) by arc discharge. *Journal of Applied Physics* **1996,** *80* (5), 3062-3067.
[12] Shi, Z. J.; Lian, Y. F.; Liao, F. H.; Zhou, X. H.; Gu, Z. N.; Zhang, Y.; Iijima, S.; Li, H. D.; Yue, K. T.; Zhang, S. L., Large scale synthesis of single-wall carbon nanotubes by arc-discharge method. *J Phys Chem Solids* **2000,** *61* (7), 1031-1036.
[13] Thess, A.; Lee, R.; Nikolaev, P.; Dai, H. J.; Petit, P.; Robert, J.; Xu, C. H.; Lee, Y. H.; Kim, S. G.; Rinzler, A. G.; Colbert, D. T.; Scuseria, G. E.; Tomanek, D.; Fischer, J. E.; Smalley, R. E., Crystalline ropes of metallic carbon nanotubes. *Science* **1996,** *273* (5274), 483-487.
[14] Zhang, Y.; Iijima, S., Formation of single-wall carbon nanotubes by laser ablation of fullerenes at low temperature. *Appl Phys Lett* **1999,** *75* (20), 3087-3089.
[15] Lee, K.; Lee, S. S.; Lee, J. A.; Lee, K.-C.; Ji, S., Carbon nanotube film piezoresistors embedded in polymer membranes. *Applied Physics Letters* **2010,** *96* (1), 013511.
[16] Choy, K. L., Chemical vapour deposition of coatings. *Prog Mater Sci* **2003,** *48*

(2), 57-170.
[17] Kumar, M.; Ando, Y., Chemical Vapor Deposition of Carbon Nanotubes: A Review on Growth Mechanism and Mass Production. *J Nanosci Nanotechno* **2010,** *10* (6), 3739-3758.
[18] Moisala, A.; Nasibulin, A. G.; Kauppinen, E. I., The role of metal nanoparticles in the catalytic production of single-walled carbon nanotubes - a review. *J Phys-Condens Mat* **2003,** *15* (42), S3011-S3035.
[19] Nasibulin, A. G.; Moisala, A.; Brown, D. P.; Kauppinen, E. I., Carbon nanotubes and onions from carbon monoxide using Ni(acac)(2) and Cu(acac)(2) as catalyst precursors. *Carbon* **2003,** *41* (14), 2711-2724.
[20] Dal, H. J.; Rinzler, A. G.; Nikolaev, P.; Thess, A.; Colbert, D. T.; Smalley, R. E., Single-wall nanotubes produced by metal-catalyzed disproportionation of carbon monoxide. *Chem Phys Lett* **1996,** *260* (3-4), 471-475.
[21] Takagi, D.; Homma, Y.; Hibino, H.; Suzuki, S.; Kobayashi, Y., Single-walled carbon nanotube growth from highly activated metal nanoparticles. *Nano Lett* **2006,** *6* (12), 2642-2645.
[22] Ivanov, V.; Nagy, J. B.; Lambin, P.; Lucas, A.; Zhang, X. B.; Zhang, X. F.; Bernaerts, D.; Vantendeloo, G.; Amelinckx, S.; Vanlanduyt, J., The Study of Carbon Nanotubules Produced by Catalytic Method. *Chem Phys Lett* **1994,** *223* (4), 329-335.
[23] Nikolaev, P.; Bronikowski, M. J.; Bradley, R. K.; Rohmund, F.; Colbert, D. T.; Smith, K. A.; Smalley, R. E., Gas-phase catalytic growth of single-walled carbon nanotubes from carbon monoxide. *Chem Phys Lett* **1999,** *313* (1-2), 91-97.
[24] Bower, C.; Zhou, O.; Zhu, W.; Werder, D. J.; Jin, S. H., Nucleation and growth of carbon nanotubes by microwave plasma chemical vapor deposition. *Appl Phys Lett* **2000,** *77* (17), 2767-2769.
[25] Hafner, J. H.; Bronikowski, M. J.; Azamian, B. R.; Nikolaev, P.; Rinzler, A. G.; Colbert, D. T.; Smith, K. A.; Smalley, R. E., Catalytic growth of single-wall carbon nanotubes from metal particles. *Chem Phys Lett* **1998,** *296* (1-2), 195-202.
[26] Flahaut, E.; Govindaraj, A.; Peigney, A.; Laurent, C.; Rousset, A.; Rao, C. N. R., Synthesis of single-walled carbon nanotubes using binary (Fe, Co, Ni) alloy nanoparticles prepared in situ by the reduction of oxide solid solutions. *Chem Phys Lett* **1999,** *300* (1-2), 236-242.
[27] Che, G.; Lakshmi, B. B.; Martin, C. R.; Fisher, E. R.; Ruoff, R. S., Chemical vapor deposition based synthesis of carbon nanotubes and nanofibers using a template method. *Chem Mater* **1998,** *10* (1), 260-267.
[28] Cheng, H. M.; Li, F.; Su, G.; Pan, H. Y.; He, L. L.; Sun, X.; Dresselhaus, M. S., Large-scale and low-cost synthesis of single-walled carbon nanotubes by the catalytic pyrolysis of hydrocarbons. *Appl Phys Lett* **1998,** *72* (25), 3282-3284.
[29] Smith, D. K.; Lee, D. C.; Korgel, B. A., High yield multiwall carbon nanotube synthesis in supercritical fluids. *Chem Mater* **2006,** *18* (14), 3356-3364.
[30] Andrews, R.; Jacques, D.; Rao, A. M.; Derbyshire, F.; Qian, D.; Fan, X.; Dickey, E. C.; Chen, J., Continuous production of aligned carbon nanotubes: a step closer to commercial realization. *Chem Phys Lett* **1999,** *303* (5-6), 467-474.
[31] He, D.; Bozlar, M.; Genestoux, M.; Bai, J., Diameter- and length-dependent

self-organizations of multi-walled carbon nanotubes on spherical alumina microparticles. *Carbon* **2010,** *48* (4), 1159-1170.
[32] Ren, Z. F.; Huang, Z. P.; Xu, J. W.; Wang, J. H.; Bush, P.; Siegal, M. P.; Provencio, P. N., Synthesis of large arrays of well-aligned carbon nanotubes on glass. *Science* **1998,** *282* (5391), 1105-1107.
[33] Zhong, G. F.; Warner, J. H.; Fouquet, M.; Robertson, A. W.; Chen, B. A.; Robertson, J., Growth of Ultrahigh Density Single-Walled Carbon Nanotube Forests by Improved Catalyst Design. *Acs Nano* **2012,** *6* (4), 2893-2903.
[34] Futaba, D. N.; Hata, K.; Yamada, T.; Hiraoka, T.; Hayamizu, Y.; Kakudate, Y.; Tanaike, O.; Hatori, H.; Yumura, M.; Iijima, S., Shape-engineerable and highly densely packed single-walled carbon nanotubes and their application as super-capacitor electrodes. *Nat Mater* **2006,** *5* (12), 987-994.
[35] Thostenson, E. T.; Li, W. Z.; Wang, D. Z.; Ren, Z. F.; Chou, T. W., Carbon nanotube/carbon fiber hybrid multiscale composites. *Journal of Applied Physics* **2002,** *91* (9), 6034-6037.
[36] Wicks, S. S.; Wang, W. N.; Williams, M. R.; Wardle, B. L., Multi-scale interlaminar fracture mechanisms in woven composite laminates reinforced with aligned carbon nanotubes. *Composites Science and Technology* **2014,** *100*, 128-135.
[37] Veedu, V. P.; Cao, A. Y.; Li, X. S.; Ma, K. G.; Soldano, C.; Kar, S.; Ajayan, P. M.; Ghasemi-Nejhad, M. N., Multifunctional composites using reinforced laminae with carbon-nanotube forests. *Nat Mater* **2006,** *5* (6), 457-462.
[38] Gui, X. C.; Zeng, Z. P.; Zhu, Y.; Li, H. B.; Lin, Z. Q.; Gan, Q. M.; Xiang, R.; Cao, A. Y.; Tang, Z. K., Three-Dimensional Carbon Nanotube Sponge-Array Architectures with High Energy Dissipation. *Advanced Materials* **2014,** *26* (8), 1248-1253.
[39] Treacy, M. M. J.; Ebbesen, T. W.; Gibson, J. M., Exceptionally high Young's modulus observed for individual carbon nanotubes. *Nature* **1996,** *381* (6584), 678-680.
[40] Yakobson, B. I.; Avouris, P., Mechanical properties of carbon nanotubes. *Top Appl Phys* **2001,** *80*, 287-327.
[41] Wong, E. W.; Sheehan, P. E.; Lieber, C. M., Nanobeam mechanics: Elasticity, strength, and toughness of nanorods and nanotubes. *Science* **1997,** *277* (5334), 1971-1975.
[42] Yu, M.-F.; Lourie, O.; Dyer, M. J.; Moloni, K.; Kelly, T. F.; Ruoff, R. S., Strength and Breaking Mechanism of Multiwalled Carbon Nanotubes Under Tensile Load. *Science* **2000,** *287* (5453), 637-640.
[43] Yu, M.-F.; Files, B. S.; Arepalli, S.; Ruoff, R. S., Tensile Loading of Ropes of Single Wall Carbon Nanotubes and their Mechanical Properties. *Phys Rev Lett* **2000,** *84* (24), 5552-5555.
[44] Peng, B.; Locascio, M.; Zapol, P.; Li, S. Y.; Mielke, S. L.; Schatz, G. C.; Espinosa, H. D., Measurements of near-ultimate strength for multiwalled carbon nanotubes and irradiation-induced crosslinking improvements. *Nat Nanotechnol* **2008,** *3* (10), 626-631.
[45] Wei, B. Q.; Vajtai, R.; Ajayan, P. M., Reliability and current carrying capacity of carbon nanotubes. *Appl Phys Lett* **2001,** *79* (8), 1172-1174.

[46] Ebbesen, T. W.; Lezec, H. J.; Hiura, H.; Bennett, J. W.; Ghaemi, H. F.; Thio, T., Electrical conductivity of individual carbon nanotubes. *Nature* **1996,** *382* (6586), 54-56.
[47] Dai, H. J., Probing electrical transport in nanomaterials: Conductivity of individual carbon nanotubes (vol 272, pg 523, 1996). *Science* **1996,** *272* (5270), 1861-1861.
[48] Berber, S.; Kwon, Y. K.; Tomanek, D., Unusually high thermal conductivity of carbon nanotubes. *Phys Rev Lett* **2000,** *84* (20), 4613-4616.
[49] Pop, E.; Mann, D.; Wang, Q.; Goodson, K. E.; Dai, H. J., Thermal conductance of an individual single-wall carbon nanotube above room temperature. *Nano Lett* **2006,** *6* (1), 96-100.
[50] De Volder, M. F.; Tawfick, S. H.; Baughman, R. H.; Hart, A. J., Carbon nanotubes: present and future commercial applications. *Science* **2013,** *339* (6119), 535-9.
[51] Dai, L. M.; Chang, D. W.; Baek, J. B.; Lu, W., Carbon Nanomaterials for Advanced Energy Conversion and Storage. *Small* **2012,** *8* (8), 1130-1166.
[52] Evanoff, K.; Khan, J.; Balandin, A. A.; Magasinski, A.; Ready, W. J.; Fuller, T. F.; Yushin, G., Towards Ultrathick Battery Electrodes: Aligned Carbon Nanotube - Enabled Architecture. *Advanced Materials* **2012,** *24* (4), 533-+.
[53] Sotowa, C.; Origi, G.; Takeuchi, M.; Nishimura, Y.; Takeuchi, K.; Jang, I. Y.; Kim, Y. J.; Hayashi, T.; Kim, Y. A.; Endo, M.; Dresselhaus, M. S., The Reinforcing Effect of Combined Carbon Nanotubes and Acetylene Blacks on the Positive Electrode of Lithium-Ion Batteries. *Chemsuschem* **2008,** *1* (11), 911-915.
[54] Matsumoto, T.; Komatsu, T.; Arai, K.; Yamazaki, T.; Kijima, M.; Shimizu, H.; Takasawa, Y.; Nakamura, J., Reduction of Pt usage in fuel cell electrocatalysts with carbon nanotube electrodes. *Chem Commun* **2004,** (7), 840-841.
[55] Le Goff, A.; Artero, V.; Jousselme, B.; Tran, P. D.; Guillet, N.; Métayé, R.; Fihri, A.; Palacin, S.; Fontecave, M., From Hydrogenases to Noble Metal–Free Catalytic Nanomaterials for H2 Production and Uptake. *Science* **2009,** *326* (5958), 1384-1387.
[56] Deheer, W. A.; Chatelain, A.; Ugarte, D., A Carbon Nanotube Field-Emission Electron Source. *Science* **1995,** *270* (5239), 1179-1180.
[57] Saito, Y.; Uemura, S., Field emission from carbon nanotubes and its application to electron sources. *Carbon* **2000,** *38* (2), 169-182.
[58] Lee, N. S.; Chung, D. S.; Han, I. T.; Kang, J. H.; Choi, Y. S.; Kim, H. Y.; Park, S. H.; Jin, Y. W.; Yi, W. K.; Yun, M. J.; Jung, J. E.; Lee, C. J.; You, J. H.; Jo, S. H.; Lee, C. G.; Kim, J. M., Application of carbon nanotubes to field emission displays. *Diam Relat Mater* **2001,** *10* (2), 265-270.
[59] Dai, H. J.; Hafner, J. H.; Rinzler, A. G.; Colbert, D. T.; Smalley, R. E., Nanotubes as nanoprobes in scanning probe microscopy. *Nature* **1996,** *384* (6605), 147-150.
[60] Akita, S.; Nakayama, Y., Manipulation of nanomaterial by carbon nanotube nanotweezers in scanning probe microscope. *Jpn J Appl Phys 1* **2002,** *41* (6B), 4242-4245.

[61] Kim, P.; Lieber, C. M., Nanotube nanotweezers. *Science* **1999,** *286* (5447), 2148-2150.
[62] Fim, F. D.; Guterres, J. M.; Basso, N. R. S.; Galland, G. B., Polyethylene/Graphite Nanocomposites Obtained by In Situ Polymerization. *J Polym Sci Pol Chem* **2010,** *48* (3), 692-698.
[63] Viculis, L. M.; Mack, J. J.; Mayer, O. M.; Hahn, H. T.; Kaner, R. B., Intercalation and exfoliation routes to graphite nanoplatelets. *J Mater Chem* **2005,** *15* (9), 974-978.
[64] Yakovlev, A. V.; Finaenov, A. I.; Zabud'kov, S. L.; Yakovleva, E. V., Thermally expanded graphite: Synthesis, properties, and prospects for use. *Russ J Appl Chem+* **2006,** *79* (11), 1741-1751.
[65] Li, J. P.; Lin, H. F.; Zhao, W. F.; Chen, G. H., Instant modification of graphite nanosheets by the grafting of a styrene oligomer under microwave radiation. *J Appl Polym Sci* **2008,** *109* (3), 1377-1380.
[66] Fan, H. L.; Wang, L. L.; Zhao, K. K.; Li, N.; Shi, Z. J.; Ge, Z. G.; Jin, Z. X., Fabrication, Mechanical Properties, and Biocompatibility of Graphene-Reinforced Chitosan Composites. *Biomacromolecules* **2010,** *11* (9), 2345-2351.
[67] Ramanathan, T.; Stankovich, S.; Dikin, D. A.; Liu, H.; Shen, H.; Nguyen, S. T.; Brinson, L. C., Graphitic nanofillers in PMMA nanocomposites - An investigation of particle size influence on nanocomposite and dispersion and their properties. *J Polym Sci Pol Phys* **2007,** *45* (15), 2097-2112.
[68] Park, S.; Ruoff, R. S., Chemical methods for the production of graphenes. *Nat Nanotechnol* **2009,** *4* (4), 217-224.
[69] Wu, Y. H.; Yu, T.; Shen, Z. X., Two-dimensional carbon nanostructures: Fundamental properties, synthesis, characterization, and potential applications. *Journal of Applied Physics* **2010,** *108* (7).
[70] Cho, D.; Lee, S.; Yang, G. M.; Fukushima, H.; Drzal, L. T., Dynamic mechanical and thermal properties of phenylethynyl-terminated polyimide composites reinforced with expanded graphite nanoplatelets. *Macromol Mater Eng* **2005,** *290* (3), 179-187.
[71] Hiura, H.; Ebbesen, T. W.; Fujita, J.; Tanigaki, K.; Takada, T., Role of sp3 defect structures in graphite and carbon nanotubes. *Nature* **1994,** *367* (6459), 148-151.
[72] Ebbesen, T. W.; Hiura, H., Graphene in 3-Dimensions - Towards Graphite Origami. *Advanced Materials* **1995,** *7* (6), 582-586.
[73] Li, B.; Zhong, W.-H., Review on polymer/graphite nanoplatelet nanocomposites. *Journal of Materials Science* **2011,** *46* (17), 5595-5614.
[74] Mack, J. J.; Viculis, L. M.; Ali, A.; Luoh, R.; Yang, G.; Hahn, H. T.; Ko, F. K.; Kaner, R. B., Graphite Nanoplatelet Reinforcement of Electrospun Polyacrylonitrile Nanofibers. *Advanced Materials* **2005,** *17* (1), 77-80.
[75] Du, X. S.; Xiao, M.; Meng, Y. Z.; Hay, A. S., Facile synthesis of exfoliated and highly conductive poly(arylene disulfide)/graphite nanocomposites. *Polym Advan Technol* **2004,** *15* (6), 320-323.
[76] Yang, H.; Tian, M.; Jia, Q. X.; Shi, J. H.; Zhang, L. Q.; Lim, S. H.; Yu, Z. Z.; Mai, Y. W., Improved mechanical and functional properties of elastomer/graphite

nanocomposites prepared by latex compounding. *Acta Mater* **2007,** *55* (18), 6372-6382.
[77] Wintterlin, J.; Bocquet, M. L., Graphene on metal surfaces. *Surface Science* **2009,** *603* (10–12), 1841-1852.
[78] Ebbesen, T. W.; Ajayan, P. M., Large-scale synthesis of carbon nanotubes. *Nature* **1992,** *358* (6383), 220-222.
[79] Iijima, S.; Wakabayashi, T.; Achiba, Y., Structures of carbon soot prepared by laser ablation. *J Phys Chem-Us* **1996,** *100* (14), 5839-5843.
[80] Ando, Y.; Zhao, X.; Ohkohchi, M., Production of petal-like graphite sheets by hydrogen arc discharge. *Carbon* **1997,** *35* (1), 153-158.
[81] Shang, N. G.; Au, F. C. K.; Meng, X. M.; Lee, C. S.; Bello, I.; Lee, S. T., Uniform carbon nanoflake films and their field emissions. *Chem Phys Lett* **2002,** *358* (3–4), 187-191.
[82] Allen, M. J.; Tung, V. C.; Kaner, R. B., Honeycomb Carbon: A Review of Graphene. *Chem Rev* **2010,** *110* (1), 132-145.
[83] Kim, H.; Abdala, A. A.; Macosko, C. W., Graphene/Polymer Nanocomposites. *Macromolecules* **2010,** *43* (16), 6515-6530.
[84] Cai, D. Y.; Song, M., Recent advance in functionalized graphene/polymer nanocomposites. *J Mater Chem* **2010,** *20* (37), 7906-7915.
[85] Wang, L. W.; Hong, J. B.; Chen, G. H., Comparison Study of Graphite Nanosheets and Carbon Black as Fillers for High Density Polyethylene. *Polym Eng Sci* **2010,** *50* (11), 2176-2181.
[86] George, J. J.; Dyopadhyay, A. B.; Bhowmick, A. K., New generation layered nanocomposites derived from ethylene-co-vinyl acetate and naturally occurring graphite. *J Appl Polym Sci* **2008,** *108* (3), 1603-1616.
[87] Planes, E.; Duchet, J.; Maazouz, A.; Gerard, J. F., Characterization of new formulations for the rotational molding based on ethylene-propylene copolymer/graphite nanocomposites. *Polym Eng Sci* **2008,** *48* (4), 723-731.
[88] Cho, J.; Chen, J. Y.; Daniel, I. M., Mechanical enhancement of carbon fiber/epoxy composites by graphite nanoplatelet reinforcement. *Scripta Materialia* **2007,** *56* (8), 685-688.
[89] Lu, J.; Drzal, L. T.; Worden, R. M.; Lee, I., Simple fabrication of a highly sensitive glucose biosensor using enzymes immobilized in exfoliated graphite nanoplatelets Nafion membrane. *Chem Mater* **2007,** *19* (25), 6240-6246.
[90] Xu, D.; Sridhar, V.; Pham, T. T.; Kim, J. K., Dispersion, mechanical and thermal properties of nano graphite platelets reinforced flouroelastomer composites. *E-Polymers* **2008**.
[91] Kim, I. H.; Jeong, Y. G., Polylactide/Exfoliated Graphite Nanocomposites with Enhanced Thermal Stability, Mechanical Modulus, and Electrical Conductivity. *J Polym Sci Pol Phys* **2010,** *48* (8), 850-858.
[92] Kai, W.; Hirota, Y.; Hua, L.; Inoue, Y., Thermal and mechanical properties of a poly (ϵ-caprolactone)/graphite oxide composite. *J Appl Polym Sci* **2008,** *107* (3), 1395-1400.
[93] Yu, C. S.; Li, B., Preparation and characterization of carboxymethyl polyvinyl

alcohol-graphite nanosheet composites. *Polym Composite* **2008,** *29* (9), 998-1005.
[94] Chen, L.; Chen, G. H.; Lu, L., Piezoresistive Behavior Study on Finger-Sensing Silicone Rubber/Graphite Nanosheet Nanocomposites. *Adv Funct Mater* **2007,** *17* (6), 898-904.
[95] Xu, K.; Erricolo, D.; Dutta, M.; Stroscio, M. A., Electrical conductivity and dielectric properties of PMMA/graphite nanoplatelet ensembles. *Superlattices and Microstructures* **2012,** *51* (5), 606-612.
[96] Li, Y. C.; Tjong, S. C.; Li, R. K. Y., Electrical conductivity and dielectric response of poly(vinylidene fluoride)–graphite nanoplatelet composites. *Synthetic Metals* **2010,** *160* (17-18), 1912-1919.
[97] Kang, J. H.; Park, C.; Scholl, J. A.; Brazin, A. H.; Holloway, N. M.; High, J. W.; Lowther, S. E.; Harrison, J. S., Piezoresistive Characteristics of Single Wall Carbon Nanotube/Polyimide Nanocomposites. *J Polym Sci Pol Phys* **2009,** *47* (10), 994-1003.
[98] Lee, S.-E.; Choi, O.; Hahn, H. T., Microwave properties of graphite nanoplatelet/epoxy composites. *Journal of Applied Physics* **2008,** *104* (3), 033705.
[99] Sarto, M. S.; D'Aloia, A. G.; Tamburrano, A.; De Bellis, G., Synthesis, Modeling, and Experimental Characterization of Graphite Nanoplatelet-Based Composites for EMC Applications. *Ieee T Electromagn C* **2012,** *54* (1), 17-27.
[100] Yu, A. P.; Itkis, M. E.; Bekyarova, E.; Haddon, R. C., Effect of single-walled carbon nanotube purity on the thermal conductivity of carbon nanotube-based composites. *Appl Phys Lett* **2006,** *89* (13).
[101] Yu, A. P.; Ramesh, P.; Itkis, M. E.; Bekyarova, E.; Haddon, R. C., Graphite nanoplatelet-epoxy composite thermal interface materials. *J Phys Chem C* **2007,** *111* (21), 7565-7569.
[102] Hung, M. T.; Choi, O.; Ju, Y. S.; Hahn, H. T., Heat conduction in graphite-nanoplatelet-reinforced polymer nanocomposites. *Appl Phys Lett* **2006,** *89* (2).
[103] Quan, H.; Zhang, B.-q.; Zhao, Q.; Yuen, R. K. K.; Li, R. K. Y., Facile preparation and thermal degradation studies of graphite nanoplatelets (GNPs) filled thermoplastic polyurethane (TPU) nanocomposites. *Composites Part A: Applied Science and Manufacturing* **2009,** *40* (9), 1506-1513.
[104] Sun, X.; Ramesh, P.; Itkis, M. E.; Bekyarova, E.; Haddon, R. C., Dependence of the thermal conductivity of two-dimensional graphite nanoplatelet-based composites on the nanoparticle size distribution. *Journal of physics. Condensed matter : an Institute of Physics journal* **2010,** *22* (33), 334216.
[105] Raza, M. A.; Westwood, A.; Brown, A.; Hondow, N.; Stirling, C., Characterisation of graphite nanoplatelets and the physical properties of graphite nanoplatelet/silicone composites for thermal interface applications. *Carbon* **2011,** *49* (13), 4269-4279.
[106] Min, C.; Yu, D.; Cao, J.; Wang, G.; Feng, L., A graphite nanoplatelet/epoxy composite with high dielectric constant and high thermal conductivity. *Carbon* **2013,** *55*, 116-125.
[107] Kalaitzidou, K.; Fukushima, H.; Drzal, L. T., Multifunctional polypropylene composites produced by incorporation of exfoliated graphite nanoplatelets. *Carbon*

2007, *45* (7), 1446-1452.
[108] Kim, S.; Do, I.; Drzal, L. T., Thermal Stability and Dynamic Mechanical Behavior of Exfoliated Graphite Nanoplatelets-LLDPE Nanocomposites. *Polym Composite* **2010,** *31* (5), 755-761.
[109] Hu, H. W.; Chen, G. H., Electrochemically Modified Graphite Nanosheets and Their Nanocomposite Films with Poly(vinyl alcohol). *Polym Composite* **2010,** *31* (10), 1770-1775.
[110] Weng, W. G.; Chen, G. H.; Wu, D. J.; Chen, X. F.; Lu, J. R.; Wang, P. P., Fabrication and characterization of nylon 6/foliated graphite electrically conducting nanocomposite. *J Polym Sci Pol Phys* **2004,** *42* (15), 2844-2856.
[111] Ma, P. C.; Siddiqui, N. A.; Marom, G.; Kim, J. K., Dispersion and functionalization of carbon nanotubes for polymer-based nanocomposites: A review. *Compos Part a-Appl S* **2010,** *41* (10), 1345-1367.
[112] Thostenson, E. T.; Chou, T. W., Processing-structure-multi-functional property relationship in carbon nanotube/epoxy composites. *Carbon* **2006,** *44* (14), 3022-3029.
[113] Sahoo, N. G.; Rana, S.; Cho, J. W.; Li, L.; Chan, S. H., Polymer nanocomposites based on functionalized carbon nanotubes. *Progress in Polymer Science* **2010,** *35* (7), 837-867.
[114] Clayton, L. M.; Sikder, A. K.; Kumar, A.; Cinke, M.; Meyyappan, M.; Gerasimov, T. G.; Harmon, J. P., Transparent poly(methyl methacrylate)/single-walled carbon nanotube (PMMA/SWNT) composite films with increased dielectric constants. *Adv Funct Mater* **2005,** *15* (1), 101-106.
[115] Yoo, H. J.; Jung, Y. C.; Sahoo, N. G.; Cho, J. W., Polyurethane-carbon nanotube nanocomposites prepared by in-situ polymerization with electroactive shape memory. *J Macromol Sci B* **2006,** *45* (4), 441-451.
[116] Xie, Z.; Zhuang, Q. X.; Wang, Q.; Liu, X. Y.; Chen, Y.; Han, Z. W., In situ synthesis and characterization of poly(2,5-benzoxazole)/multiwalled carbon nanotubes composites. *Polymer* **2011,** *52* (23), 5271-5276.
[117] Park, C.; Ounaies, Z.; Watson, K. A.; Crooks, R. E.; Smith, J.; Lowther, S. E.; Connell, J. W.; Siochi, E. J.; Harrison, J. S.; Clair, T. L. S., Dispersion of single wall carbon nanotubes by in situ polymerization under sonication. *Chem Phys Lett* **2002,** *364* (3-4), 303-308.
[118] Kang, J. H.; Park, C.; Scholl, J. A.; Brazin, A. H.; Holloway, N. M.; High, J. W.; Lowther, S. E.; Harrison, J. S., Piezoresistive Characteristics of Single Wall Carbon Nanotube/Polyimide Nanocomposites (vol 47, pg 994, 2009). *J Polym Sci Pol Phys* **2009,** *47* (16), 1635-1636.
[119] Lahiff, E.; Ryu, C. Y.; Curran, S.; Minett, A. I.; Blau, W. J.; Ajayan, P. M., Selective positioning and density control of nanotubes within a polymer thin film. *Nano Lett* **2003,** *3* (10), 1333-1337.
[120] Cadek, M.; Coleman, J. N.; Barron, V.; Hedicke, K.; Blau, W. J., Morphological and mechanical properties of carbon-nanotube-reinforced semicrystalline and amorphous polymer composites. *Appl Phys Lett* **2002,** *81* (27), 5123-5125.
[121] Park, K. S.; Youn, J. R., Dispersion and aspect ratio of carbon nanotubes in

aqueous suspension and their relationship with electrical resistivity of carbon nanotube filled polymer composites. *Carbon* **2012,** *50* (6), 2322-2330.
[122] Hirsch, A., Functionalization of single-walled carbon nanotubes. *Angew Chem Int Edit* **2002,** *41* (11), 1853-1859.
[123] Buffa, F.; Abraham, G. A.; Grady, B. P.; Resasco, D., Effect of nanotube functionalization on the properties of single-walled carbon nanotube/polyurethane composites. *J Polym Sci Pol Phys* **2007,** *45* (4), 490-501.
[124] Wang, T. L.; Tseng, C. G., Polymeric carbon nanocomposites from multiwalled carbon nanotubes functionalized with segmented polyurethane. *J Appl Polym Sci* **2007,** *105* (3), 1642-1650.
[125] Watts, P. C. P.; Hsu, W. K.; Chen, G. Z.; Fray, D. J.; Kroto, H. W.; Walton, D. R. M., A low resistance boron-doped carbon nanotube-polystyrene composite. *J Mater Chem* **2001,** *11* (10), 2482-2488.
[126] Dang, Z.-M.; Yuan, J.-K.; Zha, J.-W.; Zhou, T.; Li, S.-T.; Hu, G.-H., Fundamentals, processes and applications of high-permittivity polymer–matrix composites. *Progress in Materials Science* **2012,** *57* (4), 660-723.
[127] Dang, Z. M.; Wang, L.; Yin, Y.; Zhang, Q.; Lei, Q. Q., Giant Dielectric Permittivities in Functionalized Carbon-Nanotube/ Electroactive-Polymer Nanocomposites. *Advanced Materials* **2007,** *19* (6), 852-857.
[128] Yao, S.-H.; Dang, Z.-M.; Xu, H.-P.; Jiang, M.-J.; Bai, J., Exploration of dielectric constant dependence on evolution of microstructure in nanotube/ferroelectric polymer nanocomposites. *Applied Physics Letters* **2008,** *92* (8), 082902.
[129] Lynch, M. D.; Patrick, D. L., Organizing carbon nanotubes with liquid crystals. *Nano Lett* **2002,** *2* (11), 1197-1201.
[130] Dang, Z.-M.; Li, W.-K.; Xu, H.-P., Origin of remarkable positive temperature coefficient effect in the modified carbon black and carbon fiber cofillled polymer composites. *Journal of Applied Physics* **2009,** *106* (2), 024913.
[131] Xu, H.-P.; Dang, Z.-M.; Jiang, M.-J.; Yao, S.-H.; Bai, J., Enhanced dielectric properties and positive temperature coefficient effect in the binary polymer composites with surface modified carbon black. *Journal of Materials Chemistry* **2008,** *18* (2), 229.
[132] Zhang, W. D.; Shen, L.; Phang, I. Y.; Liu, T. X., Carbon nanotubes reinforced nylon-6 composite prepared by simple melt-compounding. *Macromolecules* **2004,** *37* (2), 256-259.
[133] Bocchini, S.; Frache, A.; Camino, G.; Claes, M., Polyethylene thermal oxidative stabilisation in carbon nanotubes based nanocomposites. *European Polymer Journal* **2007,** *43* (8), 3222-3235.
[134] Yuan, J.-K.; Yao, S.-H.; Dang, Z.-M.; Sylvestre, A.; Genestoux, M.; Bai, J., Giant Dielectric Permittivity Nanocomposites: Realizing True Potential of Pristine Carbon Nanotubes in Polyvinylidene Fluoride Matrix through an Enhanced Interfacial Interaction. *The Journal of Physical Chemistry C* **2011,** *115* (13), 5515-5521.
[135] McNally, T.; Potschke, P.; Halley, P.; Murphy, M.; Martin, D.; Bell, S. E. J.; Brennan, G. P.; Bein, D.; Lemoine, P.; Quinn, J. P., Polyethylene multiwalled carbon

nanotube composites. *Polymer* **2005,** *46* (19), 8222-8232.
[136] Potschke, P.; Bhattacharyya, A. R.; Janke, A., Morphology and electrical resistivity of melt mixed blends of polyethylene and carbon nanotube filled polycarbonate. *Polymer* **2003,** *44* (26), 8061-8069.
[137] Potschke, P.; Bhattacharyya, A. R.; Janke, A., Melt mixing of polycarbonate with multiwalled carbon nanotubes: microscopic studies on the state of dispersion. *European Polymer Journal* **2004,** *40* (1), 137-148.
[138] Zeng, J. J.; Saltysiak, B.; Johnson, W. S.; Schiraldi, D. A.; Kumar, S., Processing and properties of poly(methyl methacrylate)/carbon nano fiber composites. *Compos Part B-Eng* **2004,** *35* (2), 173-178.
[139] Haggenmueller, R.; Gommans, H. H.; Rinzler, A. G.; Fischer, J. E.; Winey, K. I., Aligned single-wall carbon nanotubes in composites by melt processing methods. *Chem Phys Lett* **2000,** *330* (3-4), 219-225.
[140] Gorga, R. E.; Cohen, R. E., Toughness enhancements in poly(methyl methacrylate) by addition of oriented multiwall carbon nanotubes. *J Polym Sci Pol Phys* **2004,** *42* (14), 2690-2702.
[141] Siochi, E. J.; Working, D. C.; Park, C.; Lillehei, P. T.; Rouse, J. H.; Topping, C. C.; Bhattacharyya, A. R.; Kumar, S., Melt processing of SWCNT-polyimide nanocomposite fibers. *Composites Part B: Engineering* **2004,** *35* (5), 439-446.
[142] Tang, W.; Santare, M. H.; Advani, S. G., Melt processing and mechanical property characterization of multi-walled carbon nanotube/high density polyethylene (MWNT/HDPE) composite films. *Carbon* **2003,** *41* (14), 2779-2785.
[143] Valentini, L.; Biagiotti, J.; Kenny, J.; Santucci, S., Morphological characterization of single-walled carbon nanotubes-PP composites. *Composites Science and Technology* **2003,** *63* (8), 1149-1153.
[144] Zeng, Y.; Ying, Z.; Du, J.; Cheng, H.-M., Effects of carbon nanotubes on processing stability of polyoxymethylene in melt-mixing process. *The Journal of Physical Chemistry C* **2007,** *111* (37), 13945-13950.
[145] Chou, T.-W.; Gao, L.; Thostenson, E. T.; Zhang, Z.; Byun, J.-H., An assessment of the science and technology of carbon nanotube-based fibers and composites. *Composites Science and Technology* **2010,** *70* (1), 1-19.
[146] Gojny, F. H.; Wichmann, M.; Köpke, U.; Fiedler, B.; Schulte, K., Carbon nanotube-reinforced epoxy-composites: enhanced stiffness and fracture toughness at low nanotube content. *Composites Science and Technology* **2004,** *64* (15), 2363-2371.
[147] Moniruzzaman, M.; Winey, K. I., Polymer nanocomposites containing carbon nanotubes. *Macromolecules* **2006,** *39* (16), 5194-5205.
[148] Biercuk, M.; Llaguno, M. C.; Radosavljevic, M.; Hyun, J.; Johnson, A. T.; Fischer, J. E., Carbon nanotube composites for thermal management. *Appl Phys Lett* **2002,** *80* (15), 2767-2769.
[149] Choi, E.; Brooks, J.; Eaton, D.; Al-Haik, M.; Hussaini, M.; Garmestani, H.; Li, D.; Dahmen, K., Enhancement of thermal and electrical properties of carbon nanotube polymer composites by magnetic field processing. *Journal of Applied physics* **2003,** *94* (9), 6034-6039.
[150] Ge, J. J.; Hou, H.; Li, Q.; Graham, M. J.; Greiner, A.; Reneker, D. H.; Harris, F.

W.; Cheng, S. Z., Assembly of well-aligned multiwalled carbon nanotubes in confined polyacrylonitrile environments: electrospun composite nanofiber sheets. *Journal of the American Chemical Society* **2004,** *126* (48), 15754-15761.
[151] Kashiwagi, T.; Du, F.; Douglas, J. F.; Winey, K. I.; Harris, R. H.; Shields, J. R., Nanoparticle networks reduce the flammability of polymer nanocomposites. *Nat Mater* **2005,** *4* (12), 928-933.
[152] Bauhofer, W.; Kovacs, J. Z., A review and analysis of electrical percolation in carbon nanotube polymer composites. *Composites Science and Technology* **2009,** *69* (10), 1486-1498.
[153] Sandler, J.; Kirk, J.; Kinloch, I.; Shaffer, M.; Windle, A., Ultra-low electrical percolation threshold in carbon-nanotube-epoxy composites. *Polymer* **2003,** *44* (19), 5893-5899.
[154] Li, J.; Ma, P. C.; Chow, W. S.; To, C. K.; Tang, B. Z.; Kim, J. K., Correlations between percolation threshold, dispersion state, and aspect ratio of carbon nanotubes. *Adv Funct Mater* **2007,** *17* (16), 3207-3215.
[155] Du, F.; Fischer, J. E.; Winey, K. I., Coagulation method for preparing single-walled carbon nanotube/poly (methyl methacrylate) composites and their modulus, electrical conductivity, and thermal stability. *Journal of Polymer Science Part B: Polymer Physics* **2003,** *41* (24), 3333-3338.
[156] Bai, J.; Allaoui, A., Effect of the length and the aggregate size of MWNTs on the improvement efficiency of the mechanical and electrical properties of nanocomposites—experimental investigation. *Composites Part A: applied science and manufacturing* **2003,** *34* (8), 689-694.
[157] Bryning, M. B.; Islam, M. F.; Kikkawa, J. M.; Yodh, A. G., Very Low Conductivity Threshold in Bulk Isotropic Single-Walled Carbon Nanotube–Epoxy Composites. *Advanced materials* **2005,** *17* (9), 1186-1191.
[158] Mehdipour, A.; Rosca, I. D.; Trueman, C. W.; Sebak, A.-R.; Van Hoa, S., Multiwall carbon nanotube–epoxy composites with high shielding effectiveness for aeronautic applications. *Electromagnetic Compatibility, IEEE Transactions on* **2012,** *54* (1), 28-36.
[159] Kumar, R.; Dhakate, S. R.; Gupta, T.; Saini, P.; Singh, B. P.; Mathur, R. B., Effective improvement of the properties of light weight carbon foam by decoration with multi-wall carbon nanotubes. *J Mater Chem A* **2013,** *1* (18), 5727-5735.
[160] Yang, Y.; Gupta, M. C.; Dudley, K. L.; Lawrence, R. W., A comparative study of EMI shielding properties of carbon nanofiber and multi-walled carbon nanotube filled polymer composites. *J Nanosci Nanotechno* **2005,** *5* (6), 927-931.
[161] Jiang, M.-J.; Dang, Z.-M.; Xu, H.-P., Giant dielectric constant and resistance-pressure sensitivity in carbon nanotubes/rubber nanocomposites with low percolation threshold. *Appl Phys Lett* **2007,** *90* (4), 042914.
[162] Jiang, M.-J.; Dang, Z.-M.; Xu, H.-P., Enhanced electrical conductivity in chemically modified carbon nanotube/methylvinyl silicone rubber nanocomposite. *European Polymer Journal* **2007,** *43* (12), 4924-4930.
[163] Jiang, M.-J.; Dang, Z.-M.; Xu, H.-P.; Yao, S.-H.; Bai, J., Effect of aspect ratio of multiwall carbon nanotubes on resistance-pressure sensitivity of rubber

nanocomposites. *Appl Phys Lett* **2007,** *91* (7), 072907.
[164] Shehzad, K.; Dang, Z.-M.; Ahmad, M. N.; Sagar, R. U. R.; Butt, S.; Farooq, M. U.; Wang, T.-B., Effects of carbon nanotubes aspect ratio on the qualitative and quantitative aspects of frequency response of electrical conductivity and dielectric permittivity in the carbon nanotube/polymer composites. *Carbon* **2013,** *54*, 105-112.
[165] Cattin, C.; Hubert, P., Piezoresistance in polymer nanocomposites with high aspect ratio particles. *ACS applied materials & interfaces* **2014,** *6* (3), 1804-11.
[166] Frediani, G.; Mazzei, D.; De Rossi, D. E.; Carpi, F., Wearable wireless tactile display for virtual interactions with soft bodies. *Frontiers in bioengineering and biotechnology* **2014,** *2*.
[167] Hanley, C. A.; Gun'ko, Y. K.; Frediani, G.; Carpi, F., Stretchable optical device with electrically tunable absorbance and fluorescence. *Smart Materials and Structures* **2014,** *23* (1), 015009.
[168] Carpi, F.; Kornbluh, R.; Sommer-Larsen, P.; Alici, G., Electroactive polymer actuators as artificial muscles: are they ready for bioinspired applications? *Bioinspiration & biomimetics* **2011,** *6* (4), 045006.
[169] Carpi, F.; Frediani, G.; Turco, S.; De Rossi, D., Bioinspired Tunable Lens with Muscle-Like Electroactive Elastomers. *Adv Funct Mater* **2011,** *21* (21), 4152-4158.
[170] Kim, M. H.; Hong, S. M.; Koo, C. M., Electric actuation properties of SEBS/CB and SEBS/SWCNT nanocomposite films with different conductive fillers. *Macromolecular Research* **2012,** *20* (1), 59-65.
[171] Yuan, W.; Brochu, P.; Ha, S. M.; Pei, Q. B., Dielectric oil coated single-walled carbon nanotube electrodes for stable, large-strain actuation with dielectric elastomers. *Sensor Actuat a-Phys* **2009,** *155* (2), 278-284.
[172] Yuan, W.; Hu, L. B.; Yu, Z. B.; Lam, T. L.; Biggs, J.; Ha, S. M.; Xi, D. J.; Chen, B.; Senesky, M. K.; Gruner, G.; Pei, Q. B., Fault-tolerant dielectric elastomer actuators using single-walled carbon nanotube electrodes. *Advanced Materials* **2008,** *20* (3), 621-+.
[173] Wang, S.; Chung, D. D. L.; Chung, J., Self-sensing of damage in carbon fiber polymer-matrix composite by measurement of the electrical resistance or potential away from the damaged region. *Journal of Materials Science* **2005,** *40* (24), 6463-6472.
[174] Chung, D., Damage detection using self-sensing concepts. *Proceedings of the Institution of Mechanical Engineers, Part G: Journal of Aerospace Engineering* **2007,** *221* (4), 509-520.
[175] Hu, N.; Fukunaga, H.; Atobe, S.; Liu, Y.; Li, J., Piezoresistive strain sensors made from carbon nanotubes based polymer nanocomposites. *Sensors* **2011,** *11* (11), 10691-10723.
[176] Li, C.; Thostenson, E. T.; Chou, T.-W., Sensors and actuators based on carbon nanotubes and their composites: A review. *Composites Science and Technology* **2008,** *68* (6), 1227-1249.
[177] Thostenson, E. T.; Chou, T. W., Carbon Nanotube Networks: Sensing of Distributed Strain and Damage for Life Prediction and Self Healing. *Advanced Materials* **2006,** *18* (21), 2837-2841.

[178] Myounggu, P.; Hyonny, K.; Jeffrey, P. Y., Strain-dependent electrical resistance of multi-walled carbon nanotube/polymer composite films. *Nanotechnology* **2008,** *19* (5), 055705.
[179] Esumi, K.; Ishigami, M.; Nakajima, A.; Sawada, K.; Honda, H., Chemical treatment of carbon nanotubes. *Carbon* **1996,** *34* (2), 279-281.
[180] Yu, R. Q.; Chen, L. W.; Liu, Q. P.; Lin, J. Y.; Tan, K. L.; Ng, S. C.; Chan, H. S. O.; Xu, G. Q.; Hor, T. S. A., Platinum deposition on carbon nanotubes via chemical modification. *Chem Mater* **1998,** *10* (3), 718-722.
[181] Sham, M. L.; Kim, J. K., Surface functionalities of multi-wall carbon nanotubes after UV/Ozone and TETA treatments. *Carbon* **2006,** *44* (4), 768-777.
[182] Ma, P. C.; Kim, J. K.; Tang, B. Z., Functionalization of carbon nanotubes using a silane coupling agent. *Carbon* **2006,** *44* (15), 3232-3238.
[183] Wang, S. C.; Chang, K. S.; Yuan, C. J., Enhancement of electrochemical properties of screen-printed carbon electrodes by oxygen plasma treatment. *Electrochim Acta* **2009,** *54* (21), 4937-4943.
[184] Avila-Orta, C. A.; Cruz-Delgado, V. J.; Neira-Velazquez, M. G.; Hernandez-Hernandez, E.; Mendez-Padilla, M. G.; Medellin-Rodriguez, F. J., Surface modification of carbon nanotubes with ethylene glycol plasma. *Carbon* **2009,** *47* (8), 1916-1921.
[185] Li, Y.; Zhang, X.; Luo, J.; Huang, W.; Cheng, J.; Luo, Z.; Li, T.; Liu, F.; Xu, G.; Ke, X., Purification of CVD synthesized single-wall carbon nanotubes by different acid oxidation treatments. *Nanotechnology* **2004,** *15* (11), 1645.
[186] Tchoul, M. N.; Ford, W. T.; Lolli, G.; Resasco, D. E.; Arepalli, S., Effect of mild nitric acid oxidation on dispersability, size, and structure of single-walled carbon nanotubes. *Chem Mater* **2007,** *19* (23), 5765-5772.
[187] Smith, B.; Wepasnick, K.; Schrote, K. E.; Cho, H.-H.; Ball, W. P.; Fairbrother, D. H., Influence of surface oxides on the colloidal stability of multi-walled carbon nanotubes: A structure− property relationship. *Langmuir* **2009,** *25* (17), 9767-9776.
[188] Kelly, K.; Chiang, I.; Mickelson, E.; Hauge, R.; Margrave, J.; Wang, X.; Scuseria, G.; Radloff, C.; Halas, N., Insight into the mechanism of sidewall functionalization of single-walled nanotubes: an STM study. *Chem Phys Lett* **1999,** *313* (3), 445-450.
[189] Stevens, J. L.; Huang, A. Y.; Peng, H.; Chiang, I. W.; Khabashesku, V. N.; Margrave, J. L., Sidewall amino-functionalization of single-walled carbon nanotubes through fluorination and subsequent reactions with terminal diamines. *Nano Lett* **2003,** *3* (3), 331-336.
[190] Zhang, Q.-H.; Chen, D.-J., Percolation threshold and morphology of composites of conducting carbon black/polypropylene/EVA. *Journal of materials science* **2004,** *39* (5), 1751-1757.
[191] Cao, L.; Yang, W.; Yang, J.; Wang, C.; Fu, S., Hyperbranched poly (amidoamine)-modified multi-walled carbon nanotubes via grafting-from method. *Chemistry Letters* **2004,** *33* (5), 490-491.
[192] Hu, N.; Zhou, H.; Dang, G.; Rao, X.; Chen, C.; Zhang, W., Efficient dispersion of multi-walled carbon nanotubes by in situ polymerization. *Polymer International*

2007, *56* (5), 655-659.
[193] Maiti, U. N.; Lee, W. J.; Lee, J. M.; Oh, Y.; Kim, J. Y.; Kim, J. E.; Shim, J.; Han, T. H.; Kim, S. O., 25th Anniversary article: chemically modified/doped carbon nanotubes & graphene for optimized nanostructures & nanodevices. *Advanced Materials* **2014,** *26* (1), 40-67.
[194] Hwang, S. K.; Lee, J. M.; Kim, S.; Park, J. S.; Park, H. I.; Ahn, C. W.; Lee, K. J.; Lee, T.; Kim, S. O., Flexible multilevel resistive memory with controlled charge trap B-and N-doped carbon nanotubes. *Nano Lett* **2012,** *12* (5), 2217-2221.
[195] Hwang, J. O.; Park, J. S.; Choi, D. S.; Kim, J. Y.; Lee, S. H.; Lee, K. E.; Kim, Y.-H.; Song, M. H.; Yoo, S.; Kim, S. O., Workfunction-tunable, N-doped reduced graphene transparent electrodes for high-performance polymer light-emitting diodes. *Acs Nano* **2011,** *6* (1), 159-167.
[196] Xue, Y.; Wu, B.; Jiang, L.; Guo, Y.; Huang, L.; Chen, J.; Tan, J.; Geng, D.; Luo, B.; Hu, W., Low temperature growth of highly nitrogen-doped single crystal graphene arrays by chemical vapor deposition. *Journal of the American Chemical Society* **2012,** *134* (27), 11060-11063.
[197] Hashim, D. P.; Narayanan, N. T.; Romo-Herrera, J. M.; Cullen, D. A.; Hahm, M. G.; Lezzi, P.; Suttle, J. R.; Kelkhoff, D.; Munoz-Sandoval, E.; Ganguli, S., Covalently bonded three-dimensional carbon nanotube solids via boron induced nanojunctions. *Scientific reports* **2012,** *2*.
[198] Sumpter, B. G.; Meunier, V.; Romo-Herrera, J. M.; Cruz-Silva, E.; Cullen, D. A.; Terrones, H.; Smith, D. J.; Terrones, M., Nitrogen-mediated carbon nanotube growth: diameter reduction, metallicity, bundle dispersability, and bamboo-like structure formation. *Acs Nano* **2007,** *1* (4), 369-375.
[199] Romo-Herrera, J. M.; Sumpter, B. G.; Cullen, D. A.; Terrones, H.; Cruz-Silva, E.; Smith, D. J.; Meunier, V.; Terrones, M., An atomistic branching mechanism for carbon nanotubes: sulfur as the triggering agent. *Angewandte Chemie International Edition* **2008,** *47* (16), 2948-2953.
[200] Yang, Z.; Yao, Z.; Li, G.; Fang, G.; Nie, H.; Liu, Z.; Zhou, X.; Chen, X. a.; Huang, S., Sulfur-doped graphene as an efficient metal-free cathode catalyst for oxygen reduction. *Acs Nano* **2011,** *6* (1), 205-211.
[201] Qu, L.; Liu, Y.; Baek, J.-B.; Dai, L., Nitrogen-doped graphene as efficient metal-free electrocatalyst for oxygen reduction in fuel cells. *Acs Nano* **2010,** *4* (3), 1321-1326.
[202] Lee, W. J.; Lee, J. M.; Kochuveedu, S. T.; Han, T. H.; Jeong, H. Y.; Park, M.; Yun, J. M.; Kwon, J.; No, K.; Kim, D. H., Biomineralized N-doped CNT/TiO2 core/shell nanowires for visible light photocatalysis. *Acs Nano* **2011,** *6* (1), 935-943.
[203] Lee, W. J.; Lee, D. H.; Han, T. H.; Lee, S. H.; Moon, H.-S.; Lee, J. A.; Kim, S. O., Biomimetic mineralization of vertical N-doped carbon nanotubes. *Chem Commun* **2011,** *47* (1), 535-537.
[204] Kong, J.; Franklin, N. R.; Zhou, C.; Chapline, M. G.; Peng, S.; Cho, K.; Dai, H., Nanotube molecular wires as chemical sensors. *Science* **2000,** *287* (5453), 622-625.
[205] Barrau, S.; Demont, P.; Perez, E.; Peigney, A.; Laurent, C.; Lacabanne, C.,

Effect of palmitic acid on the electrical conductivity of carbon nanotubes-epoxy resin composites. *Macromolecules* **2003,** *36* (26), 9678-9680.
[206] Yuan, J.; Yao, S.; Li, W.; Sylvestre, A.; Bai, J., Vertically Aligned Carbon Nanotube Arrays on SiC Microplatelets: A High Figure-of-Merit Strategy for Achieving Large Dielectric Constant and Low Loss in Polymer Composites. *The Journal of Physical Chemistry C* **2014,** *118* (40), 22975-22983.
[207] Ci, L.; Bai, J., Novel micro/nanoscale hybrid reinforcement: multiwalled carbon nanotubes on SiC particles. *Advanced Materials* **2004,** *16* (22), 2021-2024.
[208] He, D.; Bai, J., Acetylene-Enhanced Growth of Carbon Nanotubes on Ceramic Microparticles for Multi-Scale Hybrid Structures. *Chemical Vapor Deposition* **2011,** *17* (4-6), 98-106.
[209] He, D.; Li, H.; Bai, J., Experimental and numerical investigation of the position-dependent growth of carbon nanotube–alumina microparticle hybrid structures in a horizontal CVD reactor. *Carbon* **2011,** *49* (15), 5359-5372.
[210] He, D.; Li, H.; Li, W.; Haghi-Ashtiani, P.; Lejay, P.; Bai, J., Growth of carbon nanotubes in six orthogonal directions on spherical alumina microparticles. *Carbon* **2011,** *49* (7), 2273-2286.
[211] Li, W.; Yuan, J.; Lin, Y.; Yao, S.; Ren, Z.; Wang, H.; Wang, M.; Bai, J., The controlled formation of hybrid structures of multi-walled carbon nanotubes on SiC plate-like particles and their synergetic effect as a filler in poly(vinylidene fluoride) based composites. *Carbon* **2013,** *51*, 355-364.
[212] Li, W.; He, D.; Bai, J., The influence of nano/micro hybrid structure on the mechanical and self-sensing properties of carbon nanotube-microparticle reinforced epoxy matrix composite. *Composites Part A: Applied Science and Manufacturing* **2013,** *54*, 28-36.
[213] Bozlar, M.; He, D.; Bai, J.; Chalopin, Y.; Mingo, N.; Volz, S., Carbon nanotube microarchitectures for enhanced thermal conduction at ultralow mass fraction in polymer composites. *Adv Mater* **2010,** *22* (14), 1654-8.
[214] Yuan, J.-K.; Li, W.-L.; Yao, S.-H.; Lin, Y.-Q.; Sylvestre, A.; Bai, J., High dielectric permittivity and low percolation threshold in polymer composites based on SiC-carbon nanotubes micro/nano hybrid. *Appl Phys Lett* **2011,** *98* (3), 032901.
[215] Li, W.; He, D.; Dang, Z.; Bai, J., In situ damage sensing in the glass fabric reinforced epoxy composites containing CNT–Al2O3 hybrids. *Composites Science and Technology* **2014,** *99*, 8-14.
[216] Li, W.; Yuan, J.; Dichiara, A.; Lin, Y.; Bai, J., The use of vertically aligned carbon nanotubes grown on SiC for in situ sensing of elastic and plastic deformation in electrically percolative epoxy composites. *Carbon* **2012,** *50* (11), 4298-4301.
[217] Kasap, S., Principles of Electronic Materials and Devices, 2006. McGraw Hill, New York.
[218] Barber, P.; Balasubramanian, S.; Anguchamy, Y.; Gong, S.; Wibowo, A.; Gao, H.; Ploehn, H. J.; Zur Loye, H.-C., Polymer composite and nanocomposite dielectric materials for pulse power energy storage. *Materials* **2009,** *2* (4), 1697-1733.
[219] Dang, Z.-M.; Zhang, Y.-H.; Tjong, S.-C., Dependence of dielectric behavior on the physical property of fillers in the polymer-matrix composites. *Synthetic Metals*

2004, *146* (1), 79-84.
[220] Murugaraj, P.; Mainwaring, D.; Mora-Huertas, N., Dielectric enhancement in polymer-nanoparticle composites through interphase polarizability. *Journal of applied physics* **2005,** *98* (5), 4304.
[221] Vo, H. T.; Shi, F. G., Towards model-based engineering of optoelectronic packaging materials: Dielectric constant modeling. *Microelectronics Journal* **2002,** *33* (5), 409-415.
[222] Fan, B.-H.; Zha, J.-W.; Wang, D.-R.; Zhao, J.; Dang, Z.-M., Experimental study and theoretical prediction of dielectric permittivity in BaTiO3/polyimide nanocomposite films. *Appl Phys Lett* **2012,** *100* (9), 092903.
[223] Van Beek, L., Dielectric behaviour of heterogeneous systems. *Progress in dielectrics* **1967,** *7*, 69-114.
[224] Nan, C.-W., Physics of inhomogeneous inorganic materials. *Prog Mater Sci* **1993,** *37* (1), 1-116.
[225] Sihvola, A. H.; Pekonen, O. P., Effective medium formulae for bi-anisotropic mixtures. *Journal of Physics D: Applied Physics* **1996,** *29* (3), 514.
[226] Shivola, A. H., Self-consistency aspects of dielectric mixing theories. *Geoscience and Remote Sensing, IEEE Transactions on* **1989,** *27* (4), 403-415.
[227] Nelson, S.; You, T.-S., Relationships between microwave permittivities of solid and pulverised plastics. *Journal of physics D: applied physics* **1990,** *23* (3), 346.
[228] Tamura, R.; Lim, E.; Manaka, T.; Iwamoto, M., Analysis of pentacene field effect transistor as a Maxwell-Wagner effect element. *Journal of applied physics* **2006,** *100* (11), 114515.
[229] Pecharroman, C.; Esteban-Betegon, F. t.; Bartolome, J. F.; Lopez-Esteban, S.; Moya, J. S., New Percolative BaTiO 3–Ni Composites with a High and Frequency-Independent Dielectric Constant(εr≈ 80000). *Advanced Materials* **2001,** *13* (20), 1541.
[230] Dang, Z. M.; Yuan, J. K.; Yao, S. H.; Liao, R. J., Flexible Nanodielectric Materials with High Permittivity for Power Energy Storage. *Advanced Materials* **2013,** *25* (44), 6334-6365.
[231] Simoes, R.; Silva, J.; Vaia, R.; Sencadas, V.; Costa, P.; Gomes, J.; Lanceros-Méndez, S., Low percolation transitions in carbon nanotube networks dispersed in a polymer matrix: dielectric properties, simulations and experiments. *Nanotechnology* **2009,** *20* (3), 035703.
[232] He, F.; Lau, S.; Chan, H. L.; Fan, J., High Dielectric Permittivity and Low Percolation Threshold in Nanocomposites Based on Poly(vinylidene fluoride) and Exfoliated Graphite Nanoplates. *Advanced Materials* **2009,** *21* (6), 710-715.
[233] Nan, C. W.; Shen, Y.; Ma, J., Physical Properties of Composites Near Percolation. *Annual Review of Materials Research* **2010,** *40* (1), 131-151.
[234] Yi, J. Y.; Choi, G. M., Percolation behavior of conductor-insulator composites with varying aspect ratio of conductive fiber. *Journal of electroceramics* **1999,** *3* (4), 361-369.
[235] Neda, Z.; Florian, R.; Brechet, Y., Reconsideration of continuum percolation of isotropically oriented sticks in three dimensions. *Physical Review E* **1999,** *59* (3), 3717.

[236] Stankovich, S.; Dikin, D. A.; Dommett, G. H.; Kohlhaas, K. M.; Zimney, E. J.; Stach, E. A.; Piner, R. D.; Nguyen, S. T.; Ruoff, R. S., Graphene-based composite materials. *Nature* **2006,** *442* (7100), 282-286.
[237] Li, J.; Wong, P.-S.; Kim, J.-K., Hybrid nanocomposites containing carbon nanotubes and graphite nanoplatelets. *Materials Science and Engineering: A* **2008,** *483*, 660-663.
[238] Kumar, S.; Sun, L.; Caceres, S.; Li, B.; Wood, W.; Perugini, A.; Maguire, R.; Zhong, W., Dynamic synergy of graphitic nanoplatelets and multi-walled carbon nanotubes in polyetherimide nanocomposites. *Nanotechnology* **2010,** *21* (10), 105702.
[239] Wei, T.; Song, L.; Zheng, C.; Wang, K.; Yan, J.; Shao, B.; Fan, Z.-J., The synergy of a three filler combination in the conductivity of epoxy composites. *Materials Letters* **2010,** *64* (21), 2376-2379.
[240] Li, C.; Thostenson, E. T.; Chou, T.-W., Dominant role of tunneling resistance in the electrical conductivity of carbon nanotube–based composites. *Appl Phys Lett* **2007,** *91* (22), 223114.
[241] Fuhrer, M.; Nygård, J.; Shih, L.; Forero, M.; Yoon, Y.-G.; Choi, H. J.; Ihm, J.; Louie, S. G.; Zettl, A.; McEuen, P. L., Crossed nanotube junctions. *Science* **2000,** *288* (5465), 494-497.
[242] Buldum, A.; Lu, J. P., Contact resistance between carbon nanotubes. *Phys Rev B* **2001,** *63* (16), 161403.
[243] Stoyanov, H.; Mc Carthy, D.; Kollosche, M.; Kofod, G., Dielectric properties and electric breakdown strength of a subpercolative composite of carbon black in thermoplastic copolymer. *Appl Phys Lett* **2009,** *94* (23), 232905.
[244] Gyure, M. F.; Beale, P. D., Dielectric breakdown in continuous models of metal-loaded dielectrics. *Phys Rev B* **1992,** *46* (7), 3736.
[245] Balberg, I.; Azulay, D.; Toker, D.; Millo, O., Percolation and tunneling in composite materials. *International Journal of Modern Physics B* **2004,** *18* (15), 2091-2121.
[246] Simmons, J. G., Generalized formula for the electric tunnel effect between similar electrodes separated by a thin insulating film. *Journal of Applied Physics* **1963,** *34* (6), 1793-1803.
[247] Hu, N.; Karube, Y.; Yan, C.; Masuda, Z.; Fukunaga, H., Tunneling effect in a polymer/carbon nanotube nanocomposite strain sensor. *Acta Mater* **2008,** *56* (13), 2929-2936.
[248] Toker, D.; Azulay, D.; Shimoni, N.; Balberg, I.; Millo, O., Tunneling and percolation in metal-insulator composite materials. *Phys Rev B* **2003,** *68* (4), 041403.
[249] Nan, C. W., Physics of Inhomogeneous Inorganic Materials. *Prog Mater Sci* **1993,** *37* (1), 1-116.
[250] Zhang, X. W.; Pan, Y.; Zheng, Q.; Yi, X. S., Time dependence of piezoresistance for the conductor-filled polymer composites. *Journal of Polymer Science part B: polymer physics* **2000,** *38* (21), 2739-2749.
[251] Wang, L.; Han, Y., Application of carbon nanotube filled silicone rubber composite in stress measurement during ramped loading with low compression speed. *Sensors and Actuators A: Physical* **2013,** *201*, 214-221.

[252] Wang, L.; Xu, C.; Li, Y., Piezoresistive response to changes in contributive tunneling film network of carbon nanotube/silicone rubber composite under multi-load/unload. *Sensors and Actuators A: Physical* **2013,** *189*, 45-54.
[253] Hou, Y.; Wang, D.; Zhang, X.-M.; Zhao, H.; Zha, J.-W.; Dang, Z.-M., Positive piezoresistive behavior of electrically conductive alkyl-functionalized graphene/polydimethylsilicone nanocomposites. *Journal of Materials Chemistry C* **2013,** *1* (3), 515.
[254] Pang, C.; Lee, G.-Y.; Kim, T.-i.; Kim, S. M.; Kim, H. N.; Ahn, S.-H.; Suh, K.-Y., A flexible and highly sensitive strain-gauge sensor using reversible interlocking of nanofibres. *Nat Mater* **2012,** *11* (9), 795-801.
[255] Zhao, H.; Bai, J., Highly sensitive piezo-resistive graphite nanoplatelet-carbon nanotube hybrids/polydimethylsilicone composites with improved conductive network construction. *ACS applied materials & interfaces* **2015,** *7* (18), 9652-9.
[256] Hammock, M. L.; Chortos, A.; Tee, B. C.; Tok, J. B.; Bao, Z., 25th anniversary article: The evolution of electronic skin (e-skin): a brief history, design considerations, and recent progress. *Adv Mater* **2013,** *25* (42), 5997-6038.
[257] Sun, Y.; Rogers, J. A., Structural forms of single crystal semiconductor nanoribbons for high-performance stretchable electronics. *J Mater Chem* **2007,** *17* (9), 832-840.
[258] Shin, M. K.; Oh, J.; Lima, M.; Kozlov, M. E.; Kim, S. J.; Baughman, R. H., Elastomeric conductive composites based on carbon nanotube forests. *Adv Mater* **2010,** *22* (24), 2663-7.
[259] Park, S.; Vosguerichian, M.; Bao, Z., A review of fabrication and applications of carbon nanotube film-based flexible electronics. *Nanoscale* **2013,** *5* (5), 1727-1752.
[260] Coleman, J. N.; Khan, U.; Blau, W. J.; Gun'ko, Y. K., Small but strong: A review of the mechanical properties of carbon nanotube–polymer composites. *Carbon* **2006,** *44* (9), 1624-1652.
[261] Wu, Y. H.; Yu, T.; Shen, Z. X., Two-dimensional carbon nanostructures: Fundamental properties, synthesis, characterization, and potential applications. *Journal of Applied Physics* **2010,** *108* (7), 071301.
[262] Dichiara, A.; Yuan, J.-K.; Yao, S.-H.; Sylvestre, A.; Bai, J., Chemical Vapor Deposition Synthesis of Carbon Nanotube-Graphene Nanosheet Hybrids and Their Application in Polymer Composites. *J Nanosci Nanotechno* **2012,** *12* (9), 6935-6940.
[263] He D, Formation of hybrid structures of carbon nanotubes and alumina microparticles by CVD method: Mechanisms and Chemical kinetics. *Thesis of Ph.D* Ecole Centrale Paris, **2010**.
[264] Nessim, G. D.; Hart, A. J.; Kim, J. S.; Acquaviva, D.; Oh, J.; Morgan, C. D.; Seita, M.; Leib, J. S.; Thompson, C. V., Tuning of vertically-aligned carbon nanotube diameter and areal density through catalyst pre-treatment. *Nano Lett* **2008,** *8* (11), 3587-3593.
[265] Wasel, W.; Kuwana, K.; Reilly, P. T.; Saito, K., Experimental characterization of the role of hydrogen in CVD synthesis of MWCNTs. *Carbon* **2007,** *45* (4), 833-838.
[266] Li, H.; He, D.; Li, T.; Genestoux, M.; Bai, J., Chemical kinetics of catalytic chemical vapor deposition of an acetylene/xylene mixture for improved carbon

nanotube production. *Carbon* **2010,** *48* (15), 4330-4342.
[267] Prakash, R.; Mishra, A. K.; Roth, A.; Kübel, C.; Scherer, T.; Ghafari, M.; Hahn, H.; Fichtner, M., A ferrocene-based carbon–iron lithium fluoride nanocomposite as a stable electrode material in lithium batteries. *J Mater Chem* **2010,** *20* (10), 1871-1876.
[268] Fu, L.-S.; Jiang, J.-T.; Xu, C.-Y.; Zhen, L., Synthesis of hexagonal Fe microflakes with excellent microwave absorption performance. *CrystEngComm* **2012,** *14* (20), 6827-6832.
[269] Dichiara, A. B.; Yuan, J.; Yao, S.; Sylvestre, A.; Zimmer, L.; Bai, J., Effective synergistic effect of Al2O3 and SiC microparticles on the growth of carbon nanotubes and their application in high dielectric permittivity polymer composites. *J Mater Chem A* **2014,** *2* (21), 7980.
[270] Ghini, G.; Luconi, L.; Rossin, A.; Bianchini, C.; Giambastiani, G.; Cicchi, S.; Lascialfari, L.; Brandi, A.; Giannasi, A., Can nitrones functionalize carbon nanotubes? *Chem. Commun.* **2009,** *46* (2), 252-254.
[271] Grassi, G.; Scala, A.; Piperno, A.; Iannazzo, D.; Lanza, M.; Milone, C.; Pistone, A.; Galvagno, S., A facile and ecofriendly functionalization of multiwalled carbon nanotubes by an old mesoionic compound. *Chem Commun* **2012,** *48* (54), 6836-6838.
[272] Dang, Z.-M.; Wang, H.-Y.; Peng, B.; Nan, C.-W., Effect of BaTiO3 size on dielectric property of BaTiO3/PVDF composites. *Journal of Electroceramics* **2007,** *21* (1-4), 381-384.
[273] Dang, Z.-M.; Wu, J.-P.; Xu, H.-P.; Yao, S.-H.; Jiang, M.-J.; Bai, J., Dielectric properties of upright carbon fiber filled poly(vinylidene fluoride) composite with low percolation threshold and weak temperature dependence. *Appl Phys Lett* **2007,** *91* (7), 072912.
[274] Dang, Z.-M.; Xie, D.; Shi, C.-Y., Theoretical prediction and experimental study of dielectric properties in poly(vinylidene fluoride) matrix composites with micronanosize BaTiO[sub 3] filler. *Appl Phys Lett* **2007,** *91* (22), 222902.
[275] Hong, S. M.; Nam, Y. W.; Hwang, S. S.; Chae, D. W., Physical Properties of Multi-Walled Carbon Nanotube-Filled PVDF Composites Prepared by Melt Compounding. *Molecular Crystals and Liquid Crystals* **2007,** *464* (1), 195/[777]-203/[785].
[276] Martins, P.; Costa, C. M.; Benelmekki, M.; Botelho, G.; Lanceros-Mendez, S., On the origin of the electroactive poly(vinylidene fluoride) β-phase nucleation by ferrite nanoparticles via surface electrostatic interactions. *CrystEngComm* **2012,** *14* (8), 2807.
[277] Martins, P.; Lopes, A. C.; Lanceros-Mendez, S., Electroactive phases of poly(vinylidene fluoride): Determination, processing and applications. *Progress in Polymer Science* **2014,** *39* (4), 683-706.
[278] Zucolotto, V.; Avlyanov, J.; Gregorio, R.; Mattoso, L. H. C., Melt processing of composites of PVDF and carbon black modified with conducting polymers. *J Appl Polym Sci* **2004,** *94* (2), 553-557.
[279] Fan, B.-H.; Zha, J.-W.; Wang, D.; Zhao, J.; Dang, Z.-M., Size-dependent low-frequency dielectric properties in the BaTiO3/poly(vinylidene fluoride)

nanocomposite films. *Appl Phys Lett* **2012,** *100* (1), 012903.
[280] Zhao, H.; Zhang, L.; Yang, M. H.; Dang, Z. M.; Bai, J. B., Temperature-dependent electro-mechanical actuation sensitivity in stiffness-tunable BaTiO3/polydimethylsiloxane dielectric elastomer nanocomposites. *Appl Phys Lett* **2015,** *106* (9).
[281] He, R.; Yang, P., Giant piezoresistance effect in silicon nanowires. *Nat Nanotechnol* **2006,** *1* (1), 42-46.
[282] Benight, S. J.; Wang, C.; Tok, J. B. H.; Bao, Z., Stretchable and self-healing polymers and devices for electronic skin. *Progress in Polymer Science* **2013,** *38* (12), 1961-1977.
[283] Stassi, S.; Cauda, V.; Canavese, G.; Pirri, C. F., Flexible tactile sensing based on piezoresistive composites: a review. *Sensors* **2014,** *14* (3), 5296-332.
[284] Canavese, G.; Stassi, S.; Fallauto, C.; Corbellini, S.; Cauda, V.; Camarchia, V.; Pirola, M.; Pirri, C. F., Piezoresistive flexible composite for robotic tactile applications. *Sensors and Actuators A: Physical* **2014,** *208*, 1-9.
[285] Castano, L. M.; Flatau, A. B., Smart fabric sensors and e-textile technologies: a review. *Smart Materials and Structures* **2014,** *23* (5), 053001.
[286] Kong, J. H.; Jang, N. S.; Kim, S. H.; Kim, J. M., Simple and rapid micropatterning of conductive carbon composites and its application to elastic strain sensors. *Carbon* **2014,** *77*, 199-207.
[287] Ramuz, M.; Tee, B. C.; Tok, J. B.; Bao, Z., Transparent, optical, pressure-sensitive artificial skin for large-area stretchable electronics. *Adv Mater* **2012,** *24* (24), 3223-7.
[288] Zhou, J. F.; Song, Y. H.; Zheng, Q.; Wu, Q.; Zhang, M. Q., Percolation transition and hydrostatic piezoresistance for carbon black filled poly(methylvinylsilioxane) vulcanizates. *Carbon* **2008,** *46* (4), 679-691.
[289] Yan, C.; Wang, J.; Kang, W.; Cui, M.; Wang, X.; Foo, C. Y.; Chee, K. J.; Lee, P. S., Highly stretchable piezoresistive graphene-nanocellulose nanopaper for strain sensors. *Adv Mater* **2014,** *26* (13), 2022-7.
[290] Zhu, S.-E.; Krishna Ghatkesar, M.; Zhang, C.; Janssen, G. C. A. M., Graphene based piezoresistive pressure sensor. *Appl Phys Lett* **2013,** *102* (16), 161904.
[291] Lee, C.; Jug, L.; Meng, E., High strain biocompatible polydimethylsiloxane-based conductive graphene and multiwalled carbon nanotube nanocomposite strain sensors. *Appl Phys Lett* **2013,** *102* (18), 183511.
[292] Luo, S., Processing-Structure-Property Relationships Of Carbon Nanotube And Nanoplatelet Enabled Piezoresistive Sensors. **2013**.
[293] Zhao, H.; Wang, D.-R.; Zha, J.-W.; Zhao, J.; Dang, Z.-M., Increased electroaction through a molecular flexibility tuning process in TiO2–polydimethylsilicone nanocomposites. *J Mater Chem A* **2013,** *1* (9), 3140.
[294] Luheng, W.; Tianhuai, D.; Peng, W., Effects of conductive phase content on critical pressure of carbon black filled silicone rubber composite. *Sensors and Actuators A: Physical* **2007,** *135* (2), 587-592.
[295] Luheng, W.; Tianhuai, D.; Peng, W., Influence of carbon black concentration on piezoresistivity for carbon-black-filled silicone rubber composite. *Carbon* **2009,** *47*

(14), 3151-3157.
[296] Song, X.; Liu, S.; Gan, Z.; Lv, Q.; Cao, H.; Yan, H., Controllable fabrication of carbon nanotube-polymer hybrid thin film for strain sensing. *Microelectronic Engineering* **2009,** *86* (11), 2330-2333.
[297] Wang, P.; Geng, S.; Ding, T., Effects of carboxyl radical on electrical resistance of multi-walled carbon nanotube filled silicone rubber composite under pressure. *Composites Science and Technology* **2010,** *70* (10), 1571-1573.
[298] Darren J. Lipomi , M. V., Benjamin C-K. Tee , Sondra L. Hellstrom,Jennifer A. Lee, Courtney H. Fox and Zhenan Bao, Skin-like pressure and strain sensors based on transparent elastic films of carbon nanotubes. *Nat Nanotechnol lett* **2011,** *6*, 788-792.
[299] Hwang, J.; Jang, J.; Hong, K.; Kim, K. N.; Han, J. H.; Shin, K.; Park, C. E., Poly(3-hexylthiophene) wrapped carbon nanotube/poly(dimethylsiloxane) composites for use in finger-sensing piezoresistive pressure sensors. *Carbon* **2011,** *49* (1), 106-110.
[300] Zha, J.-W.; Li, W.-K.; Zhang, J.; Shi, C.-Y.; Dang, Z.-M., Influence of the second filler on the positive piezoresistance behavior of carbon nanotubes/silicone rubber composites. *Materials Letters* **2014,** *118*, 161-164.
[301] Castillo-Castro, T.; Castillo-Ortega, M. M.; Encinas, J. C.; Herrera Franco, P. J.; Carrillo-Escalante, H. J., Piezo-resistance effect in composite based on cross-linked polydimethylsiloxane and polyaniline: potential pressure sensor application. *Journal of Materials Science* **2011,** *47* (4), 1794-1802.

Publications

[1] **Hang Zhao**, Jinbo Bai. Highly sensitive piezo-resistive graphite nanoplatelet-carbon nanotubes hybrids /polydimethylsilicone composites with improved conductive network construction. *ACS Applied Materials & Interfaces*, **2015**, 7 (18) 9652–9659.

[2] **Hang Zhao**, Ling Zhang, Min-Hao Yang, Zhi-Min Dang, Jinbo Bai. Temperature-dependent electro-mechanical actuation sensitivity in stiffness-tunable $BaTiO_3$/polydimethylsilixane dielectric elastomers nanocomposites. *Applied Physics Letters*, **2015**, 106, 092904.

[3] **Hang Zhao**, Dong-Rui Wang, Jun-Wei Zha, Jun Zhao, Zhi-Min Dang. Increased electroaction through a molecular flexibility tuning process in TiO_2 – polydimethylsilicone nanocomposites. *Journal of Material Chemistry A*, **2013**, 1, 3140–3145.

[4] **Hang Zhao**, Zhi-Min Dang, Yu-Juan Xia, Jun-Wei Zha, Guo-Hua Hu, Composition dependence of dielectric properties, elastic modulus and electroactivity in (carbon black-$BaTiO_3$)/silicone rubber nanocomposites. *Journal of Applied Polymer Science*. **2013**, 38044, 4440-4445.

[5] **Hang Zhao**, Zhi-Min Dang, Jun-Wei Zha, Jun Zhao, Dong-Rui Wang, Guo-Hua Hu, Explanation for bulge deformation of electroactive silicone based composites by employing infinitesimal method. *Journal of Advanced Physics*, **2013**, 2, 1-7.

[6] Yi Hou, Dong-Rui Wang, **Hang Zhao**, Zhi-Min Dang. graphene/PDMS nanocomposites with sensitive dynamic piezoresistive behavior. *Journal of Material Chemistry C*, **2013**, 1,515-520.